Establishment of An Automated Digital Prion Infectivity Cell Assay and PrP-HPFRET Based High-throughput siRNA Screening Platform

---

Dissertation

zur

Erlangung der naturwissenschaftlichen Doktorwürde

(Dr. sc. nat.)

vorgelegt der

Mathematisch-naturwissenschaftlichen Fakultät

der

Universität Zürich

von

Bei Li

aus

China, PRC

Promotionskomitee

Prof. Dr. Adriano Aguzzi (Vorsitz)

Prof. Dr. Charles Weissmann

Prof. Dr. Ben Schuler

Zürich, 2016

Table of Contents

1 Summary

Prion diseases are a group of transmissible fatal neurodegenerative diseases, including the Creutzfeldt-Jakob disease (CJD), fatal familial insomnia (FFI), Gerstmann-Sträussler-Scheinker syndrome (GSS) and Kuru in humans, bovine spongiform encephalopathy (BSE) in cattle, scrapie in sheep and goat, chronic wasting disease (CWD) in deer, moose and elk. The disease causing agents consists of aggregated PrP^{Sc}, a misfolded isoform of the host cellular prion protein (PrP^{C}). In a prion replication process, PrP^{Sc} acts as a propagon that is capable of seeding a self-perpetuating reaction to convert more PrP^{C} to PrP^{Sc}. The number of monomers in each prion propagon is variable; therefore, prion infectivity titers cannot be predicted by merely measuring PrP^{Sc} but necessitate bioassays, which require inoculation of serially diluted prions into susceptible animals. The conventional animal bioassay is time-consuming, cost-ineffective and ethically problematic; hence, it is imperative to establish a rapid, economic and sensitive method to determine prion infectivity titers.

The PrP^{C} expression level is the main determinant of prion pathogenesis. $Prnp^{-/-}$ homozygous mice are resistant to prion infection. Reduction of PrP^{C} by 50% ($Prnp^{+/-}$ heterozygous mice) significantly prolongs the incubation time of prion disease, whereas overexpression of PrP^{C} remarkably shortens disease progression. However, the intrinsic molecular mechanisms underlying prion protein expression and replication are currently far less understood. This is mainly because the conventional detection methods for prion proteins have inherent limitations in applicability to high-throughput research, leading to the dearth of high-throughput technology that can be used to characterize the fundamental molecular mechanisms.

In the first part of the thesis, I developed homogeneous-phase fluorescence resonance energy transfer (HPFRET) assays for detecting prion proteins, designated as PrP^{C}-HPFRET and PrP^{Sc}-HPFRET. Next, I established an automated digital prion infectivity cell assay (DPICA), which requires minimal manipulation of infectious materials. The DPICA readout is based on highly parallel cell-based PrP^{Sc}-HPFRET bioassays: 100 prion susceptible cells/well were seeded in 384-well plates and exposed to prions. After ten days of culture, lysis buffer containing proteinase K, denaturing buffer, neutralizing buffer and a pair of fluorescently labelled anti-PrP antibodies were sequentially added. PrP^{Sc}-HPFRET signal in each well was detected by a RT-FRET reader. The results were analysed with sophisticated numerical methods intended to filter noise from the binomially distributed biological data. The DPICA detected $10^{6.5}$ propagons/g and $10^{5.4}$ propagons/g in two distinct mouse prion strains, RML6 and Me7, thus demonstrating the number of propagons in the samples. This bioassay can be applied to a fully automated platform, and is therefore suitable for high-throughput screening (HTS) applications.

In the second part of the thesis, I utilized the PrP^{C}-HPFRET and PrP^{Sc}-HPFRET to assess RNAi-mediated gene silencing in neuronal cells, and established an automated PrP-HPFRET based high-throughput siRNA screening platform to identify genes affecting cellular prion protein expression. Next, I screened an arrayed murine siRNA library including 3153 siRNAs targeting 780 genes that are involved in endocytosis pathways. I identified the transferrin receptor 1 (Tfr1 or Tfrc) as an interesting hit, such that Tfr1-siRNA treatment efficiently downregulated PrP^{C} expression and blocked PrP^{Sc} replication in neuronal cells. By qPCR analysis, I found that Prnp mRNA levels in Tfr1-siRNA transfected wide-type neuronal cells were also significantly reduced, suggested that silencing Tfr1 repressed endogenous PrP^{C} expression at the transcriptional/post-transcriptional level. Further, genome-wide transcriptome analysis of Tfr1-siRNA treated CAD5 cells by RNAseq confirmed the qPCR results and showed that 99 genes were significantly changed with >4-fold-change, p-value < 1e-5, in which 48 genes were down-regulated (Tfr1 was top7 and Prnp was top11 down regulated) and 51 genes were upregulated. Finally, I modulated the Tfr1 level in a cell culture model and mouse model by iron supplement or chelator treatment, and found that PrP^{C} expression can be significantly altered. These results imply that Tfr1 may represent a potential therapeutic target for prion diseases. The PrP-HPFRET based high-throughput siRNA screening platform will provide a powerful tool for discovering unknown molecular mechanisms and even novel approaches for prion therapy.

2 Zusammenfassung

Prionenerkrankungen bilden eine Gruppe von übertragbaren, tödlich verlaufenden neurodegenerativen Erkrankungen. Bei Menschen gehören Creutzfeldt-Jakob-Krankheit, Fatale Familiäre Insomnie, Gerstmann-Sträussler-Scheinker-Syndrom und die Kuru Krankheit dazu. Zu den Prionenerkrankungen bei Tieren zählen die Bovine Spongiforme Encephalopathie bei Rindern (BSE), die Schaberkrankheit („Scrapie") bei Schafen und Ziegen und die Chronic Wasting Disease» (CWD) der Hirsche und Elche.

Das die Krankheit auslösende Agens besteht aus aggregiertem PrPSc, einer fehlgefalteten Isoform des körpereigenen Prion Proteins (PrP^{C}). PrP^{Sc} wirkt bei dieser Erkrankung als Propagon, das in einem Replikationsprozess dazu befähigt ist PrP^{C} in PrP^{Sc} umzuwandeln. Die Zahl von Monomeren in jedem Prionpropagon ist variabel, deshalb lässt sich der Prionentiter nicht von der detektierten Menge von PrP^{Sc} ableiten, sondern bedarf eines Bioassays, der durch Inokulationsexperimente in Tiere mit verschiedenen Verdünnungen der Prionen bestimmt werden kann. Der klassische Tier-Bioassay ist ineffizient, kostspielig und ethisch problematisch, daher ist eine schnellere, preisgünstige und sensitive Methodik zwingend erforderlich.

Bei der Pathogenese von Prionenerkrankungen spielt die PrP^{C} Expressionsmenge eine entscheidende Rolle, wobei $Prnp^{-/-}$ homozygote Mäuse infektionsresistent sind bzw. Mäuse mit einer 50% igen Verminderung von PrP^{C} ($Prnp^{+/-}$ heterozygous mice) eine signifikante Verlängerung der Inkubationszeit von Prionenerkrankungen zeigen. Im Gegensatz dazu führt eine Überexpression von PrP^{C} zu einer deutlich kürzeren Erkrankungsdauer. Allerdings sind die Mechanismen, die zur Prionenreplikation führen, noch nicht vollständig geklärt.

Das ergibt sich vor allem dadurch, dass die herkömmlichen Nachweismethoden durch das Fehlen von High throughput Technologien limitiert sind, die für die Aufklärung dieser Fragestellung eine entscheidende Rolle spielen.

Im ersten Teil meiner Doktorarbeit, um Prionenproteine zu detektieren, habe ich einen Försters Fluorescenz Resonanz Emissionstransfer (HPFRET) Assay, als PrP^{C}-HPFRET and PrP^{Sc}-HPFRET bezeichnet, verwendet. Als Nächstes habe ich einen automatisierten, digitalen Prionen Infektivitäts Assay (DPICA), der minimale Manipulation von infektiösem Material benötigt. Der Readout basiert auf einem parallel-angeordneten zellbasierten PrP^{Sc}-HPFRET Bioassay. 100 Zellen pro Well wurden ausplattiert und mit Prionen infiziert. Nach 10 Tagen Zellkultivierung wurden nacheinander Lysepuffer, welcher Proteinase K enthält, Denaturierungspuffer, Neutralisationspuffer und ein Fluoreszenz gelabeltes Antikörperpaar hinzugegeben.

Das PrP^{Sc}-HPFRET Signal wird mittels eines RT-FRET detektiert. Die Ergebnisse werden als numerische Methoden bewertet, welche Rauschen von binomial verteilten biologischen

Daten filtrieren. Der DPICA-Assay detektierte $10^{6.5}$ Propagone/g und $10^{5.4}$ Propagone/g in den zwei verschiedenen Mausprionenstämmen RML6 und Me7. Dies entspricht der Zahl der Propagone innerhalb der Proben. Dieser Bioassay lässt sich komplett automatisiert durchführen und ist daher als High throughput screen (HTS) geeignet.

Im zweiten Teil meiner Arbeit habe ich den PrP^{C}-HPFRET und PrP^{Sc}-HPFRET genutzt, um RNAi-mediiertes „gene silencing“ in neuronalen Zellen zu bestimmen. Des Weiteren habe ich einen automatisierten PrP-HPFRET Assay etabliert, basierend auf dem high-throughput siRNA screen, um Gene zu identifizieren, die die Expression des zellulären Prion Proteins beeinflussen. Anschliessend habe ich einen Array von Maus siRNA gescreened , welcher 3153 siRNAs umfasst, die 780 Gene betreffen, welche den Endozytose Signalweg beeinflussen. Dabei habe ich den Transferrin Rezeptor 1 (Tfr1 oder Tfrc) als möglichen Kandidaten detektiert, bei dem die siRNA Behandlung zu einer Runterregulation der PrPC Expression und somit Verhinderung der PrP^{Sc} Replikation in neuronalen Zellen geführt hat. Mittels quantitativer PCR Analyse, konnte ich zeigen, dass die mRNA Level von Prnp in Tfr1-siRNA transfizierten neuronalen Zellen also signifikant vermindert waren, was darauf hinweist, dass silencing von Tfr1 die endogene PrP^{C} Expression auf transkriptionaler/ posttranskriptionaler Ebene unterdrückt. Weiterhin konnten die Genom basierten Transkriptom Analysen der -siRNA behandelten CAD5 Zellen mittels RNAseq die PCR Ergebnisse untermauert und gezeigt werden, dass 99 Gene eine signifikante Änderung, > als 4 fach, und p-Wert < 1e-5, unter denen 48 Gene runterreguliert waren (mit Tfr1 als 7. und Prnp als 11. runterreguliert) und 51 genes waren hochreguliert. Zu guter letzt habe ich das Tfr1 level in einem Zellkultur Modell durch Eisen Zusatz oder Chelator Behandlung moduliert. Dabei zeigte sich, dass die PrPC Expression sich signifikant änderte. Diese Ergebnisse weisen darauf hin, dass Tfr1 ein potentielles therapeutisches Target für Prionenerkrankungen darstellen könnte. Der PrP-HPFRET basierte high-throughput siRNA screen stellt sich als ein wichtiges Werkzeug für die Aufdeckung unbekannter molekularer Mechanismen und neuen Ansätzen der Prionen Therapie dar.

3 Abbreviations

AA	amino acid
Aβ	amyloid-β
AD	Alzheimer's diseases
ALS	amyotrophic lateral sclerosis
APP	amyloid precursor protein
BH	brain homogenate
BSA	bovine serum albumin
BSE	bovine spongiform encephalopathy
CJD	Creutzfeldt-Jakob disease
CNS	central nervous system
CWD	chronic wasting disease
DPICA	digital prion infectivity cell assay
dpi	days post infection
ER	endoplasmic reticulum
fCJD	familial Creutzfeldt-Jakob disease
FFI	familial fatal insomnia
FTD	frontotemporal dementia
GPI	glycosylphosphatidylinositol
GSS	Gerstmann-Sträussler-Scheinker syndrome
HPFRET	homogeneous-phase fluorescence resonance energy transfer
KD	kilo Dalton
LD_{50}	median lethal dose
MSA	multiple system atrophy
NBH	non-infectious brain homogenate
PD	Parkinson's diseases
PK	proteinase K
POM 1-19	set of 19 anti-PrP monoclonal antibodies
Prnp	murine prion gene
PRNP	human prion gene
PrP	prion protein
PrP^{C}	cellular prion protein
PrP^{Sc}	scrapie-associated prion protein
RML6	Rocky Mountain laboratory strain, passage 6
SEM	standard error of the mean
SD	standard deviation
sCJD	sporadic Creutzfeldt-Jakob disease

SCEPA	scrapie cell assay in end point format
$TCID_{50}$	tissue culture infectivity 50% dose
Tga20	transgenic mice overexpressing PrP^C
TSE	transmissible spongiform encephalopathies
vCJD	variant Creutzfeldt-Jakob disease
WT	wild-type
KO	knockout
263K	hamster adapted scrapie prions

4 Introduction

4.1 Prion diseases

Prion diseases also known as transmissible spongiform encephalopathies (TSEs), are a group of fatal neurodegenerative disorders marked by neuronal loss, vacuolization, gliosis, and spongiform changes in the brain (Aguzzi, Nuvolone et al. 2013). In animals, prion diseases include scrapie in sheep and goats (Cuille J and Chelle PL 1939), chronic wasting disease (CWD) in deer, moose and elk (Williams and Young 1980), and bovine spongiform encephalopathy (BSE) in cattle (Hope J, Ritchie L et al. 1989). In humans, prion diseases include Creutzfeldt-Jacob diseases (CJD) (Gibbs, Gajdusek et al. 1968), fatal familial insomnia (FFI) (Medori, Tritschler et al. 1992), Gerstmann-Sträussler-Scheinker syndrome (GSS) (Gajdusek 1977) and Kuru (Gajdusek, Gibbs et al. 1966).

The disease causing agent consists of PrP^{Sc}, which is an isoform of the host-encoded cellular prion protein PrP^{C}. PrP^{Sc} that acts as a propagon, which is capable of seeding a self-perpetuating reaction to convert PrP^{C} to itself within a bioassay system (Aguzzi, Nuvolone et al. 2013). This process is termed as prion replication. The cellular prion protein PrP^{C} is encoded by the PRNP gene (Basler, Oesch et al. 1986). Its expression is indispensable for prion replication and prion-induced neurodegeneration (Bueler, Aguzzi et al. 1993). However, the intrinsic molecular mechanisms of prion replication and subsequent neurodegeneration are still largely unknown (Weissmann 2005).

4.1.1 Animal prion diseases

The first case of scrapie was reported in Spanish merino sheep in 1732 (Liberski 2012). The name “scrapie” was derived from the observation that diseased sheep scrape themselves against objects. Scrapie was proven to represent a transmissible disease among sheep and goats (Cuille J and Chelle PL 1939, Gordon 1946). The first case of CWD was reported in Colorado, then spread around North America and to South Korea (Sigurdson and Aguzzi 2007). In 1986, the first case of BSE, later known by the popular name "mad-cow disease", was described in in the UK (Wells, Scott et al. 1987). Subsequently, the disease rapidly developed into a major epidemic in European countries. In the last 30 years, over 280,000 animals were affected by prion diseases (Aguzzi and Calella 2009). The use of prion-infected bone and meat in cattle food was considered a major source of BSE (Weissmann and Aguzzi 1997). Other possible routes of infection described in animals include the milk of sheep suffering from scrapie or mastitis (Ligios, Sigurdson et al. 2005), the urine of mice affected by scrapie and nephritis (Seeger, Heikenwalder et al. 2005), and the saliva and blood of deer with CWD (Mathiason, Powers et al. 2006). It is mandatory to implement stringent control measures to eliminate the risk of infectious materials in animal feed, and thereby reduce the incidence of prion disease (Hope 2013)

4.1.2 Human prion diseases

Five human prion diseases have been recognized so far: Creutzfeldt-Jakob disease (CJD), variant Creutzfeldt-Jakob disease (vCJD), fatal familial insomnia (FFI), Gerstmann-Sträussler-Scheinker syndrome (GSS) and Kuru. Sporadic CJD comprises 85% of human prion diseases, 10 – 15% cases are familial (fCJD) and 1% cases are iatrogenic. Human prion diseases can be subdivided into inherited, sporadic and infectious forms, based on their clinical presenation, genetic and neuropathological features (Aguzzi and Calella 2009).

The inherited prion diseases fCJD, FFI and GSS are associated with an autosomal dominant mutation in PRNP (Johnson and Gibbs 1998). In general, fCJD is associated with point mutations, insertions or deletions in the PRNP gene, and presents at an earlier age, with a more prolonged clinical course than sporadic CJD (Johnson and Gibbs 1998, Aguzzi and Calella 2009). FFI is characterized by a mutation in PRNP that replaces the amino acid asparagine (N) with methionine (M) at codon 129 and aspartic acid (D) at codon 178 (Gambetti, Parchi et al. 1995). GSS is inherited in an autosomal dominant manner with mutations in PRNP mostly at codons 102 and 198, and characterized histopathologically by multicentric amyloid plaques positive for PrP (Collins, McLean et al. 2001).

4.2 The cellular prion protein

4.2.1 PrP^C expression pattern

The host cellular prion protein (PrP^C) is highly conserved in mammals, implying important functions of PrP^C. Although PrP-deficient ($Prnp^{-/-}$) mice are generally believed to perform well, an evolutionary pressure must exist to counterbalance the susceptibility of Prnp-expressing individuals to prion disease (Mead, Stumpf et al. 2003). PrP^C is highly expressed in the central nervous system (CNS), and also in several peripheral tissues and cells including heart, skeletal muscle, kidney and lymphocytes (Dodelet and Cashman 1998, Ford, Burton et al. 2002). Inflammatory conditions can trigger ectopic PrP^C expression and prion replication competence in organs that normally express low amounts of PrP^C (Heikenwalder, Zeller et al. 2005). In the CNS, PrP^C is ubiquitously expressed with the highest levels found in neuronal and glial cells (Aguzzi, Baumann et al. 2008).

4.2.2 Biosynthesis of PrP^C

Murine PrP gene (Prnp) has three exons. Exon 3 contains an open reading frame (ORF) and a 3' untranslated region (3' UTR), whereas Human PrP gene (PRNP) has two known exons and one putative exon. So far, the equivalent of murine exon 2 has not been found in human RNA transcripts. The murine PrP^C protein is 254 amino acids (aa) in length, which includes a 22 amino acid signal peptide, five octapeptide repeats, one disulphide bond (S–S) between cysteine residues 178 and 213, and two potential sites for N-linked glycosylation (CHO) at

residues 180 and 196. A glycosylphosphatidylinositol (GPI) anchor is attached to the C-terminus of PrP at residues 231 to 254. The human PrP^C protein consists of 245 amino acids and has the same structural features as murine PrP^C protein. PrP^C is synthesized in the endoplasmic reticulum (ER) (Stahl, Borchelt et al. 1987). The key signal peptide for directing PrP^C into the ER is located in amino acids 1 – 22, and is subsequently cleaved off. Two glycans chains are attached at asparagine 181 and 197, and a disulphide bridge is formed between cysteine 197 and 214. After removing the C-terminal peptide, a GPI anchor is attached (Harris 2003). PrP^C is folded and transported to the Golgi, where additional modifications are made in glycans and the GPI anchor, before being sent to the cell surface. Finally, mature PrP^C at the cell surface is endocytosed into internal endosomal compartments, where it can either be recycled into the cell membrane or sent to lysosomes for degradation (Chakrabarti, Ashok et al. 2009). In cell culture, most PrP^C is degraded through the lysosome or proteasome pathway (Caughey and Lansbury 2003). Roughly less than one third of PrP^C is shed into the medium (Borchelt, Scott et al. 1990).

4.2.3 Structure of PrP^C

PrP^C proteins in mammals have a similar three-dimensional structure that consists of two distinct domains: a C-terminal structured globular domain (aa 126 – 231) and an N-terminal unstructured flexible tail (aa 23 – 125) (Aguzzi and Calella 2009). The structured C-terminal globular domain consists of double-stranded antiparallel β-pleated sheets (aa 128-131 and 161 – 164), three α-helices (aa 144 – 154, 173 – 194 and 200 – 228) and a disulphide bond linking helices two and three. (Riek, Hornemann et al. 1996). The unstructured N-terminal flexible tail contains a segment of five repeats so called “octarepeat” region, which is flanked by two positively charged clusters CC1 (aa 23 –27) and CC2 (aa 95 – 110). The octarepeat region may be involved in copper binding and inherited prion diseases with insertion of mutations (Aguzzi and Calella 2009). The two domains are linked by a highly conserved hydrophobic core (aa 111 – 134).

4.2.4 Physiological function of PrP^C

Several physiological roles of PrP^C are recognized including myelin homeostasis, circadian rhythm, memory formation, and immunological processes such as phagocytosis, and the self-renewal of hematopoietic stem cells (Steele, Lindquist et al. 2007). Many of these functions are still controversial because of the mixed background of *Prnp*$^{-/-}$ mice and the problem of flanking genes (Nuvolone, Kana et al. 2013). Our lab has shown that neuronal ablation of PrP^C or the prevention of PrP^C cleavage produces chronic demyelinating polyneuropathy in *Prnp*$^{-/-}$ mice of various genetic backgrounds (Bremer, Baumann et al. 2010)

and recent studies have demonstrated that the PrP^{C} promotes myelin homeostasis through FT-mediated Gpr126 agonism in Schwann cells (Küffer et al., 2016 in press).

4.3 Models of prion replication

The protein-only hypothesis proposes that the nature of the infectious entity responsible for triggering of any prion disease consists mainly of PrP^{Sc}, which is an abnormally-folded, protease-resistant and β-sheet-rich isoform of PrP^{C} (Prusiner 1991). A 'unified theory' of prion propagation defined by Charles Weissmann (Weissmann 1991) indicates that prion is an infectious protein that does not contain any informational nucleic acids, and propagates by recruitment and the “autocatalytic” conformational conversion of normal PrP^{C} into disease-associated PrP^{Sc} (Aguzzi, Heikenwalder et al. 2007). PrP^{C} is soluble in mild detergents and sensitive to proteinase K (PK) digestion. PrP^{Sc} forms insoluble aggregates and is partially resistant to PK (Bolton, Mckinley et al. 1982, Oesch, Westaway et al. 1985, Meyer, Mckinley et al. 1986). Correlation of the mass of the purified PrP^{Sc} protein fractions to the infectivity showed that the most infectious prion particle has a mass corresponding to 14-28 PrP molecules (Silveira, Raymond et al. 2005).

There have been two models proposed for the pathological conversion of PrP^{C} into PrP^{Sc} (**Figure 4.1**): **(A)** the 'refolding' or template directed assistance model (Gajdusek 1988) and **(B)** the 'seeding' or nucleation–polymerization model (Jarrett and Lansbury 1993). In the 'refolding' model, a kinetic energy barrier prevents the spontaneous misfolding from PrP^{C} into PrP^{Sc}. An exogenously introduced PrP^{Sc}, probably with the assistance of a chaperone (Telling, Scott et al. 1995) or another type of molecule (Priola, Chesebro et al. 2003), acts as a template that catalyzes the conversion of PrP^{C} into PrP^{Sc} (Weissmann 1999). In the 'seeding' model, the natural equilibrium between PrP^{C} and PrP^{Sc} is strongly shifted towards PrP^{C} (Weissmann 1999). Exposure to monomeric PrP^{Sc} induces a nucleation-polymerisation process that promotes the stabilization of PrP^{Sc} and further recruitment of more monomeric PrP^{Sc}, which results in the formation of amyloid. The propagation through fragmentation is predicted as a crucial step that determines the degree of infectivity during prion replication (Knowles, Waudby et al. 2009, Cohen, Vendruscolo et al. 2011)

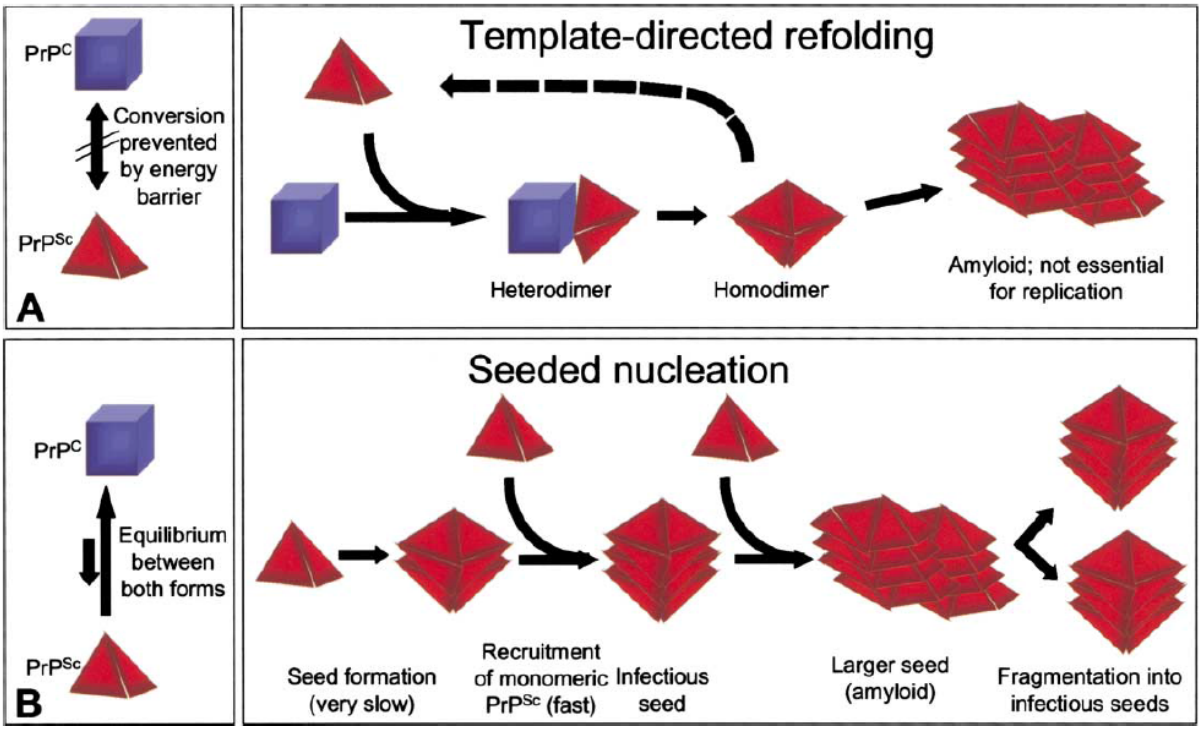

Figure 4.1 Models of prion replication. A. The 'refolding' or template-directed assistance model. **B.** The 'seeding' or nucleation–polymerization model. Figure adapted from (Aguzzi and Polymenidou 2004).

4.4 Prion pathogenesis

The precise molecular mechanisms of prion pathogenesis that lead to glial activation, neuronal cell death and the association of PrP^{Sc} and prion plaques to neurotoxicity are not yet well understood. A basic question is whether prion diseases are caused by PrP^{C} associated loss of function (Aguzzi, Baumann et al. 2008). First, PrP^{C} deficient mice did not show a significant phenotype of prion-like neuropathological changes (Bueler, Fischer et al. 1992), prion replication after intracerebral (i.c.) inoculation with prions was not observed (Bueler, Aguzzi et al. 1993), indicating that PrP^{C} expression is necessary for prion replication. The *Prnp*$^{-/-}$ mice transplanted with PrP^{C} overproducing neuroectodermal grafts into brains and intracerebrally inoculated with prions showed high levels of PrP^{Sc} accumulation and prion infectivity in grafts, and developed typical scrapie-induced histopathological changes. However, the surrounding tissue lacked PrP^{C} expression and without pathological changes, suggesting that PrP^{C} was required for scrapie – induced neurotoxicity (Brandner, Isenmann et al. 1996, Brandner, Raeber et al. 1996). Then, early signs of prion pathology such as spongiotic degeneration and neuronal cell loss were reversed by conditionally removing PrP^{C} selectively in neurons after prion inoculation (Mallucci, Dickinson et al. 2003, Mallucci, White et al. 2007), confirming that scrapie – induced toxicity requires target cells expressing PrP^{C}. Besides, transgenic mice that express a secreted PrP molecule lacking the glycosylphosphatidylinositol-anchor (GPI) were still able to replicate PrP^{Sc} but without any

signs of neurotoxicity (Chesebro, Trifilo et al. 2005), suggesting that PrP must be membrane-bound to induce cellular toxicity.

Some recent studies reported that prion replication and neurotoxicity may occur in two different phases: First, an exponential phase without clinical signs, where PrP^{C} is misfolded into PrP^{Sc} and prion titers are exponentially increased. This phase is not rate limited by PrP^{C} expression and prion infectivity can increase until a plateau is reached. Second, a plateau phase of prion infectivity determines the time to clinical onset and is inversely proportional to prion protein concentration (Sandberg, Al-Doujaily et al. 2011, Sandberg, Al-Doujaily et al. 2014). These studies hypothesized a toxic PrP species termed PrP^{L} that might be an oligomeric species of PrP^{Sc}.

4.5 Prionoid in PMDs

Protein misfolding disorders (PMDs) are classified by the coalescence of proteins into highly ordered aggregates that can affect entire organ systems with preferential deposition in the CNS, resulting in progressive neurodegeneration (Aguzzi and Lakkaraju 2016). So far, more than 20 different misfolding proteins have been reported, including mainly α-synuclein in Parkinson's diseases (PD) and multiple system atrophy (MSA), amyloid precursor protein (APP) and tau in Alzheimer's diseases (AD), transactive response DNA binding protein 43 kDa (TDP-43) in amyotrophic lateral sclerosis (ALS) and frontotemporal dementia (FTD), huntingtin in Huntington disease, and amyloid polypeptide in systemic amyloid disorders (Aguzzi and Lakkaraju 2016). Some of the proteins have been recognized and characterised according to the cellular localization of protein deposits: in prion diseases, PrP^{Sc} aggregates in extracellular spaces; amyloid-β (Aβ) deposits in extracellular and cytoplasmic space in AD; in PD, α-synuclein deposits in cytoplasm; in Huntington's diseases, polyglutamine accumulates in the nucleus.

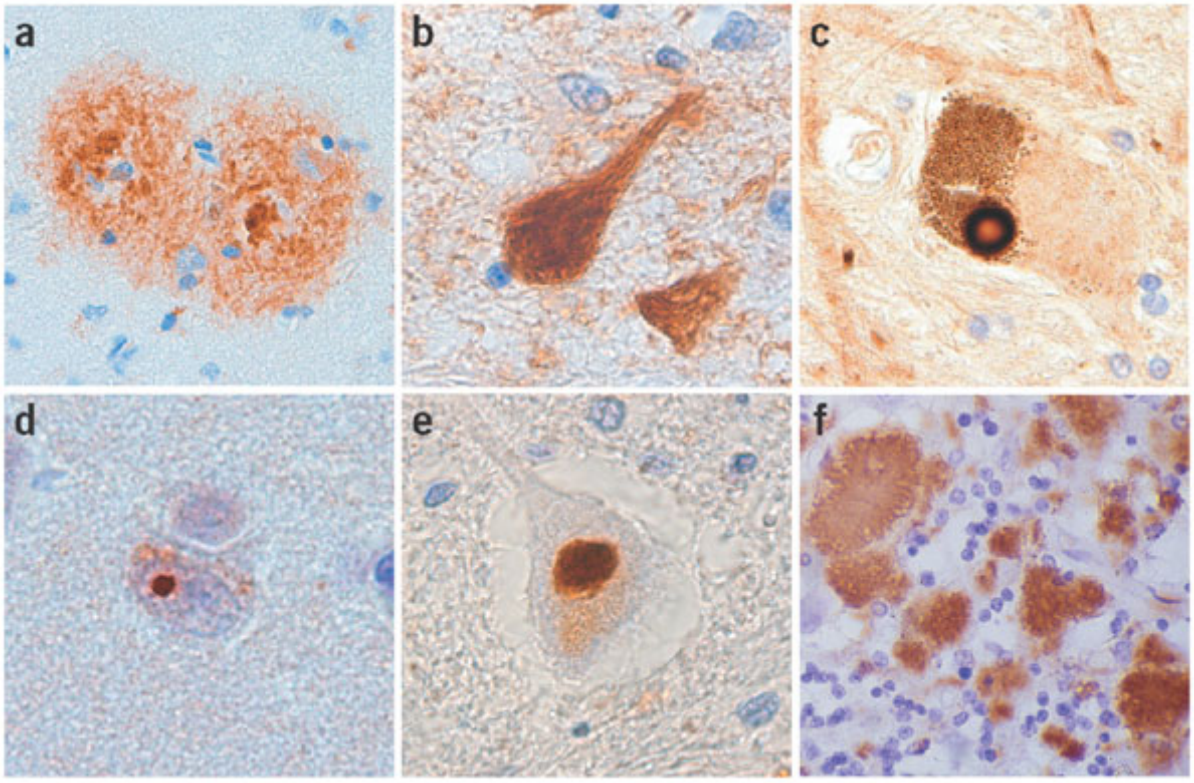

Figure 4.2 Protein aggregates in neurodegenerative disease. (a) Senile plaques in the neocortex of a brain with AD. **(b)** NFTs in hippocampus of FTDP-17. **(c)** Lewy body in the substantia nigra of PD. **(d)** Intranuclear polyglutamine inclusion in neocortex of Huntington disease. **(e)** Ubiquitinated inclusion in spinal cord motor neuron of ALS. **(f)** Protease-resistant PrP in cerebellum of CJD. Figure adapted from (Forman, Trojanowski et al. 2004)

The best-characterized PMDs are prion diseases that result from the aggregation of misfolded cellular prion proteins into highly ordered and β-sheet-enriched PrP^{Sc}. Although prion diseases are unique among neurodegenerative disorders because of their transmissibility between individuals and can cause epidemics, the ability of misfolding and self-propagation is not exclusive to prions. The amino acid sequence of each culprit protein in PMDs is different, but they all have a similarly insoluble and highly ordered structure containing β-sheets. The principles governing aggregation and propagation are quite similar to prions, in that under some certain conditions, the conformation of physiologically soluble proteins can change into β-sheet-enriched forms. Such protein aggregates spread from cell to cell, which triggers insolubility, aggregation propensity, and the resistance of protein aggregates to physical denaturants. Therefore, the term 'prionoids' (Aguzzi 2009) was applied to protein aggregates that act in a prion like manner but are not identical to prions, because they have not been found to be transmitted between humans. For example, the cell-to-cell transmission of pathologic α-synuclein and Parkinson's like Lewy pathology was found in wild-type (wt) non-transgenic mice with a single intracerebral injection of synthetic α-synuclein (Luk, Kehm et al. 2012). Additionally, recent studies have shown that Aβ can seed

aggregates of identical conformation in a particular conformation (Stohr, Condello et al. 2014, Watts, Condello et al. 2014), and other studies have reported some evidence for human transmission of Aβ pathology and cerebral amyloid angiopathy (Jaunmuktane, Mead et al. 2015, Frontzek, Lutz et al. 2016, Kovacs, Lutz et al. 2016). Therefore, fundamental studies focusing on the mechanisms of prion replication and prion-induced neurodegeneration can help advance the understanding the mechanisms of other PMDs diseases.

4.6 Strategies for potential therapeutic targets of prion diseases

Several strategies have been explored to target different stages of prion pathogenesis (**Figure 4.2**): a) Knock down the Prnp gene or pharmacologically down regulate PrP^{C} to block conversion of PrP^{C} into PrP^{Sc}; b) Specifically capture prions by antibodies or compounds to prevent the process of prion replication; c) Interfere with the formation of higher-order aggregates by antibodies or compounds; d) Stabilize prion fibrils by compounds to prevent the process of prion replication; e) Enhance natural protein-aggregate-clearing mechanisms by antibodies or compounds to prevent the process of prion replication; f) Use compounds to interfere with PrP^{C}-mediated neurotoxic pathway at the neuronal cell membrane (Aguzzi, Nuvolone et al. 2013).

To date, a large number of compounds have been screened with several compounds showing promising results in the suppression of prion proteins in cell-free or cell-based models, but showed no efficacy in follow-up validation using *in vivo* animal models. The majority of potential compounds showed little efficacy after the key pathologic features had occurred (Trevitt and Collinge 2006). Besides, antibody therapy has the inherent limitation that treatment should start before the onset of clinical signs (Aguzzi, Heikenwalder et al. 2007). However, in patients treatment is normally initiated is after the clinical diagnosis is made, at late stages of the disease. Therefore, potential therapeutics must exhibit high efficiency after prion-related pathology is already present. Unfortunately, disease-modifying therapies are not yet available. Hopefully, better understanding of the fundamental molecular mechanisms of prion diseases will facilitate the discovery of novel therapeutic approaches.

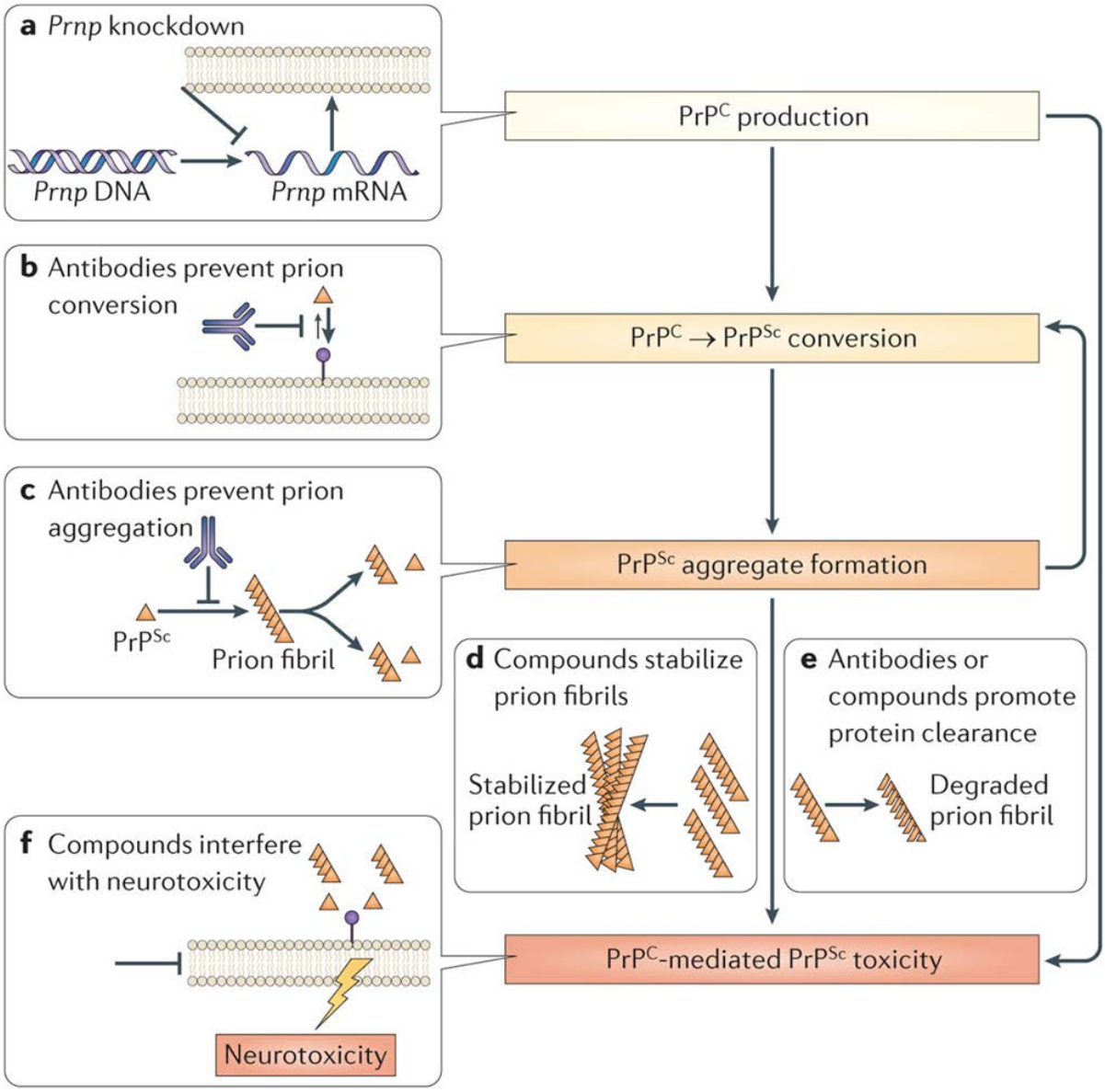

Figure 4.2 Potential therapeutic targets at different stages of prion pathogenesis. Figure adapted from (Aguzzi, Nuvolone et al. 2013)

4.7 Aims of the thesis

For my PhD thesis, I have proposed to develop new methods and technologies available for high-throughput measurements of prion proteins and infectivity. Then, I intend to apply these high-throughput assays to large scale murine siRNA screens, to identify genes that are involved in endogenous PrP^C expression and prion replication, to improve the understanding of molecular mechanisms of prions, and to find novel therapeutic targets for prion diseases.

a) Develop homogeneous-phase fluorescent resonance energy transfer assays for mouse prion protein detection (PrP^C-HPFRET, PrP^{Sc}-HPFRET).
b) Establish a cell-based bioassay “DPICA” for prion infectivity measurement that can be adapted to a fully automated platform.

c) Establish an RNAi HTS system for a comprehensive genome-wide study of prion diseases by combining novel technologies (PrP^{C}-/PrP^{Sc}-HPFRET, small RNAi, automated liquid handling platforms).

d) Apply the RNAi HTS system to a mouse siRNA library screen to identify genes that regulate endogenous PrP^{C} expression and prion replication.

5 Results PART I: Establishment of an automated digital prion infectivity cell assay (DPICA)

5.1 Introduction

5.1.1 Prion infectivity

Prion diseases are characterized by the deposition within the CNS and other organs of PrP^{Sc}, a misfolded and aggregated isoform of the host-encoded PrP^{C}, (Aguzzi and Zhu 2012). Prion diseases are unique among neurodegenerative conditions because of their transmissibility between individuals. The infectious agent consists of PrP^{Sc}, which acts as a propagon (Tuite and Cox 2003) capable of seeding a self-perpetuating reaction of templated nucleation (Aguzzi, Nuvolone et al. 2013). Because of these conditions, PrP^{Sc} concentrations are often used by scientists and regulatory agencies as surrogates of prion infectivity titers. However, this practice is fraught with problems. PrP^{Sc} is defined as the fraction of PrP that is resistant to proteolysis (Prusiner 1982), yet up to 99% of infectivity resides in a protease-sensitive fraction. Moreover, since the number of PrP^{Sc} monomers in each prion propagon is variable, infectious prion titers cannot be predicted by directly measuring PrP^{Sc}. These limitations indicate that it is unreliable to extrapolate prion titers from PrP^{Sc} determinations. Instead, accurate prion titrations continue to require bioassays in which infectivity is transferred to entities susceptible to infection.

5.1.2 Conventional prion infectivity bioassays

The standard prion infectivity assay is conducted by inoculating serial dilutions of the sample intracerebrally into indicator animals (Chandler 1961) and determining the dilution at which 50% of the animals acquire scrapie (end-point method) (Reed J 1938, Dougherty 1964). This method requires vast cohorts of animals and is prohibitively expensive. Prusiner introduced the incubation time method (Bolton, Mckinley et al. 1982), which relies on the inverse relationship between the logarithm of the inoculum size and latency time of the clinical disease. The latter method requires much smaller number of animals, but is notoriously imprecise. Moreover, both animal bioassays require several months to years for completion. Furthermore, clinically apparent prion disease creates a significant animal-welfare burden.

A landmark innovation was achieved by Charles Weissmann's "scrapie cell assay in end-point format (SCEPA)"(Klohn, Stoltze et al. 2003). The SCEPA takes 2-3 weeks to be completed, and is as sensitive as the mouse bioassay. In the SCEPA, prion susceptible cells are plated in 96-well plates and exposed to serial dilutions of prion-containing samples for 3 days. Cells are consecutively split 1:10 for three times every 3 days. Finally, cells in each well are transferred to membranes of ELISPOT plates and PrP^{Sc}-positive cells identified by immunoblotting. The tissue culture infectivity 50% dose ($TCID_{50}$) is calculated

accordingly(Reed J 1938, Dougherty 1964). Although the SCEPA significantly accelerates prion titrations, it still requires intensive pipetting for cell culture. Moreover, the handling of infectious culture medium can pose biohazards to the experimenters through the generation of highly infectious aerosols (Haybaeck, Heikenwalder et al. 2011). Moreover, the ELISPOT immunoreactions can only be partially automated. Here, we propose to develop a new cell-based prion infectivity bioassay, which can be adapted to a fully automated platform, and is therefore suitable for HTS applications.

5.2 Specific aims of the project

Here, I planned to develop a new cell-based assay for prion infectivity detection, termed "digital prion infectivity cell assay (DPICA)". The DPICA was designed to be applicable for automation and high-throughput applications.

a) Develop homogeneous-phase fluorescent resonance energy transfer assays for prion proteins detection (PrP^{C}-HPFRET, PrP^{Sc}-HPFRET).
b) Utilize PrP^{Sc}-HPFRET to establish a new cell-based bioassay (DPICA) for prion infectivity measurement, which can be adapted to a fully automated platform.
c) Establish automated HPFRET and DPICA programs on our robotic platform.

5.3 Development of HPFRET assays for detecting prion proteins

Fluorescence resonance energy transfer (FRET) is based on the energy transfer between two fluorophores, Europium (Eu^{3+}) and allophycocyanin (APC), which are separately labelled to anti-PrP antibodies (**Table 5.1**). When the Eu^{3+} and APC labelled anti-PrP antibodies bind to a single molecule and are closely apposed (<10 nm), the donor Eu^{3+} is excited and transfers the energy to the acceptor APC by nonradiative dipole-dipole coupling. Then the APC emits photons at a wavelength that can be measured.

To measure prion proteins in a fast and automated manner, I[#] developed homogeneous-phase FRET assays (HPFRET) for the quantification either PrP^{C} (Falsig, Sonati et al. 2012) or PrP^{Sc}. I established the HPFRET in a 96-well format and then optimized the assays for the 384-well format.

[#] I use the first-person narrative in my thesis in order to unequivocally identify those experiments that I personally performed, compared to when I use the “we” designation, which indicates that I was either involved in designing experiments, analysis and/or in the interpretation of the data.

5.3.1 Establishment of PrP^C-HPFRET

To detect PrP^C in a homogeneous phase, a variety of anti-PrP holoantibody pairs (POMs) (Polymenidou, Moos et al. 2008, Sonati, Reimann et al. 2013) were labeled with Eu^{3+} and APC, respectively. I tested different FRET holoantibody pairs and found the best FRET pair for PrP^C detection with the highest sensitivity and signal-to-noise ratio (SNR) is Eu^{2+}-POM2 and APC-POM1. The detection limit was about 0.4 ng/mL monomeric recombinant PrP (recPrP). In normal mouse brain homogenates (BH), PrP^C was detectable when the brain homogenate was 50,000 times diluted. In CAD5 cell lysates, PrP^C was detectable when the CAD5 cell lysate was diluted to 25 µg/mL (=1.25 µg/well total protein) (**Figure 5.1**). Normally, when the CAD5 cells are confluent in 384-well plates, there are about 5 µg/well total proteins, which is more than enough for PrP^C-HPFRET.

Table 5.1 Molecular characteristics of fluorophores used for labelling FERT antibodies.

Fluorophore	Molecular weight	Excitation λmax	Emission λmax	Extinction coefficient	Chemistry	Reactive group
Europium (Eu^{3+})	151 g/mol	340 nm	615 nm	at 335nm: 27,500 $cm^{-1}M^{-1}$	Amine reactive ($-NH_2$)	NHS ester
Allophycocyanin APC	104 kDa	650 nm	665 nm	at 650nm: 700,000 $cm^{-1}M^{-1}$	Thiol reactive (-SH)	Maleimide

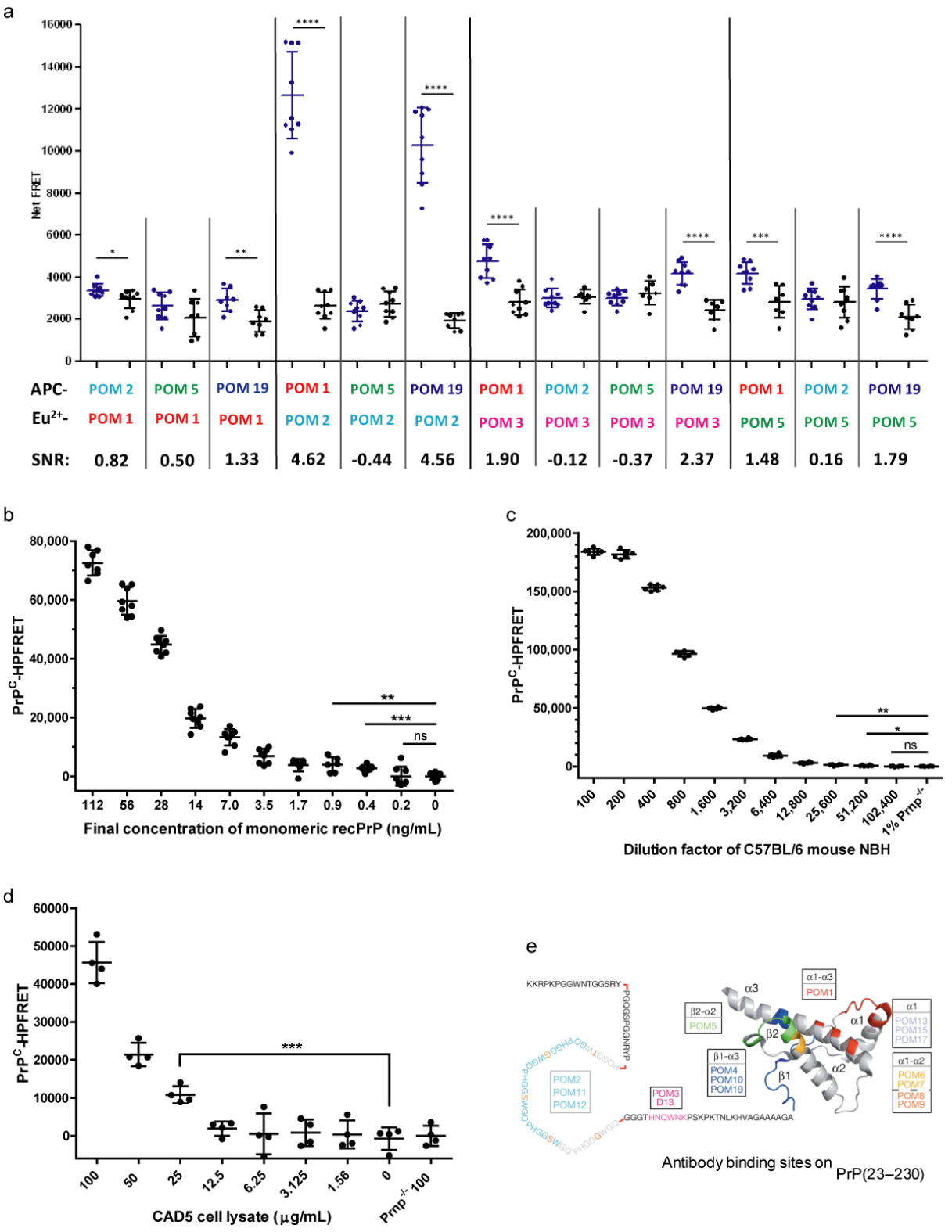

Figure 5.1 Establishment of PrP^C-HPFRET. (a) Comparison of FRET holoantibody pairs. Blue dot: normal mouse brain homogenate. Black dot: PrP-/- mouse brain homogenate. **(b)** PrP^C titration in monomeric recPrP^C. The FRET antibody pair was POM2-Eu^{2+} and POM1-APC. When the monomeric recPrP^C was diluted to around 0.4 ng/mL, the PrP^C signal was still detectable (***P<0.001). **(c)** PrP^C titration in mouse BH. The sample was 1% NBH from C57BL/6 mouse, then 1:1 diluted with 1% *Prnp*$^{-/-}$ BH**.** The FRET antibody pair was POM19-Eu^{2+} and POM1-APC. When the NBH was 51,200 times

diluted, the PrP^{C} signal was still detectable (*P<0.05). **(d)** PrP^{C} titration in CAD5 cell lysate. The sample was 100 µg/mL CAD5 cell lysate, then 1:1 diluted with 100 µg/mL CAD5 *Prnp*$^{-/-}$ cell lysate**.** When the CAD5 cell lysate was diluted to 25 µg/mL (1.25 µg/well total protein), the PrP^{C} signal was still detectable (***P<0.001). **(e)** Epitopes of the α-PrP antibody library. Adapted from (Sonati, Reimann et al. 2013)

5.3.2 Establishment of PrP^{Sc}-HPFRET

To detect PrP^{Sc} in the homogeneous phase (**Figure 5.2a**), tissue samples were homogenized in 0.32M sucrose or PBS and treated with a lysis/digestion buffer containing detergents and proteinase K (PK). Any cellular PrP^{C} present in samples is fully degraded by PK, whereas PrP^{Sc} aggregates indicative of prion infection are PK-resistant and therefore preserved. After PK inactivation by PMSF, concentrated sodium hydroxide was added to disassemble PrP^{Sc} aggregates into monomers (Peretz, Scott et al. 2001), followed by phosphate buffer for pH neutralization. Residual PrP was detected by a mixture of two monoclonal antibodies (Polymenidou, Moos et al. 2008, Sonati, Reimann et al. 2013) directed against two non-overlapping epitopes of PrP and labeled Europium (Eu^{3+}) and allophycocyanin (APC), respectively. By bridging the two antibodies, any PrP present in the sample enabled concentration-dependent FRET, thereby providing homogeneous-phase readout with extremely little background, a broad linear dynamic range, and sufficient sensitivity. I found that complete disassembly of PrP^{Sc} aggregates into monomers was crucial for obtaining an optimal FRET signal. We therefore titrated the NaOH concentration necessary to disassemble the PrP^{Sc} aggregate after PK digestion (**Figure 5.2b**). A concentration of 42 mM NaOH was found to increase the PrP^{Sc} FRET signal to a plateau, whereas higher concentrations did not improve the signal. Since 57 mM of NaOH resulted in a highest and least variable signal, it was defined as a standard concentration for following experiments.

To apply the PrP^{Sc}-HPFRET to the assessment of PrP^{Sc} level in mouse samples, I tested various antibodies from the POM library developed in-house (Polymenidou, Moos et al. 2008). Antibody pairs were scored according to the Z' factor and the signal-to-noise (S/N) ratio of the assay, and were considered acceptable if the Z' factor was ≥0.5 (with 1 being the maximum) and the S/N ratio was ≥5. Several antibody pairs were found to satisfy these requirements (**Figure 5.2c**). I used the FRET antibody pair Eu^{2+}-POM19 and APC-POM1 to further validate the fast and robust readout of the PrP^{Sc}-HPFRET. In CD1 mice brains which were infected with the Rocky Mountain Laboratory (RML) (Mahal, Baker et al. 2007) prion strain, PrP^{Sc} signal was still detectable (****p < 0.0001) when the RML6 BH was 6,400 times diluted in 1% *Prnp*$^{-/-}$ mouse (**Figure 5.2d**). I also found a good FRET antibody pair Eu^{2+}-3F4 and APC-POM1 to detect PrP^{Sc} in 263K prion-infected hamster brain homogenates (BH,

Figure 5.2e). This antibody pair recognizes epitopes, which are conserved between mouse and human PrP (Polymenidou, Moos et al. 2008, Polymenidou, Prokop et al. 2011), and can therefore potentially be used for the detection of human PrP^{Sc} by HPFRET.

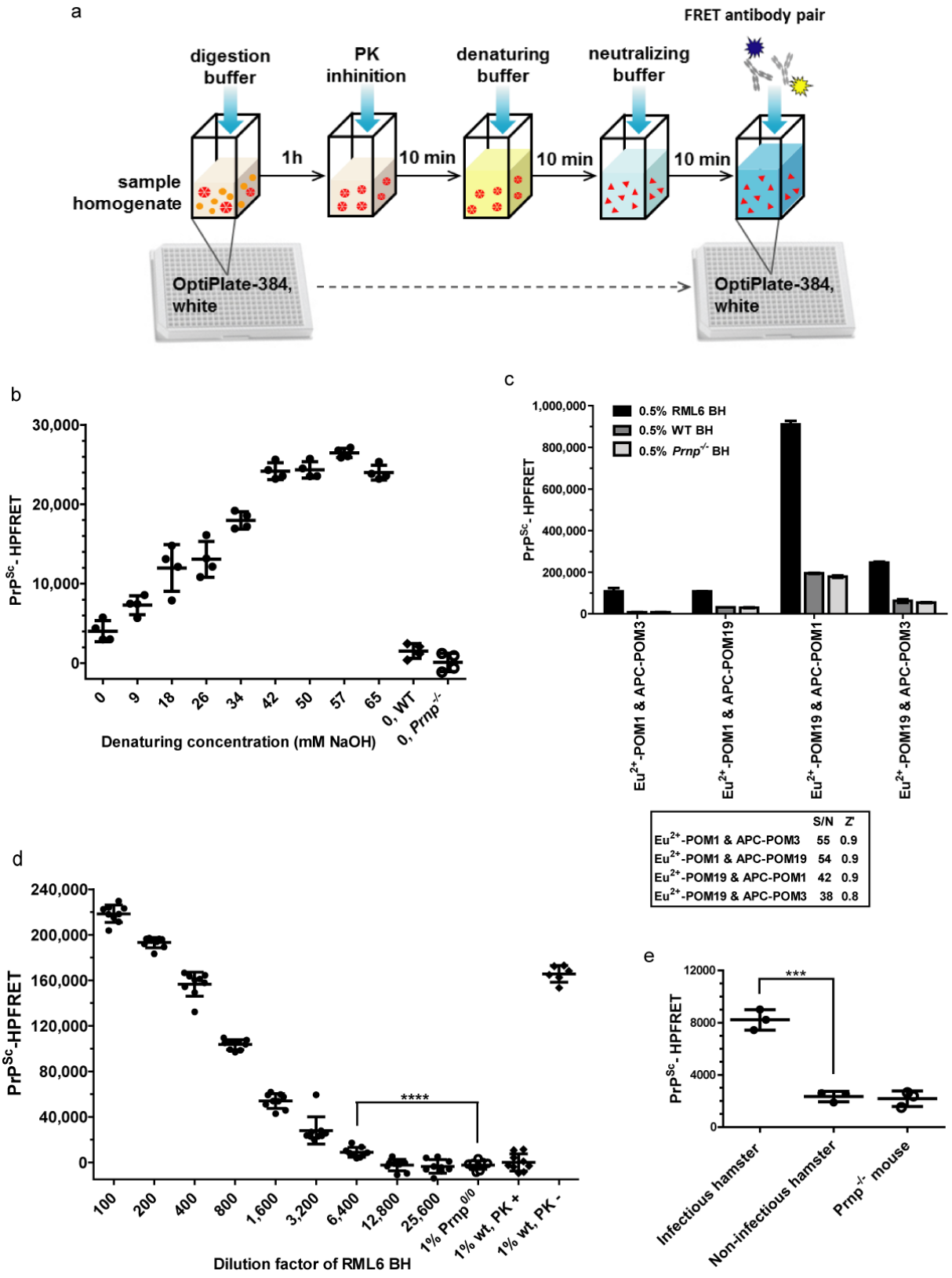

Figure 5.2 Establishment of PrP^{Sc}-HPFRET. (a) Scheme of the PrP^{Sc}-HPFRET assay. Samples are treated with PK digestion, denatured, and neutralized. Then PK-resistant PrP^{Sc} is determined by FRET using a donor-acceptor pair of antibodies to distinct PrP epitopes. **(b)** Titration of the NaOH concentration to disassemble PrP^{Sc} aggregates. The sample was 0.5% RML6 BH. Negative controls were 0.5% NBH and 0.5% *Prnp*$^{-/-}$ BH without denaturation. 57 mM NaOH was sufficient to increase the PrP^{Sc}-HPFRET signal to a plateau. **(c)** The samples were 0.5% RML6 BH, 0.5% NBH and 0.5% *Prnp*$^{-/-}$ BH. All the antibody pairs had a good Z' factor>0.5 and a high S/N>5. The FRET pair Eu^{2+}-POM19 and APC-POM1 had the highest PrP^{Sc}-HPFRET signal. **(d)** PrP^{Sc} titration in prion infected mouse BH. 1% RML6 BH was 1:1 serially diluted with 1% *Prnp*$^{-/-}$ BH. The FRET antibody pair was Eu^{2+}-POM19and APC-POM1. When the RML6 BH was diluted 6,400 times, the PrP^{Sc} signal was still detectable (****P<0.0001). **(e)** Samples were 0.5% BH from the 263K prion-infected hamster, 0.5% NBH from normal hamster and 0.5% BH from *Prnp*$^{-/-}$ mouse. The FRET antibody pair was Eu^{2+}-3F4 and APC-POM1. The PrP^{Sc} in hamster BH was significantly detectable (***P<0.001).

To further validate the robust and high-throughput readout of PrP^{Sc}-HPFRET, I used the assay to detect PrP^{Sc} in various C57BL/6 mouse brain regions (hippocampus, frontal brain, cerebellum, cortex/midbrain and olfactory bulb) at 8 different time points of the prion incubation period (**Figure 5.3a-e**). The PrP^{Sc}-HPFRET results indicate that PrP^{Sc} were first detectable from 82~96 dpi at various brain regions and PrP^{Sc} levels were constantly increased to the end point of the incubation period. Hippocampus has the highest PrP^{Sc} level at the terminal stage (**Figure 5.3f**). In general, the HPFRET assays were found to be acceptably rapid, scalable, and sensitive. The new assays require minimal manipulation of samples and do not involve any washing, liquid-replacement, and centrifugation steps. In addition, it enables HTS-compatible detection of prion proteins and compliance with best biosafety practices.

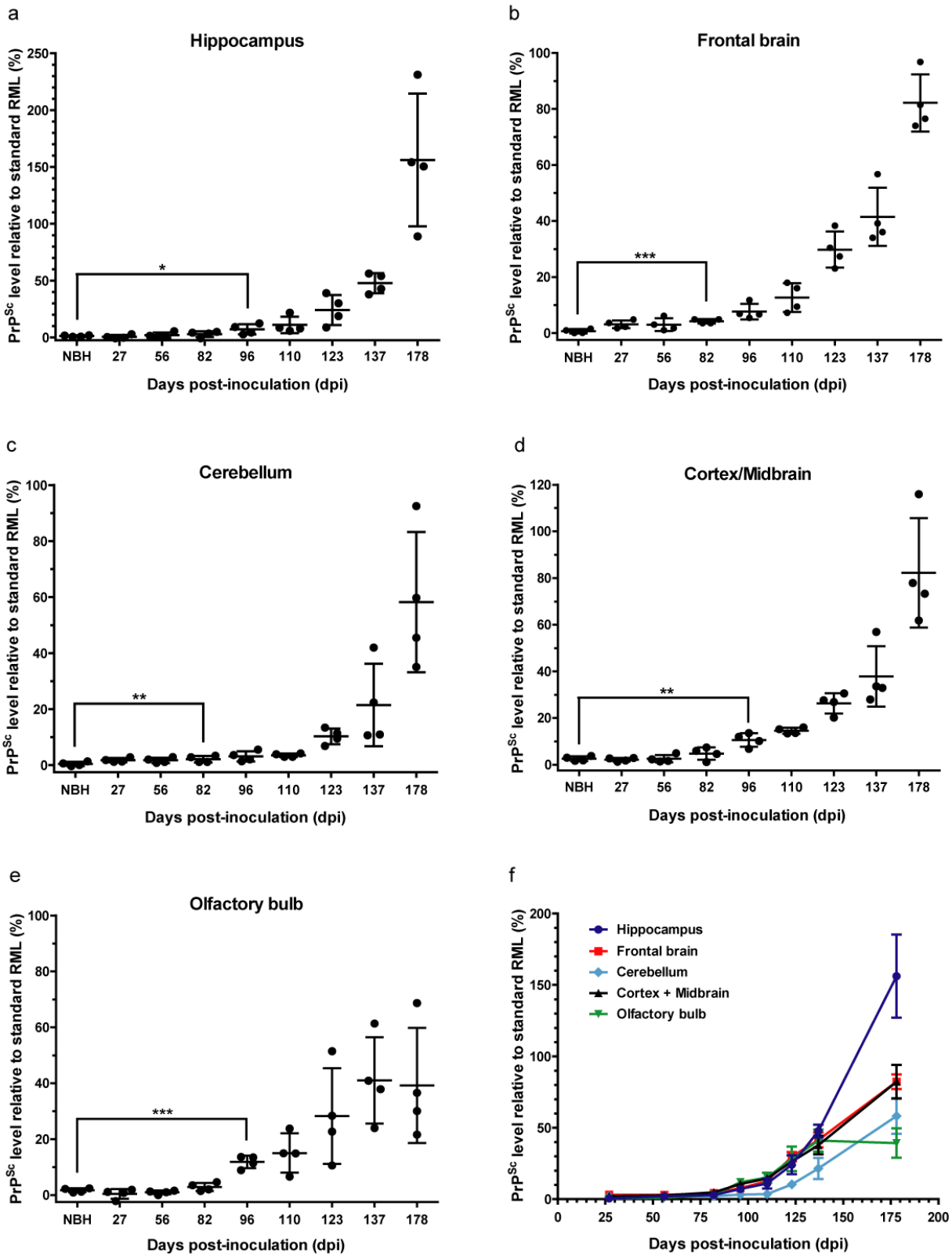

Figure 5.3 Validation of PrP^{Sc}-HPFRET for automated high-throughput measurements. The samples were 0.5% tissue: **(a)** hippocampus, **(b)** cerebellum, **(c)** frontal brain, **(d)** cortex/midbrain and **(e)** olfactory bulb. Homogenates were prepared from the RML6 BH inoculated C57BL/6 mice. Negative controls were 0.5% NBH prepared from non-infectious CD1 BH inoculated C57BL/6 mice.

Four mice per time point. Serial dilutions of standard RML6 BH were included in each assay plate as a standard curve. Technical triplicates were done for each sample. The FRET antibody pair was Eu^{2+}-19 and APC-POM1. FRET signals of samples were normalized to standard RML6 BH. PrP^{Sc} was first detectable from 82~96 dpi at various brain regions (*P<0.05, **P<0.01, ***P<0.001) and constantly increased to the end point of incubation period.

5.4 Establishment of digital prion infectivity cell assay (DPICA)

5.4.1 Overview of DPICA scheme

To apply the PrP^{Sc}-HPFRET, I established a cell-based homogeneous-phase bioassay for prion infectivity titration, which was designated the "Digital Prion Infectivity Cell Assay" (DPICA). When prion-containing test samples were subjected to limiting dilutions, the infection of individual wells containing susceptible cells was assumed to follow a Poisson distribution with each well assuming one of two binary states (infected vs non-infected, hence digital). We reasoned that the PrP^{Sc}-HPFRET could be optimally exploited for the binary assignment of parallel wells to either state in a high-throughput manner (**Figure 5.4**).

First, a small number of prion-susceptible cells (typically 100 cells/well) were seeded in 384-well microtiter plates, and exposed to limiting dilutions of prion-infected samples. Then, cells were cultured for 10 days (until cells reached confluence) to allow for prion replication without medium changes. Finally, cells were lysed directly in culture medium, and PrP^{Sc} was measured by PrP^{Sc}-HPFRET. In order to reliably extract prion infectivity measurements from potentially noisy raw signals, a numerical method ("Global Threshold Fitter") was developed to iteratively apply a sliding series of thresholds to the global dataset until the solution converged onto the best estimate of infected vs non-infected wells.

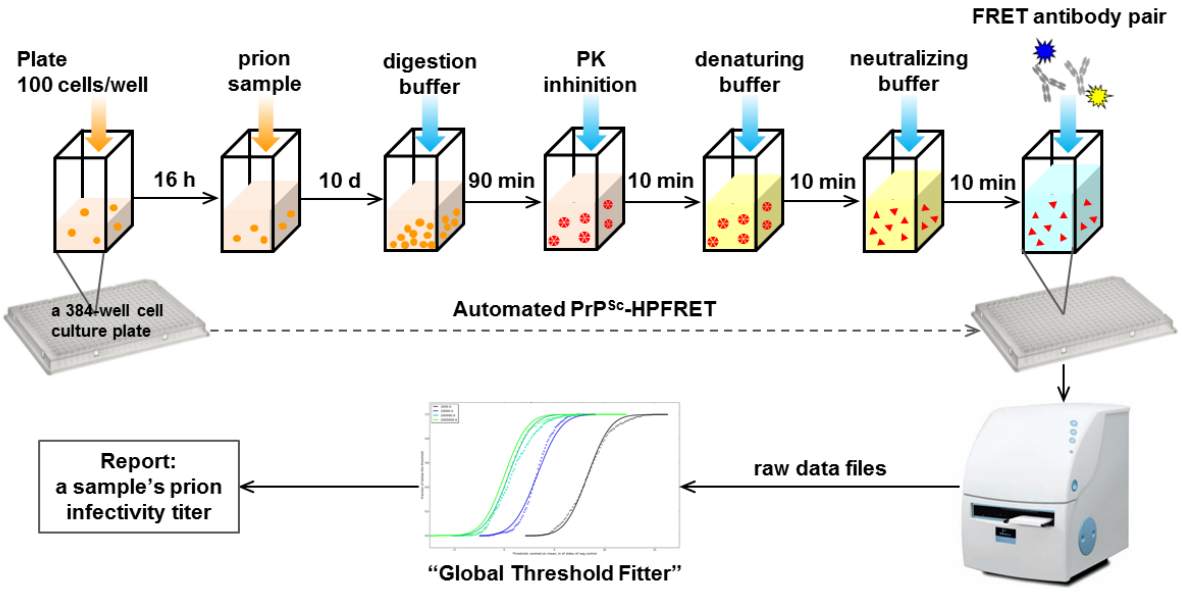

Figure 5.4 Scheme of DPICA. The whole procedure of DPICA takes about 11 days. The prion susceptible cells are seeded in 384-well plates and exposed to a highly diluted prion sample. The

post-infected cells are cultured for about 10 days for prion replication without medium change until the cells reach confluence. Then, the PrP^{Sc}-HPFRET is performed: cells are lyzed directly in culture medium; PrP^{C} proteins are digested by PK; PK-resistant PrP^{Sc} aggregates are denaturated to monomers; pH is adjusted by neutralization for FRET; FRET antibody pair is added; the PrP^{Sc} level in each well is measured by the Envision reader and raw data files are reported. Finally, raw signal files are analysed by the "Global Threshold Fitter" and the prion infectivity titer of sample is calculated automatically.

5.4.2 Numerical treatment of DPICA data

For DPICA data analysis, we verify the thresholds over the entire data range and thereby obtain traces of the fraction of points below the threshold, with varying threshold. Then, we globally fit the fraction below the threshold to equations (1) at all thresholds and concentrations.

$$f_{below} = \sum_{i=0}^{\infty} P(i)Q(T,i) \quad (1)$$

P(i) in equations (1) is the probability mass function of the Poisson distribution. The number of prions in a given volume, for a fixed concentration, follows the Poisson distribution:

$$P(i) = \frac{\lambda^i e^{-\lambda}}{i!} \quad (2)$$

where "i" is the number of propagons and "λ" is the average number of propagons per unit of experimental volume, which can therefore be related to concentration by λ = c • V, where "V" is the volume of the sample and "c" is the concentration of propagons related to the initial propagon concentration c_0 by the dilution D as $c = c_0/D$. Therefore determining "λ" will allow determination of the initial concentration of propagons.

Q(T, i) in equations (1) is the probability of below threshold "T", given that it has """" propagons. We define the probability distribution of signal intensity as S(y, i) (i.e. S(y, i) is the probability to obtain a signal of intensity "y", given that there are "i" propagons in the sample). By integrating this distribution to a threshold "T", we obtained the probability to yield a signal below the threshold for a given number of propagon "i", which is Q(T, i). We assume the intrinsic spread in signal intensity, $S(y, i)$, is still Gaussian in "y", with the same standard deviation as the negative control and a mean, μ(i), which depends on the number of propagons i. Then Q(T; i) is given by the integral:

$$Q(T,i) = \int_{-\infty}^{T} S(y,i)dy = \int_{-\infty}^{T} \frac{1}{\sigma_{nc}\sqrt{2\pi}} e^{-\frac{(y-\mu_{nc})^2}{2\sigma_{nc}^2}} dy = \frac{1}{2}\,\mathrm{erfc}\left(\frac{\mu(i)-T}{\sqrt{2}\sigma_{nc}}\right) \quad (3)$$

where "erfc(x)" is the complementary error function of "x".

Based on the statistical model described above, we used the Python programming language to develop the "Global Threshold Fitter" software, by which the standard deviation σ_{nc} and

mean μ_{nc} of the negative control can be determined from experiments and the "λ" of the sample is calculated by the "Global Threshold Fitter" software automatically.

5.4.3 Automation of DPICA

We opted for a plate layout containing 352 experimental wells (288 wells/diluted sample, 64 wells/negative control), 32 control wells. On a Perkin-Elmer Janus liquid handling platform, the procedure for plating out cells into 384-well plates and overlaying them with prion-containing samples was found to average around 10 minutes/plate. Under typical production conditions, this translated to a throughput of 55,296 wells/24 hours. Since the optimal cell culture period was 10 days, sustained throughput required an automated cell-culture incubator interfaced with the liquid handling equipment and capable of hosting 144 384-well microplates. Finally, the readout sequence (including cell lysis, proteolysis of PrP^{C}, disaggregation of PrP^{Sc}, and detection of residual PrP by FRET) had a maximal throughput of 15360 wells/24 hours. Considering that the prion titration of each sample required 352 experimental wells and 32 control wells, amounting to 40 384-well microplates, the system allowed for precise infectivity determination of 20-40 samples/day.

5.4.4 Validation of DPICA

To assess the sensitivity of the DPICA, I prepared five samples (S1 to S5) by ten-fold serial dilutions (10^{-3} to 10^{-7}) of the standard prion strain RML6 derived from CD1 mouse. The prion-susceptible mouse neuronal cells CAD5 (Mahal, Baker et al. 2007) were seeded in 384-well plates and exposed to the five samples. Cells were cultured for 10 days, and PrP^{Sc}-HPFRET was performed using the antibody conjugate pair Eu^{2+}-POM19 and APC-POM1. The global threshold fitting of plates (S1 to S5, S2 to S5) was analysed (**Figure 5.5a**), then each sample was analyzed separately (**Figure 5.5b**). The results demonstrated that there were about 55 propagons/well in S1 plate, 16 propagons/well in S2 plate, 1.1 propagons/well in S3 plate, 0.5 propagons/well in S4 plate and 0.01 propagons/well in S5 plate (**Table 5.1**). Since the limit of detection (LOD) of the PrP^{Sc}-HPFRET is around 10^{-4} dilution of RML6 BH (**Figure 5.2d**), a positive signal reported by the DPICA from high dilutions (10^{4} to 10^{7}) represented bona fide prion replication by the recipient CAD5 cells, which followed the linear dilution series. The sample S5 (10^{-7} dilution of RML6 BH) approached the LOD of DPICA in 384-well format, corresponding to about 3 propagons/plate.

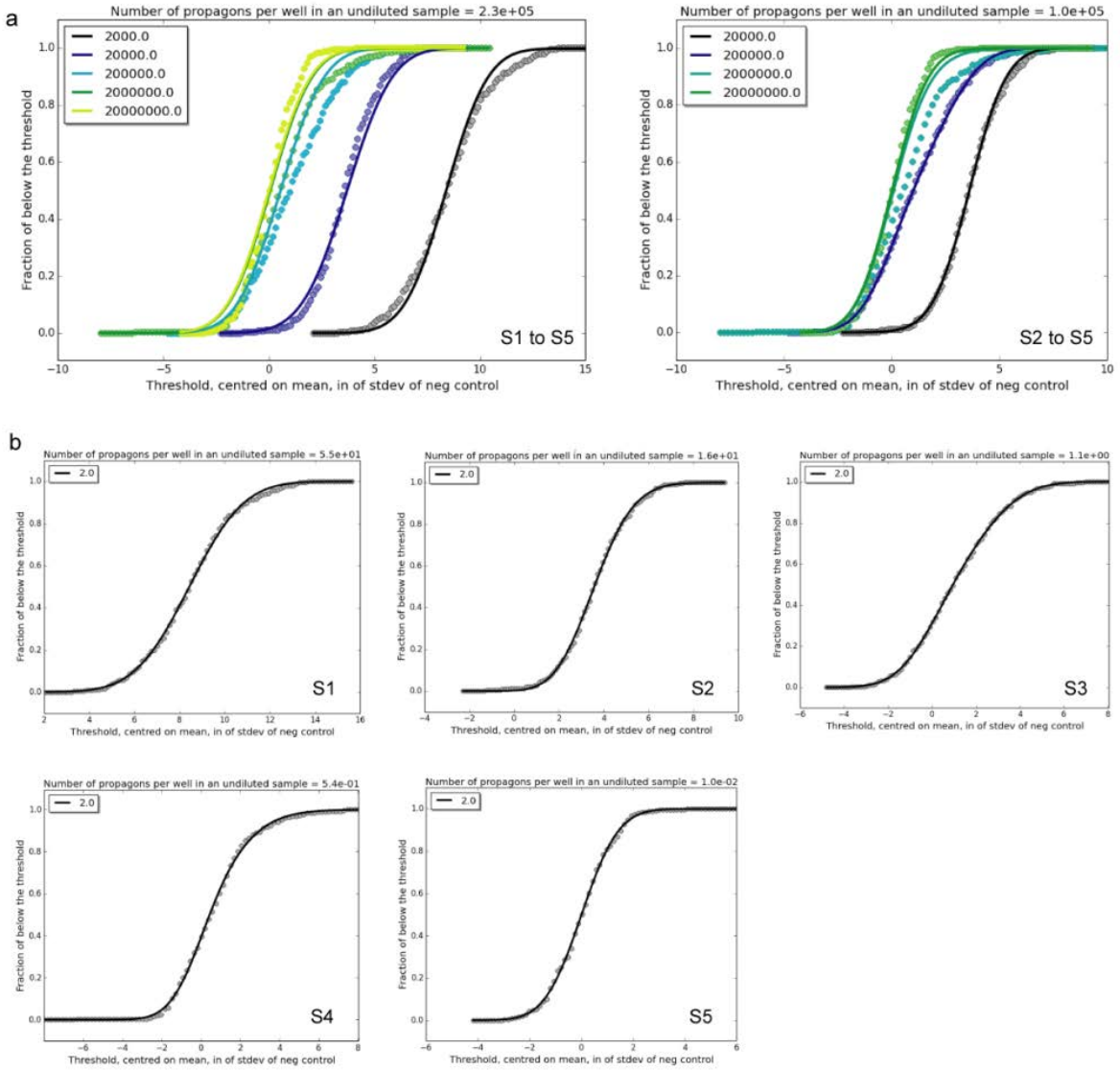

Figure 5.5 Validation of DPICA using standard prion strain RML6. (a) The sensitivity of DPICA was determined by five samples (S1 to S5) prepared from ten-fold serial dilutions (10^{-3} to 10^{-7}) of the standard prion strain RML6 BH. Prion-susceptible mouse neuronal cells CAD5 were seeded in 384-well plates and exposed to the five samples. Cells were cultured for 10 days and PrP^{Sc}-HPFRET was performed using the antibody conjugate pair Eu^{2+}-POM19 and APC-POM1. The global threshold fitting of plates (S1 to S5, S2 to S5) was analyzed. **(b)** Each sample was analyzed separately by the Global Threshold Fitter software and showed that there were about 55 propagons/well in S1 plate, 16 propagons/well in S2 plate, 1.1 propagons/well in S3 plate, 0.5 propagons/well in S4 plate and 0.01 propagons/well in S5 plate.

To further validate the prion titration of RML6 BH, I performed three independent DPICA tests (**Figure 5.6b**) and confirmed that RML6 BH contains about $10^{6.5}$ propagons/g. The prion titration of RML6 BH indicated that there was approximately ≤1 propagon/well in assay plates when RML6 BH was highly diluted to more than 10^{-5}.

To assess the background signal of the DPICA, I performed the DPICA test using non-infectious brain homogenates (NBH). CAD5 cells were seeded in 384-well plates and exposed to 10^4 dilutions of NBH from CD1 mice. Cells were cultured for 10 days, and PrP^{Sc}-HPFRET was performed using the antibody conjugate pair Eu^{2+}-POM19 and APC-POM1. The raw signals were analyzed by the Global Fitter software and showed that there was no propagon in NBH samples (**Figure 5.6f**), indicating that there is essentially no background when testing non-infectious materials by DPICA. Finally, I validated the robustness and versatility of the DPICA titration system using other mouse prion inocula (**Figure 5.6c-e**) (**Table 5.1**): Me7 (Mahal, Baker et al. 2007) BH derived from C57BL/6 mice, RML6-inoculated C57BL/6 mice BH (RML6-C57BL/6) and RML6-inoculated Tga20 mice BH (RML6-Tga20) (Fischer, Rulicke et al. 1996).

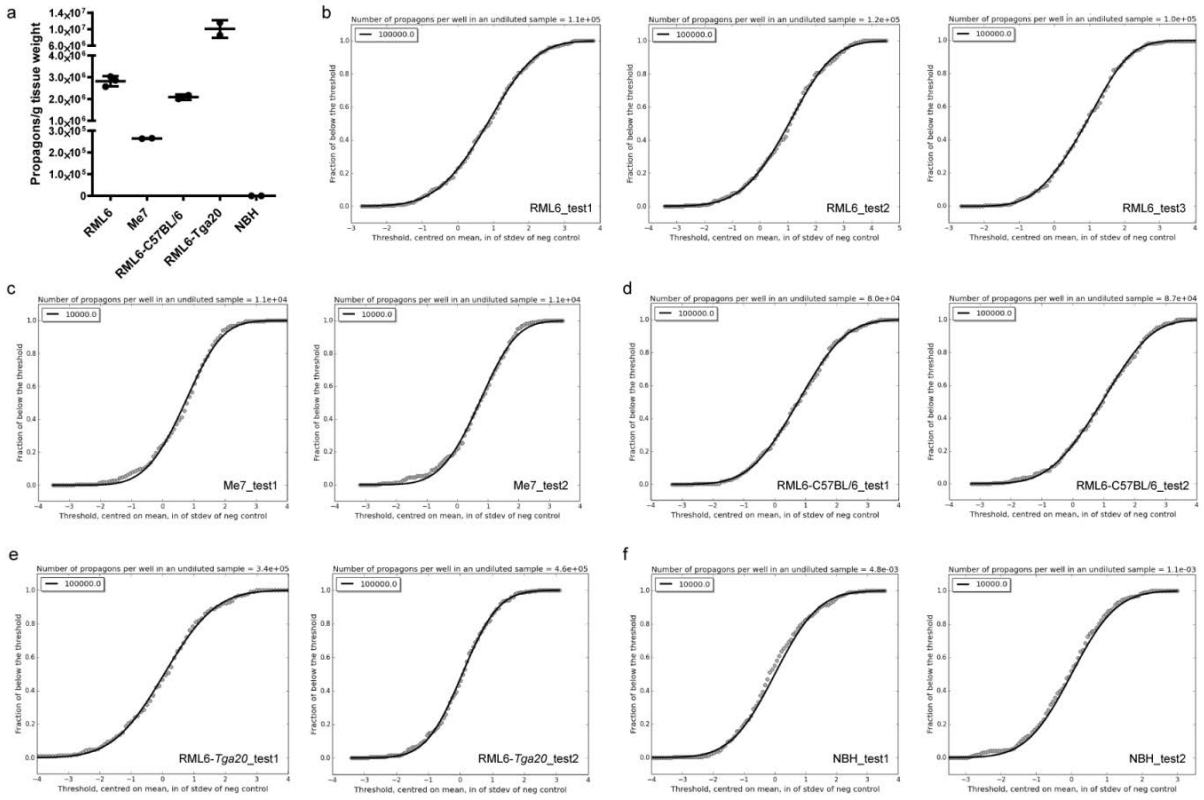

Figure 5.6 Validation of the DPICA using different mouse prion inocula. (a) Prion infectivity was determined in several mouse prion inocula derived from different mouse strain CD1, C57BL/6, Tga20. The cell line was mouse prion susceptible neuronal cell CAD5. The FRET antibody pair was Eu^{2+}-POM19 and APC-POM1. **(b)** The prion inoculum was RML6 BH and the negative control was NBH from non-infectious CD1 mice. The infectivity titer of RML6 BH was determined as $10^{6.5}$ propagons/g. **(c)** Prion inoculum was Me7 BH and the negative control was NBH from non-infected C57BL/6 mice. The infectivity titer of Me7 BH was determined as $10^{5.4}$ propagons/g. **(d)** The prion inoculum was RML6-C57BL/6 BH and the negative control was BH from non-infected C57BL/6 mice. The infectivity titer of RML6-C57BL/6 BH was determined as $10^{6.3}$ propagons/g. **(e)** The prion inoculum was RML6-

Tga20 BH and the negative control was BH from non-infected Tga20 mice. The infectivity titer of RML6-Tga20 BH was determined as $10^{7.0}$ propagons/g. **(f)** Sample was NBH from non-infectious CD1 mouse. The result showed that there was no propagon in this non-infectious sample.

Table 5.1 Validation of the DPICA with mouse prion inoculum

Sample	Global Threshold Fitter (Figure 5.5) undiluted propagons/well	medium ml/well	C_0 (propagons/ml)	Propagons/ml sample	Log propagons/ml sample	Predicted value of Log propagons/ml sample from results of Fig. 4b
S1 (10^{-3} RML6)	55	0.04	1'381	2.48E+03	3.14	3.45
S2 (10^{-4} RML6)	16	0.04	403	4.03E+02	2.61	2.45
S3 (10^{-5} RML6)	1.1	0.04	27	2.65E+01	1.42	1.45
S4 (10^{-6} RML6)	0.5	0.04	13	1.34E+01	1.13	0.45
S5 (10^{-7} RML6)	0.01	0.04	0.3	2.55E-01	-0.59	-0.55
Sample	Global Threshold Fitter (Figure 5.6) undiluted propagons/well	medium ml/well	C_0 (propagons/ml)	Propagons/g tissue weight	Log propagons/g tissue weight	CV%
RML6_test1	1.14E+05	0.04	2'855'154	2'855'154	6.46	8
RML6_test2	1.21E+05	0.04	3'031'091	3'031'091	6.48	
RML6_test3	1.03E+05	0.04	2'569'239	2'569'239	6.41	
Me7_test1	1.05E+04	0.04	263'048	263'048	5.42	1
Me7_test2	1.06E+04	0.04	265'067	265'067	5.42	
RML6-C57BL/6_test1	7.99E+04	0.04	1'998'635	1'998'635	6.30	6
RML6-C57BL/6_test2	8.69E+04	0.04	2'173'734	2'173'734	6.34	
RML6-Tga20_test1	3.41E+05	0.04	8'530'082	8'530'082	6.93	21
RML6-Tga20_test2	4.62E+05	0.04	11'562'264	11'562'264	7.06	
NBH_test1	0	0.04	0	0	Not Detectable	
NBH_test2	0	0.04	0	0	Not Detectable	

5.4.5 Comparison of the DPICA, SCEPA and mouse bioassay

I compared the DPICA to the traditional mouse bioassay and SCEPA. RML6 BH was serially diluted and 30µl aliquots of each dilution were intracerebrally (i.c.) infected into each group of

CD1 mice. Using the Reed-Muench formula (Reed J 1938), the infectivity of RML6 BH was calculated as $10^{9.6}$ LD_{50} units/g. The SCEPA (Klohn, Stoltze et al. 2003) was performed in 96-well plates for RML6 BH. Using the Reed-Muench formula (Reed J 1938), the infectivity of RML6 BH was found to be $10^{6.8}$ $TCID_{50}$ units/g. The DPICA was performed in 384-well plates for RML6 BH. Using the Global Threshold Fitter algorithm, the infectivity of RML6 BH was detected to be $10^{6.5}$ propagons/g. The novelty of DPICA as a method to determine the absolute number of propagons in samples is based on a completely new model, delivering high sensitivity, while enabling sufficient throughput for large-scale HTS applications (**Table 5.2**).

Table 5.2 Comparison of the DPICA, SCEPA and mouse bioassay

	DPICA	SCEPA	Animal
Materials	Prion susceptible cells	Prion susceptible cells	About 50 mice/sample
Format	In 384-well plates. 288 wells/dilution. one dilution.	In 96-well plates. 12-24 wells/dilution. Serial dilutions from 100% to 0% infected.	6 mice/dilution. Serial dilutions from 100% to 0% infected.
Signal readout	PrP^{Sc}-HPFRET	ELISPOT-ELISA	Clinical symptom
Numerical treatment	«Global Threshold Fitter» algorithm	Median infectivity dose (ID_{50}) model. Calculation: Reed-Muench formula	Median infectivity dose (ID_{50}) model. Calculation: Reed-Muench formula
Time cost	11 days	2-3 weeks	Several months
Labor intensitity	Fully automated system.	Intensive labor for splitting cells and ELISPOT-ELISA.	Moderate labor for mouse injection and frequently checking.
Automation	Full	Half	No
High throughput	Yes (20-40 plates/day)	No (1-4 plates/day)	No
Prion titration report* (Log_{10} ± SD)	Log propagons/g tissue weight RML6: 6.45 ± 0.04	Log $TCID_{50}$/g tissue weight RML6: 6.89 ± 0.52	Log LD_{50}/g tissue weight RML6: 9.62 ± 0.28

5.4.6 Application of DPICA to assessment of prion decontamination

The characterization of prion toxicity and replication may greatly profit from proteomics studies. However, it is difficult to justify the contamination of expensive mass spectrometers with prions. We therefore applied the DPICA to measuring prion removal during the pre-analytical steps preceding mass spectrometry. Samples consisted of prion pellet aliquots

prepared from terminally sick, RML6-Tga20 mice BH. Before decontamination, prion infectivity in samples was ca. $10^{5.8}$ propagons/sample as determined by DPICA (**Figure 5.7a**). We chose to assess four prion decontamination methods relying on distinct physical principles: chaotropic salt guanidinium hydrochloride (GdnHCl) with different detergents, nanofiltration, exposure to sodium hydroxide (NaOH), and exposure to concentrated formic acid (FA) (**Figure 5.7a-b**). After chemical treatment (6M GdnHCl, 1M NaOH, or 100% FA), samples were dialyzed against sterile PBS, and prion infectivity was determined by DPICA.

CAD5 cells were seeded in 384-well plates and exposed to 1:40 or 1:60 dilution of a treated sample. Cells were cultured for 10 days, and PrP^{Sc}-HPFRET was performed using the antibody conjugate pair Eu^{2+}-POM19 and APC-POM1. The raw signals were analyzed with the Global Threshold Fitter. We found that each of the three decontamination methods (1M NaOH and 100% FA, nanofiltration) reduced prion infectivity below detectability. Because the input infectivity was $10^{5.8}$ propagons, we conclude that each of the procedures yielded a reduction of >5 log. The decontamination method of 6M GdnHCl with 1% b-octylglucoside yielded a reduction of >3 log. Since the physical principles underlying each method of decontamination do not overlap, these data demonstrate a nominal total titer reduction of >18 log.

To understand the effect of GdnHCl and pH properties on the reduction of prion infectivity, we applied the DPICA to measure prion removal of samples treated with different GdnHCl concentrations and pH values. The detergent we used was 1% b-octylglucoside, which showed the best results in **Figure 5.7a**. The samples were aliquots from terminally sick, RML6-Tga20 mice BH, containing ca. $10^{5.3}$ propagons/sample. After treatment of GdnHCl (from 0 to 5 M) at different pH (from 2.5 to 12), samples were dialyzed against sterile PBS, and prion infectivity was determined by DPICA. These results demonstrated that treatments of 5M GdnHCl and pH≤7.5 reduced prion infectivity below detectability, and the higher GdnHCl and the lower pH are more efficient to remove prions (**Figure 5.7c**).

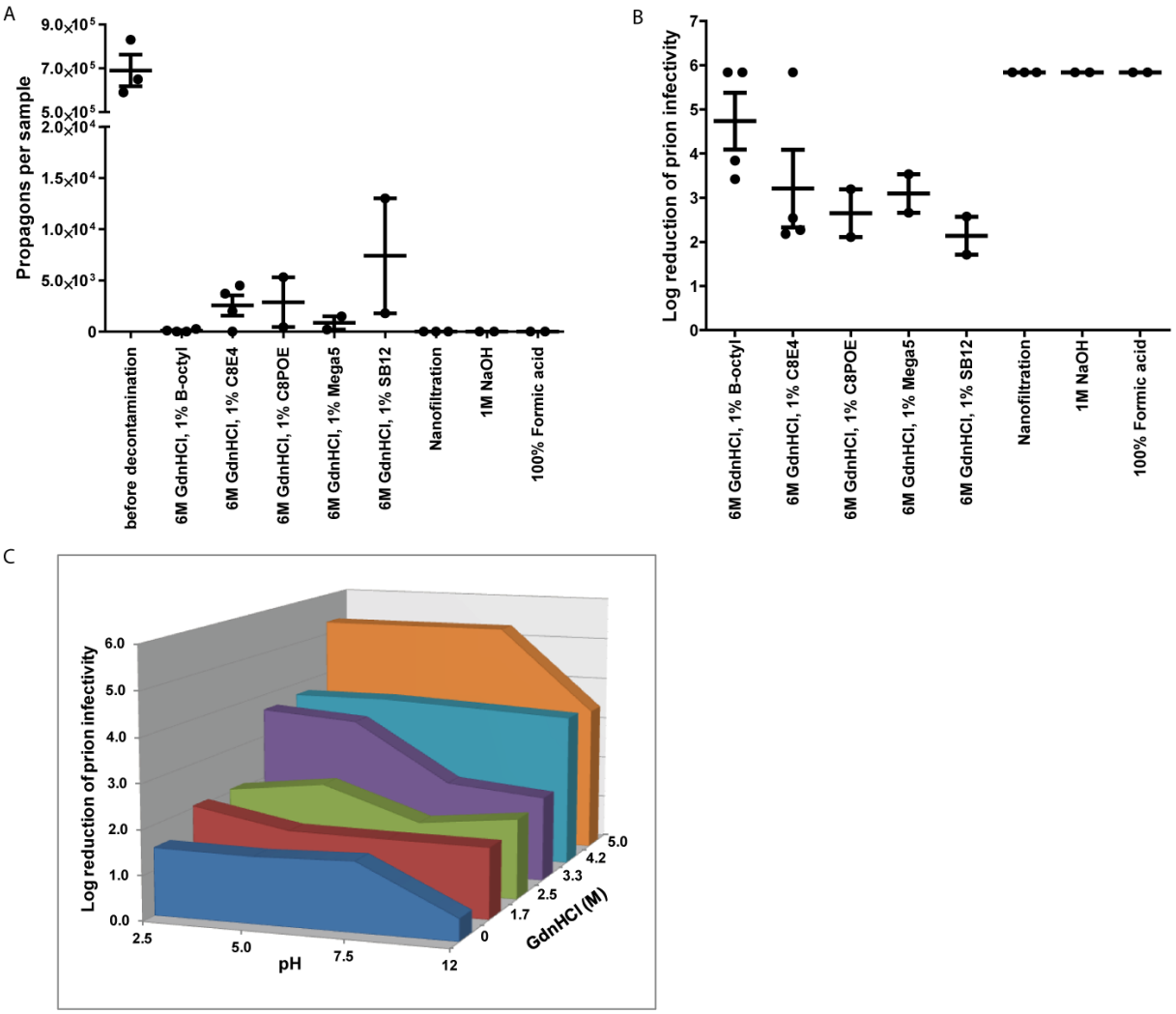

Figure 5.7 Application of DPICA to assessment of prion decontamination. (a-b) The infectivity titer of prion pellet sample aliquots before decontamination treatment was $10^{5.8}$ propagons/sample. After each treatment of 1M NaOH, 100% formic acid and Nanofiltration, the prion infectivity reduced below detectability, delivering a reduction of over 5 Log. The treatment of 6M GdnHCl with 1% b-octyl glucoside detergent yielded a reduction of over 3 Log. The treatment of 6M GdnHCl with other detergents roughly yielded a reduction of over 2 Log. **(c)** Determination of prion removal in GdnHCl (from 0 to 5 M) and pH (from 2.5 to 12) treated samples. The infectivity titer of RML6-*Tga20* BH sample aliquots before treatment was $10^{5.3}$ propagons/sample. After treatments of 5M GdnHCl and pH≤7.5, the prion infectivity reduced below detectability, delivering a reduction of over 5 Log. The higher GdnHCl and the lower pH were more efficient in reducing prion infectivity.

5.4.7 Application of DPICA to assessment of prion infectivity in various mouse brain regions

I applied the automated DPICA to measure prion infectivity in various brain regions (hippocampus, frontal brain, cerebellum, cortex/midbrain and olfactory bulb). C57BL/6 mice were i.c. inoculated with RML6 BH (30 µl of 0.1% BH containing 105 LD50 units) and

samples were collected at 8 time points: 27, 56, 82, 96, 123, 137 and 178 days post inoculation (dpi). At each time point, four mice were sacrificed and tissue samples from various brain regions were harvested. As a negative control group, four C57BL/6 mice were i.c. inoculated with uninfected 0.1% CD1 mouse BH. The prion titres in these brain regions were determined by the automated DPICA system (**Figure 5.8**). The DPICA results showed that different kinetics of prion propagation occurring in different brain regions. The prion titres at various regions reached a plateau at different time points: hippocampus (56 dpi) → cerebellum (82 dpi), frontal brain (82 dpi) → olfactory bulb (110 dpi) → cortex/midbrain (rises to terminal). The kinetics of prion infectivity propagation generally follows a sigmoid curve.

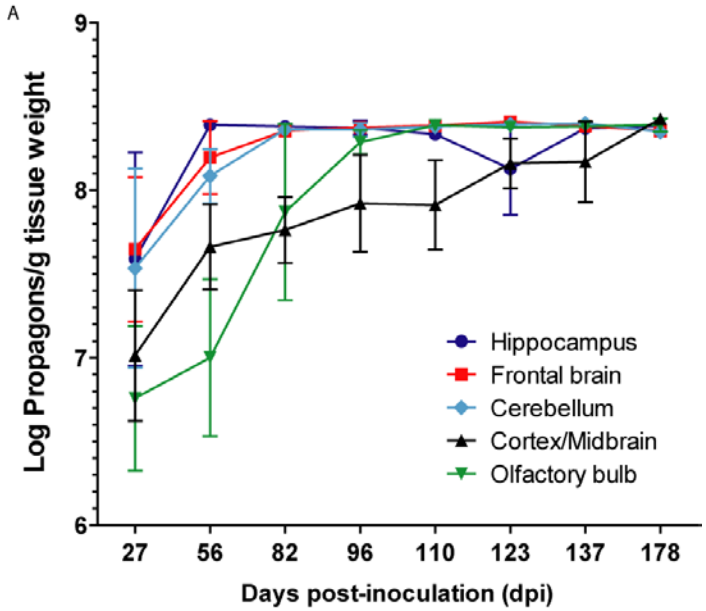

Figure 5.8 Application of DPICA to assessment of prion infectivity in various mouse brain regions. The prion infectivity was measured in mouse brain TH of cortex/midbrain, cerebellum, frontal brain, hippocampus and olfactory bulb. Different brain regions showed different kinetics of prion propagation.

5.5 Discussion

Infectivity is the best-characterized biological property of prions. Instead, the basic physical properties of the prion, such as the exact number and atomic structure of PrP monomers included in one prion, are largely unknown. A precise, massively parallel method for prion infectivity determination would be instrumental in addressing many questions regarding basic prion science, diagnostic aspects as well as drug discovery against prion diseases.

The Digital Prion Infectivity Cell Assay (DPICA), which is based on a homogeneous-phase FRET assay for prion proteins (PrP^{Sc}-HPFRET), offers far-reaching advantages over existing prion infectivity bioassays. In contrast to SCEPA, the DPICA does not require cell splitting and washing steps. All cell culture and subsequent reactions are carried out sequentially in

the same microwell, thus creating ideal preconditions for automation with simple liquid handling equipment.

The high-density microplate format allows for dilutions of each sample to be tested in 288 wells independently, whereas the mouse bioassay typically uses only 5-6 mice per dilution. Even SCEPA can only yield 12-24 wells per dilution. The larger number of measurements leads to vastly increased robustness of results. Moreover, the use of high-density microplates has allowed us to measure infectivity in extremely small samples.

The "digital" properties of the DPICA originate from the property that each well can theoretically assume only one of two binary states, either infected or uninfected. In reality, however, acquisition of prion infectivity by a well containing several hundred cells is a gradual process, which can make it difficult to define a threshold for assigning a specific state to individual wells. This issue has been addressed by developing the "Global Threshold Fitter" statistical method. Rather than attempting to assign binary values to individual wells, the Global Threshold Fitter takes into account the entire collection of wells and combines the Poisson statistical basis (Rissin and Walt 2006, Rissin, Kan et al. 2010) with analyses of bioassay signals and modeling of the reaction system (Klohn, Stoltze et al. 2003, Knowles, Waudby et al. 2009). Thus, DPICA is able to determine the prion titer with a much higher precision than the mouse bioassay and the SCEPA, which are based on the traditional median infectivity dose model (Reed J 1938, Dougherty 1964).

5.6 Outlook

For future prion studies, which requires the titration of a large number of samples and cannot be analysed by the mouse bioassay or SCEPA, I anticipate that the automated DPICA will provide a powerful platform for basic and applied prion research, including e.g. high-throughput screens for the identification of chemicals interfering with prion secretion, infection, and/or replication (Karapetyan, Sferrazza et al. 2013), and genome-wide siRNA or CRISPR/Cas9 screens aimed at understanding the mechanisms of prion transmissibility and replication.

5.7 Material and Methods

5.7.1 PrP^C-HPFRET

Europium (Eu^{3+}) donor and allophycocyanin (APC) acceptor fluorophores were coupled to anti-PrP holoantibodies POM1 and POM2 recognizing the globular domain and the octarepeats, respectively. The donor Eu^{2+}-POM2 conjugate is excited at wavelength 340 nm and transfers energy to the acceptor conjugate APC-POM1 when the distance between acceptor and donor is <10 nm. POM1-APC then emits light at wavelength 665 nm, which can

be measured with a suitable time-resolving fluorescence. To detect PrP^C level in homogenates, samples were lysed in 1x standard lysis buffer (50 mM Tris-HCl pH 8, 150 mM NaCl, 0.5% Na deoxycholate, and 0.5% Triton X-100, stored at room temperature (RT)). The Eu^{2+}-POM2 and APC-POM1 antibody pair was added, FRET plate was sealed and shaking at 37°C for 1 h at 300 rpm. FRET signal of PrP^C was detected by EnVision Multilabel Reader.

5.7.2 PrP^{Sc}-HPFRET

A homogeneous-phase Förster/fluorescence resonance energy transfer (FRET) assay was established for the measurement of PrP^{Sc} in tissue homogenates. Organ tissues were homogenized in 0.32 M sucrose (or PBS) to 10% (w/v, 100 mg of tissue per 900 µl homogenization buffer) and stored at -80°C. Chemicals for buffers were purchased from Sigma-Aldrich.

PrP^{Sc}-HPFRET was performed in a 384-well FRET plate (white OptiPlate™-384 plates, PerkinElmer) with the following steps: 1) homogeneous sample was diluted with 1x standard lysis buffer (50 mM Tris-HCl pH 8, 150 mM NaCl, 0.5% Na deoxycholate, and 0.5% Triton X-100, stored at room temperature (RT)). 2) Digestion of PrP^C: proteinase K (PK) (Roche) was added to the diluted sample, the FRET plate was sealed and shaking at 37°C for 1 hour at 700 rpm. The PK concentration was related to total protein concentration of the diluted sample quantified by bicinchoninic acid assay (BCA). For 0.5 µg/µl total proteins, the final concentration for PK was 1 µg/ml. The total reaction volume was 50 µl/well. 3) Inactivation of PK: 4 µl/well of 30 mM PMSF (stored at -20°C) was added to reach a final concentration of 2.2 mM. The FRET plate was sealed and shaking at RT for 10 min at 700 rpm. 4) Denaturation: to disassemble PK-resistant PrP^{Sc} aggragates to monomers, 7 µl/well of denaturing buffer (sodium hydroxide buffer containing 0.5M NaOH, pH 14.0, stored at RT) was added to reach a final concentration of 57.3 mM. The FRET plate was sealed and shaking at RT for 10 min at 700 rpm. 5) Neutralization: to adjust the pH for FRET, 8 µl/well of neutralizing buffer (phosphate buffer containing 0.5M NaH_2PO_4, pH 4.0, stored at RT) was added to yield a final concentration of 57.9 mM. The FRET plate was sealed and shaking at RT for 10 min at 700 rpm. 6) The FRET antibody pair incubation: Europium donor (Eu, Activated QuickAssay EU-1024 chelate kit was purchased from PELO Biotech) and the allophycocyanin acceptor (APC, AnaTag™ APC labeling kit was purchased from AnaSpec) fluorophores were coupled to anti-PrP holoantibodies(Polymenidou, Moos et al. 2008) POM19 and POM1 recognizing the different domain of mouse PrP^{Sc}, respectively. The Eu^{2+}-POM19 and APC-POM1 stock was diluted with 1x Lance buffer (LANCE® Detection Buffer for FRET,10x stock, diluted with dH_2O for use) to 67.5 nM (concentration of POM antibody). 6 µl/well of 67.5 nM Eu^{2+}-POM19 and APC-POM1 was added separately. The final total volume was 81 µl/well. The FRET plate was sealed and shaking at 37°C for 1 h at 300 rpm. 7)

The FRET signal of PrP^{Sc} was detected by the EnVision Multilabel Reader. Donor Eu^{2+}-POM19 conjugate is excited at wavelength 340 nm and transfers energy to the acceptor conjugate APC-POM1 only when the FRET antibody pair binds to one protein with a distance <10 nm. APC-POM1 then emits light at wavelength 665 nm, measured by a time-resolved FRET reader.

5.7.3 FRET calculation

FRET is the number of APC channel counts that are due specifically to FRET. It is determined by subtracting the APC background and the adjusted europium background from the total counts. The FRET signal of each well is calculated by the following equation:

$$\mathrm{FRET} = (\mathrm{T_a} - \mathrm{Mean\ A_a}) - [(\mathrm{Mean\ E_a} - \mathrm{Mean\ B_a})/(\mathrm{Mean\ E_e} - \mathrm{Mean\ B_e})](\mathrm{T_e} - \mathrm{Mean\ B_e})$$

Here,

T_a: test well signal, from APC channel.

T_e: test well signal, from europium channel.

A_a: APC-POM1 blank, from APC channel (all reagents except Eu^{2+}-POM19)

E_a: Eu^{2+}-POM19 blank, form APC channel (all reagents except APC-POM1)

E_e: Eu^{2+}-POM19 blank, form europium channel (all reagents except APC-POM1)

B_a: buffer blank, form APC channel (all reagents except Eu^{2+}-POM19 and APC-POM1)

B_e: buffer blank, form Europium channel (all reagents except Eu^{2+}-POM19 and APC-POM1)

5.7.4 Preparation of FRET antibody pairs

The monoclonal full length POM antibodies were labelled in house for HPFRET assays. The donor fluorophore was Europium chelate (Eu-W1024 ITC chelate, AD0096, PerkinElmer). Coupling of proteins to Eu chelate occurs at alkaline pH via reaction of lysine residues and free N termini with the aromatic isothiocyanate group of the Europium chelate. To remove compounds interfering with labelling, proteins were dialyzed overnight. POM antibodies were diluted in 1 ml 100 mM sodium carbonate (Na_2CO_3), pH 9-9.3. Dialysis cassettes (Slide-A-Lyzer®, Thermo scientific) were pre-incubated in ddH2O for 2 min and proteins were loaded with a 24G syringe. A dialysis cassette with a cut-off of 10-20 kDa was used for POM antibodies. Dialysis was done under stirring in a volume of 2 L of 100 mM Na_2CO_3 at 4°C overnight. Dialysis buffer was changed after 4-6 h of incubation at 4°C. Proteins and peptides were concentrated by Centricon concentrators (Millipore). Protein concentration was adjusted by the Bradford or BCA to a concentration of about 5 mg/ml. Lyophilized Eu-W1024 ITC chelate (0.1 mg) was stored at - 20°C and immediately before use reconstituted in 100 µl distilled water which gives a concentration of 1.4 mM. A molar excess of 24x of Europium chelate over IgG was added into the protein (peptide) solution on ice and incubated in 100 mM Na_2CO_3 over night at 4°C. Separation of the labelled protein from non-reacted chelate

was performed by size exclusion chromatography (Superdex 200 column, GE Healthcare). Elution from column was done with 50 mM Tris-HCl pH 7.8 + 0.9% sodium chloride. Sample fractions of 500 µl were collected. Superdex column was decontaminated with 10 mM phthalate buffer pH 4.1 containing 0.01% DTPA. Fractions were pooled and concentrated with Micron centrifugal filters (Amicon). Labelling ratio and concentration of labelled proteins were assessed by a Eu standard solution (Perkin Elmer) and Nano drop measurement, respectively. Aliquots of antibodies were stored in liquid nitrogen.

Allophycocyanin (APC, AnaTagTM Labeling Kit 72111, Anaspec) was used as the acceptor fluorophore for conjugation to POM antibodies. Maleimide groups of APC react with sulfhydryl groups on the target antibody to form a covalent bond during conjugation. POM antibodies were concentrated to 2-10 mg/ml in a volume of 100 µl with Centricon concentrators (Millipore). Antibodies were reduced with 20 µl dithiothreithol (DTT) per mL of IgG solution for 30 min without agitation at room temperature. Depending on reaction volume, reduced antibodies were desalted either by spin or gravity columns. Protein concentration was assessed by Nanodrop. For the conjugation reaction, 1.5 mg of activated APC per mg reduced IgG was added to the reduced antibodies solution and incubated for 1 h at room temperature with agitation. By adding DMSO and NEM for 30 min at room temperature, free thiol groups were blocked. To remove free APC molecules from antibody solution, reaction mixture was purified via a protein G sepharose column (Sigma). The column was washed with water and 10 volumes of 20 mM phosphate buffer pH 7 to equilibrate. Samples were added and washed with five volumes 20 mM phosphate buffer pH 7. Flow through was collected. The column was eluted with 0.1 M glycine pH 2.3 and diluted with 1 M TrisHCl pH 8. APC-labelled POM antibodies were characterized with Nanodrop (A280 and A650). Aliquots of antibodies were stored at 4°C and protected from light.

5.7.5 Mouse prion susceptible cell line and prion inoculum

Mouse cell line CAD-2A2D5 (CAD5) cells was derived from Cath.a-differentiated cells (Mahal, Baker et al. 2007). Mouse cell line N2aPK1 (Klohn, Stoltze et al. 2003) was a subclone of neuroblastoma cell line (N2a).

20% RML6 brain homogenate (BH) was from Rocky Mountain Laboratory strain RML (RML; passage #6) infected CD1 mice by intracerebral inoculation (i.c.). 10% Me7 BH was from prion strain Me7-infected C57BL/6 (BL6) mice. 10% RML6-C57BL/6 BH was from RML6-infected C57BL/6 mice. RML-Tg20 BH was from prion strain RML6-infected Tg20 mice.

5.7.6 DPICA protocol

1) Cell culture for DPICA

DPICA plate was 384-well ViewPlate plate (white, Optically Clear Bottom, TissueCulture Treated, Sterile, 384-Well with Lid, PerkinElmer). Cell culture medium (OFBS) was Opti-MEM® I Reduced-Serum Medium (no phenol red) plus 10% FBS (HyClone), 1% GlutaMaxTM (Gibco) and 1% penicillin/streptomycin (Gibco).

On day-1, 20 µl/well of CAD5 cells were plated to a density of around 100 cells/well. 16 hours after cell plating, a homogeneous mouse brain sample was diluted in OFBS medium to the level around 10-4 to 10-5 (w/v). Then, 20 µl/well infectious medium was added to the plates, corresponding to a homogenate with a tissue weight of 0.01 mg/ml and 0.001 mg/ml. The total final volume of culture medium was 40 µl/well. A whole 384-well plate was used for testing one dilution, so each sample required one DPICA plate. The dilution of the negative control (non-infectious sample) in each plate was the same as the sample dilution. Regular controls for reagents in all DPICA plates were the same: control^{+} was RML6 BH of 10-3 dilution and the control^{-} was CD1 BH of 10-3 dilution. After infection, DPICA plates were cultured in cell incubator (37°C, 5% CO_2 and 95% humidity) for 10 days.

2) PrP^{Sc}-HPFRET for DPICA

On day-11, PrP^{Sc}-HPFRET was performed in DPICA plates with the following steps: 1) cell lysis and PrP^{C} digestion in culture medium: 10 µl/well of 5x digestion buffer (5x standard lysis buffer containing 25µg/ml PK) was added directly without medium removal. The final concentration in each well was 1x standard lysis buffer and 5 µg/ml PK for about 10^5 cells. The DPICA plate was shaken at 37°C for 90 min at 700 rpm. 2) Inactivation of PK: 4 µl/well of 30 mM PMSF (stored at -20°C) was added to yield a final concentration of 2.2 mM. The DPICA plate was shaking at RT for 10 min at 700 rpm. 3) Denaturation: 7 µl/well of denaturing buffer (sodium hydroxide buffer containing 0.5M NaOH, pH 14.0, stored at RT) was added to yield a final concentration of 57.3 mM. The DPICA plate was shaken at RT for 10 min at 700 rpm. 4) Neutralization: 8 µl/well of neutralizing buffer (phosphate buffer containing 0.5M NaH_2PO_4, pH 4.0, stored at RT) was added to yield a final concentration of 57.9 mM. The DPICA plate was shaken at RT for 10 min at 700 rpm. 5) FRET antibody pair incubation: FRET antibody pair Eu^{2+}-POM19 and APC-POM1 stock was diluted with 1x Lance buffer to 67.5 nM (concentration of POM antibody). 6 µl/well of 67.5 nM Eu^{2+}-POM19 and APC-POM1 was added separately. The final total volume was 81 µl/well. The DPICA plate was shaken at 37°C for 1 h at 300 rpm. 7) The DPICA plate's clear bottom was sealed with white BackSeal-384 (PerkinElmer) for the top read of time-resolved FRET. The FRET signal of PrP^{Sc} was detected by EnVision Multilabel Reader.

3) Mathematics for DPICA

The number of prions at a fixed concentration in a given volume, follows the Poisson distribution:

$$P(i) = \frac{\lambda^i e^{-\lambda}}{i!} \quad (1)$$

Where "i" represents the number of prions and λ is the average number of prions per unit experimental volume, and is therefore related to concentration by λ = c • V, where "V" is the volume of the sample and "c" the concentration of prions related to the original prion concentration c0 by the dilution D as c = c_0/D. Therefore, determining "λ" will allow the determination of the original concentration of prions. However, it is not possible to simply fit a Poisson distribution to the distribution of signal intensities at a given concentration, as it is unclear how the signal strength scales with the number of prions. Nevertheless it should be possible to distinguish between samples that contain some prions and samples that do not have any prions at all and thereby determine P(i = 0), from which "λ" can be calculated.

When we analyze the PrP^{Sc}-HPFRET data from a diluted concentration, we assume a certain threshold, T, has been chosen. Then the fraction of points below the threshold f_{below} can be related to P(0) as follows:

$$f_{below} = \sum_{i=0}^{\infty} P(i)Q(T,i) \quad (2)$$

This is the probability that the sample contains i prions, P(i), times the probability that the resulting measurement is below the threshold, given that "i" prions were in the sample, Q(T; i).

We have included these conditional probabilities in order to account for experimental errors resulting in a spread of data, i.e., a sample containing no prions could still give a signal that is above the threshold and a sample containing some prions could give a signal below the threshold. For an ideal system with no spread, Q(T,0) = 1 and Q(T|i) = 0 for i ≠ 1, and therefore, the fraction of points below the threshold in this ideal case is equivalent to the probability of not having any prions, P(0).

If we consider a real system with significant spread, we need to find expressions for the conditional probabilities, which will be functions of the threshold, and the number of prions, "i". The probability to be below the threshold, "T", if no prions are present, Q(T,0), can be determined from the negative control experiment: by fitting a Gaussian distribution to the distribution of negative controls,

$$Q(T,0) = \int_{-\infty}^{T} \frac{1}{\sigma_{nc}\sqrt{2\pi}} e^{-\frac{(y-\mu_{nc})^2}{2\sigma_{nc}^2}} dy \quad (3)$$

i.e., we integrate the probability of obtaining a signal of intensity "y" to the threshold intensity. Calculating the probability of being below the threshold, if some prions are present, Q(T, i > 0), is more complex. We can consider the question as consisting of two parts: one is the intrinsic spread, similar to the case above, due to differences in cell cultures, prion propagation, etc. The other part is the effect due to the variable number of prions injected into the system, which brings us back to the initial problem of having to relate the injected number of prions to the signal intensity, or rather, how the initial number of prions is related to the final concentration of PrP^{Sc}.

We define the probability distribution of signal intensity as S(y, i), which is the probability to obtain a signal of intensity "y", given that there are "i" prions in the sample. By integrating this distribution up to a threshold "T", we obtain the probability to obtain a signal below the threshold for a given number of prions "i", which is Q(T, i). We assume the distribution of intrinsic spread in signal intensity, $S(y,\ i)$, is still Gaussian in "y", with the same standard deviation as the negative control and a mean, μ(i), which depends on the number of prions i. Then, Q(T; i) is given by the integral

$$Q(T,i) = \int_{-\infty}^{T} S(y,i)dy = \int_{-\infty}^{T} \frac{1}{\sigma_{nc}\sqrt{2\pi}} e^{-\frac{(y-\mu_{nc})^2}{2\sigma_{nc}^2}} dy = \frac{1}{2}\,\mathrm{erfc}\left(\frac{\mu(i)-T}{\sqrt{2}\sigma_{nc}}\right) \qquad (4)$$

where erfc(x) is the complementary error function of "x".

When we analyze the PrP^{Sc}-HPFRET data, we vary the thresholds over the entire data range of all dilution curves and thereby obtain traces of the fraction of points below the threshold, with varying threshold for each concentration. Then, we globally fit the fraction below the threshold to equation 2 at all thresholds and concentrations.

5.7.7 Automated liquid handling platform

The fully automated DPICA program was established on the Janus liquid handling platform including the instruments: "JANUS Varispan + MDT Automated Workstation" (PerkinElmer), robotic cell incubator (LICONIC), EnVision Multilabel Reader (PerkinElmer). The automated DPICA program is fully automated with the running controlled by "JANUS Project Manager" scheduling software (PerkinElmer).

5.7.8 Sample preparation from various mouse brain regions

Animal care and experimental protocols were performed in accordance with the "Swiss Ethical Principles and Guidelines for Experiments on Animals" and with the Swiss Animal Protection Law, under the approval of the Veterinary office of the Canton Zurich (animal permit 41/2012). All efforts were made to minimize animal discomfort and suffering. C57BL/6J male mice were purchased from Charles River. Mice were kept in a conventional

hygienic grade facility, housed in groups of 3-5 in type IIL cages, under a 12 h light/12 h dark cycle (light from 7 am to 7 pm) at 22±1°C, with unrestricted access to sterilized food (Kliba No. 3340, Provimi Kliba, Kaiseraugst, Switzerland) and water.

Mice were anesthetized with isofluorane and injected in the right hemisphere with 30 µl of 0.1% of RML6 or of 0.1% of NBH from CD-1 mice as control. Prion-infected and control mice were sacrificed at 4, 8, 12, 16, 18 and 20 weeks post-inoculation (wpi) or when they reached the terminal stage of prion disease. An additional group of control mice injected with NBH was sacrificed one week after the last prion-injected mouse reached the terminal stage. Euthanasia was performed by transcardial perfusion with PBS after deep anesthesia with ketamine and xylazinium. Brain areas were dissected, snap frozen and kept at -80°C until further processing. Ten percent (w/vol) tissue homogenates were prepared in 0.25 M sucrose in PBS using a Ribolyzer (Bio-Rad).

5.7.9 Scrapie cell assay in end point format

17,500 cells/well prion-susceptible neuroblastoma cells N2aPK were plated in 96-well plates and exposed to 300-µl brain homogenates using 6-12 replicas per dilution (ten-fold serial dilution from 10^{-3} to 10^{-8}) for 3 days. Cells were subsequently split three times 1:10 every 3 d. After the cells reached confluence, 25'000 cells from each well were filtered onto the membrane of ELISPOT plates, treated with PK (0.5 µg/ml for 90 min at 37°C), and denatured. PrP^{Sc}-positive cells were identified by immunocytochemistry using alkaline phosphatase-conjugated POM1 mouse anti-PrP and an alkaline phosphatase-conjugated substrate kit (Bio-Rad). Samples were quantified in endpoint format by counting positive wells according to established methods (Klohn, Stoltze et al. 2003).

5.7.10 Mouse bioassay

Serial dilutions of the 20% RML6 BH were prepared with PBS containing 5% BSA. CD1 mice, about eight week old, were intracerebrally (i.c.) inoculated with 30 µl of serially diluted RML6 BH. In parallel groups, CD1 mice were intraperitoneally (i.p.) inoculated with 100µl 30 µl of serially diluted RML6 BH. Mice were monitored every second day for the occurrence of clinical signs and were euthanized at the terminal stage of prion disease.

5.7.11 Preparation of prion decontaminated samples

Brain tissue was harvested from RML6 inoculated Tga20 (Fischer, Rulicke et al. 1996) (RML6-Tg20) mice at terminal stage and stored frozen at -80°C. Semipurified PrP^{Sc} samples were prepared according to the procedure described by Xanthopoulos (Xanthopoulos, Polymenidou et al. 2009), excluding Proteinase K treatment.

1) Decontamination with chaotropic salt guanidinium hydrochloride (GdnHCl)

The semipurified PrP^{Sc} sample was homogenized with Potter homogenisator in 6 M GdnHCl (Prusiner, Groth et al. 1993, Caughey, Raymond et al. 1997) (G4505, Sigma) solution in 20mM HEPES, 5mM imidazole, 0.5M NaCl, pH7.5 containing 1% of the one of the following detergents: C8E4 (T3394, Sigma), b-octylpyranoside (O8001, Sigma), and incubated for 24h at 25°C with constant agitation.

To eliminate cytotoxic GdnHCl and detergents from the samples, prior analysis by DPICA samples were either dialysed or the protein was precipitated. Dialysis was done against PBS using Slide-A-Lyzer Dialysis Cassettes, 10K MWCO (Pierce) with exchanges of the dialysis buffer after 2, 4, 16 and 24 hours of dialysis. Protein was precipitated after dilution of the sample to 1M GdnHCl with 10% cold TCA (final concentration) and subsequently washed with cold ethanol. Resulting samples were harvested and the changes in protein loss were assessed with BCA assay (Pierce).

2) Decontamination with NaOH

The semipurified PrP^{Sc} sample was homogenized in 1M NaOH (Prusiner, Groth et al. 1981, Bauman, Lawrence et al. 2006, Unal, Thyer et al. 2007, Bellon, Comoy et al. 2014) and incubated for 24h. Afterwards sample were dialyzed against PBS using Slide-A-Lyzer Dialysis Cassettes, 10K MWCO (Pierce) with exchange of the dialysis buffer after 2, 4, 16 and 24 hours of dialysis.

3) Decontamination with formic acid

The semipurified PrP^{Sc} sample with 100% formic acid (Brown, Wolff et al. 1990, Taylor, Brown et al. 1997) for 24h. Afterwards samples were dialyzed against PBS using Slide-A-Lyzer Dialysis Cassettes, 10K MWCO (Pierce) with exchange of the dialysis buffer after 2, 4, 16 and 24 hours of dialysis.

4) Decontamination with nanofiltration (Golker, Whiteman et al. 1996, Tateishi, Kitamoto et al. 2001)

The semipurified PrP^{Sc} sample was homogenized in PBS, then filtered through Sartorius filters Vivaclear (polyethersulfone, 0.8 µm, cat#VK01P042) at 14000g for 45min, followed by filtration through Vivaspin 6 (polyethersulfone, 0.2 µm, cat# VS0671) at 4000g for 1h and finally through Vivaspin 15R Hydrosart Membrane (2000 MWCO, cat# VS15RH91) for 15h. Changes of the sample volume were noted.

5) Decontamination with different GdnHCl concentrations and pH values

The RML6-Tg20 BH samples were homogenized with Potter homogenisator in (0, 1.7, 2.5, 3.3, 4.2, 5.0 M) GdnHCl (G4505, Sigma) solution in 20mM HEPES, 5 mM imidazole, 0.5 M NaCl, pH (2.5, 5.0, 7.5, 12) containing 1% of b-octylpyranoside (O8001, Sigma), and incubated for 48h at 25°C with constant agitation. Dialysis was done against PBS using Slide-A-Lyzer Dialysis Cassettes, 10K MWCO (Pierce) with exchange of the dialysis buffer after 2, 4, 16 and 24 hours of dialysis.

6 Results PART II: Establishment of an automated PrP-HPFRET based high-throughput siRNA screening platform

6.1 Introduction

6.1.1 RNA profile change upon prion infection

Upon prion infection of neuronal cell lines, transcriptome profile changes reflect the direct response to prion and could indicate potential pathways of prion pathogenesis. Using a cDNA microarray, distinct expression profiles in ScN2a and ScGT1 cell lines were reported (Greenwood, Horsch et al. 2005). However, by applying high-density oligonucleotide microarray analysis and exhaustive bioinfomatical interrogation of the data, another transcriptional study analyzed the transcriptome of several prion infected cell lines (N2aPK1, CAD and GT1) under more stringently controlled conditions and identified only modest differential expression after prion infection (Julius, Hutter et al. 2008). The discrepancy between the two studies may due to differences in experimental design, cell culture conditions and/or prion infection processes. The transcriptional profile of cell culture might change after prion infection. The transcriptome of cell lines could also affect the susceptibility to prion infection. Different cell lines have distinct susceptibilities to prion infection. These differences cannot be explained by the PrP^C expression levels alone, which are required but not sufficient for prion replication (Mahal, Baker et al. 2007). By comparing the transcriptome of prion-resistant revertants to susceptible cells, Marbiah et al. identified a gene regulatory network for extracellular matrix remodeling that was associated with prion propagation (Marbiah, Harvey et al. 2014). By using microarray and RT-PCR, miRNA expression changes were profiled in the brains of mice intracerebrally inoculated with mouse scrapie. Fifteen miRNAs were found to be de-regulated during the disease and only has previously been shown to be de-regulated in neurodegenerative disease (Saba, Goodman et al. 2008). With proper experimental strategy and the application of new RNA analysis technologies such as RNA sequencing (RNAseq), the understanding of the cellular transcriptional response to prion infection will be deepened. The identification of RNA profile changes upon prion infection may have potential as a biomarker for prion diagnostics and as a target for therapeutics.

6.1.2 Small RNAs based targets identification for prion disease

PrP^C is indispensable for prion replication and prion-induced pathogenesis. Mice devoid of PrP^C showed resistance to prion infection (Bueler, Aguzzi et al. 1993). A 50% reduction of of PrP^C ($Prnp^{+/-}$ heterozygous mice) significantly prolongs the incubation time of prion disease in

mouse, while overexpression of PrP^C markedly shortens prion disease progression (Manson, Clarke et al. 1994). Therefore, the identification of genes involved in PrP^C biosynthesis by small RNA based screening, and RNA-mediated modulation the PrP^C expression have great potential to mitigate the PrP^C-PrP^{Sc} conversion, diminish prion-induced neurotoxicity and consequently slow disease progression.

Since Prnp is the main determinant for prion pathogenesis, small RNAs specifically and directly targeting Prnp have been extensively studied for prion therapeutics both in vitro and in vivo. siRNA duplexes targeting *Prnp* gene effectively suppressed the expression of PrP^C in prion-infected N2a cells and inhibited the PrP^{Sc} accumulation (Daude, Marella et al. 2003). The liposome-siRNA-peptide complex was later developed to suppress PrP^C expression and eliminate PrP^{Sc} formation in prion-infected N2a cells (Pulford, Reim et al. 2010). Additionally, the vector-based shRNA was successfully applied to decrease PrP^C expression in rabbit kidney epithelial cells (Tilly, Chapuis et al. 2003) and mouse N2a cells (Mahal, Baker et al. 2007). Lentiviral vector delivered shRNA also decreased PrP^C levels and extended the incubation time in mice (Pfeifer, Eigenbrod et al. 2006, White, Farmer et al. 2008). Similar effects were observed in transgenic livestock (Golding, Long et al. 2006, Wongsrikeao, Sutou et al. 2011), Therefore, RNAi based Prnp knockdown represents a promising approach for prion therapeutics. However, certain considerations about RNAi based therapeutics, such as immunogenicity, cytotoxicity induced by off-target must be taken into account. Hence, a modified version of small RNA or novel small RNA targeting Prnp may circumvent those pitfalls. Recently, miRNA (Kang, Roh et al. 2011), DNA-based antisense oligonucleotides (ASO) (Nazor Friberg, Hung et al. 2012), and RNA aptamers (Weiss, Proske et al. 1997, Proske, Gilch et al. 2002) targeting *Prnp*/PrP^C have been studied as a method to prevent prion disease progression.

6.1.3 HTS applications for discovering prion therapeutic target

PrP^C is indispensable for prion replication and prion-induced pathogenesis. Mice devoid of PrP^C showed resistance to prion infection (Bueler, Aguzzi et al. 1993). A 50% reduction of PrP^C ($Prnp^{+/-}$ heterozygous mice) significantly prolongs the incubation time of prion disease in mouse, while overexpression of PrP^C markedly shortens prion disease progression (Manson, Clarke et al. 1994). Therefore, the identification of genes involved in PrP^C biosynthesis by small RNA based screening, and RNA-mediated modulation the PrP^C expression have great potential to mitigate the PrP^C-PrP^{Sc} conversion, diminish the prion-induced neurotoxicity and consequently slow disease progression. PrP^C is indispensable for prion replication and prion-induced pathogenesis. Mice devoid of PrP^C were resistant to prion infection (Bueler, Aguzzi et al. 1993). Because Prnp is the main determinant for prion pathogenesis, small RNAs specifically and directly targeting Prnp have been extensively studied for prion therapeutics.

siRNA duplexes targeting *Prnp* gene effectively suppressed PrP^C expression in mouse neuronal N2a cells and inhibited prion replication (Daude, Marella et al. 2003). Later, a liposome-siRNA-peptide complex was developed to suppress PrP^C expression and eliminate PrP^{Sc} accumulation in N2a cells (Pulford, Reim et al. 2010). The vector-based shRNA was applied to decrease PrP^C expression in rabbit kidney epithelial cells (Tilly, Chapuis et al. 2003) and mouse N2a cells (Pfeifer, Eigenbrod et al. 2006). The lentiviral vector delivered shRNA also decreased PrP^C level and extended the incubation time in mice (Pfeifer, Eigenbrod et al. 2006, White, Farmer et al. 2008), Similar effects were observed in transgenic livestock (Golding, Long et al. 2006, Wongsrikeao, Sutou et al. 2011). Therefore, RNAi based Prnp knockdown represents a promising approach for prion therapeutics. However, there are considerations about RNAi based therapeutics, such as immunogenicity, cytotoxicity induced by off-target that needs to be taken into account. Hence, a modified version of small RNA or novel small RNA targeting Prnp may circumvent those pitfalls. Recently, miRNA (Kang, Roh et al. 2011), DNA-based antisense oligonucleotides (ASO) (Friberg, Hung et al. 2012), and RNA aptamers (Weiss, Proske et al. 1997, Proske, Gilch et al. 2002) targeting *Prnp*/PrP^C have been studied to prevent the prion disease progression.

In addition, small RNA based high throughput screening (HTS) is expected to be used in the prion field. However, this application is challenging because the conventional approaches for prion proteins quantification are either time consuming or demand substantial manual work, hence are not applicable for HTS. Therefore, new methodologies and technologies complementary to an automated high-throughput system are required that facilitate HTS of entire small RNA libraries including siRNA, shRNA or newly developed sgRNA libraries, compounds and peptides towards the identification of disease relevant genes, proteins, early molecular markers and novel therapeutics (Hruska-Plochan, Li et al. 2015).

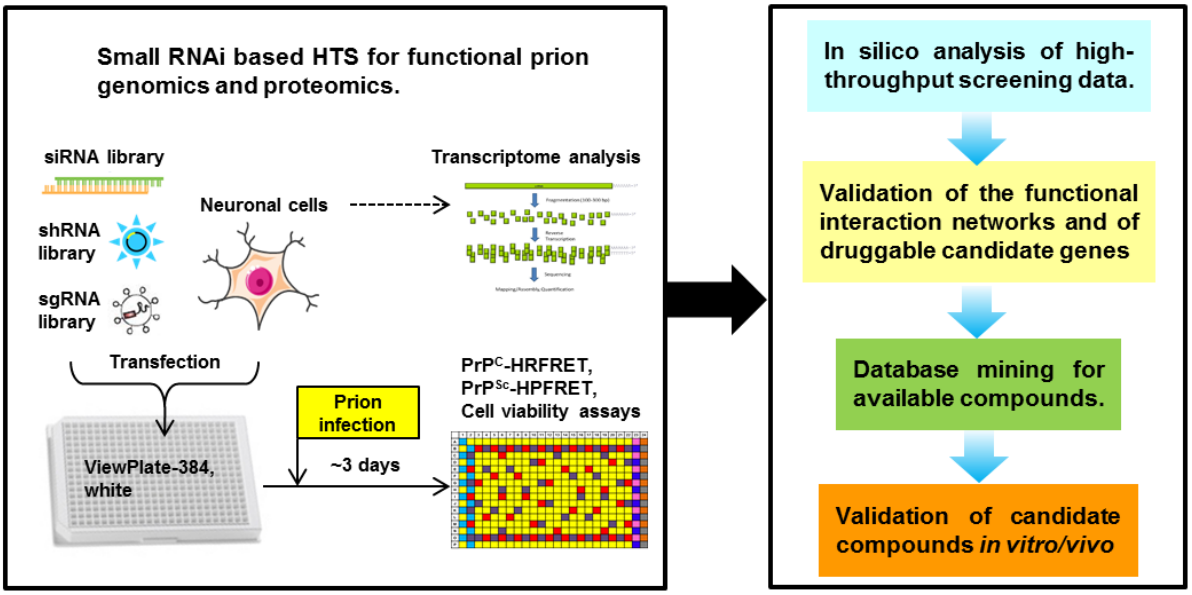

Figure 6.1 Novel strategies for RNAi HTS to discover prion molecular mechanisms and therapeutic targets. Figure adapted from (Hruska-Plochan, Li et al. 2015).

6.2 Specific aims of the project

Here, I planned to combine the PrP-HPFRET assays and RNAi HTS technologies to establish an automated PrP-HPFRET based high-throughput siRNA screening platform, and to apply a siRNA library screen to identify genes affecting cellular prion protein expression and replication.

a) Apply PrP^{C}-HPFRET and PrP^{Sc}-HPFRET for assessing RNAi-mediated gene silencing in mouse neuronal cells.
b) Establish an automated PrP-HPFRET based high-throughput siRNA screening platform.
c) Apply the siRNA HTS platform for an arrayed murine siRNA library screen to identify genes regulating endogenous PrP^{C} expression and prion replication.

6.3 Application of PrP^{C}-HPFRET and PrP^{Sc}-HPFRET for assessing RNAi-mediated gene silencing in neuronal cells

To expand the power of PrP^{C}-HPFRET and PrP^{Sc}-HPFRET to RNAi HTS technologies, I utilized them to determine RNAi-mediated gene silencing and block of prion replication. The siRNAs targeting mouse *Prnp* mRNA were used to develop the new assays in a mouse neuronal cell line Cath.a differentiated cell line 2A2D5 (CAD5), which is susceptible to various mouse prion strains (Weissmann, Li et al. 2011). CAD5 cells were plated in a 384-well plate and transfected with *Prnp*-siRNA. After 72 hours incubation, cell viability assay and PrP^{C}-HPFRET (**Figure 6.2a**) were performed to quantify PrP^{C}. I found two out of four *Prnp*-siRNAs (*Prnp*-siRNA1 and *Prnp*-siRNA4) could efficiently reduce *Prnp* expression. Since the PrP^{C} level is the most important determinant for prion infection and replication, and it has been reported that knockdown of *Prnp* significantly reduces prion replication *in vivo*, *Prnp*-siRNA silencing was expected to also reduce prion replication *in vitro*. Next, CAD5 cells were plated in a 384-well plate and treated with *Prnp*-siRNA for 24 hours, then exposed to RML6. 72 hours after infection, cell viability assay and PrP^{Sc}-HPFRET (**Figure 6.2b**) were performed to quantify PrP^{Sc}. The results confirmed that both *Prnp*_siRNA1 and *Prnp*-siRNA4 could significantly block PrP^{Sc} replication in CAD5 cells. Besides, a *Prnp* gene knockout cell line (*Prnp*$^{-/-}$ CAD5) was generated by CRISPR/Cas9 technology and used as a control for cell-based HPFRET assays. The newly developed assays for assessing RNAi-mediated gene silencing in neuronal cells confirmed that silencing *Prnp* gene could efficiently downregulate PrP^{C} expression, and significantly block PrP^{Sc} replication. Therefore, PrP^{C}-HPFRET and

PrP^{Sc}-HPFRET can be well combined with RNAi HTS to identify genes that affect prion protein expression and replication.

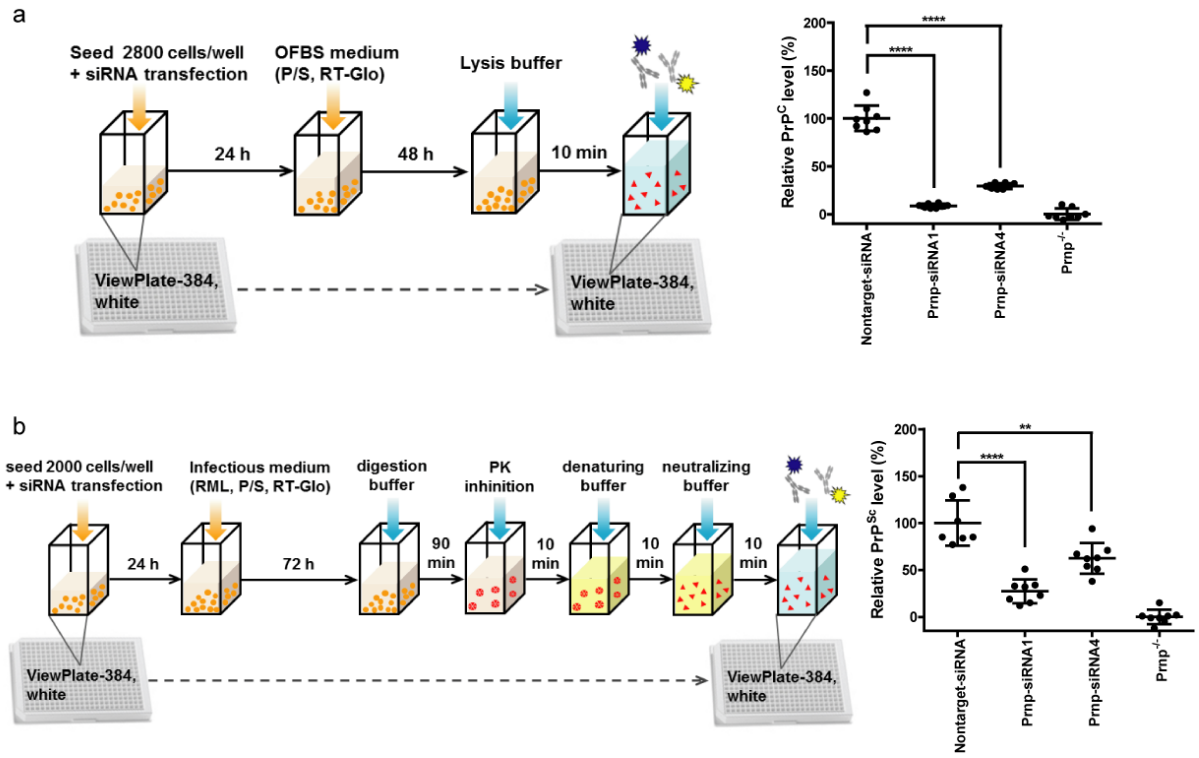

Figure 6.2 Apply PrP-HPFRET assays to assessing RNAi-mediated gene silencing. (a) 2800 cells/well CAD5 cells were plated in a 384-well plate and transfected with *Prnp*-siRNA. After 72 hours, cell viability assay and PrP^{C}-HPFRET were performed to quantify PrP^{C} protein in cell lysate (Relative PrP^{C} level = relative PrP^{C}-HPFRET / Relative cell number). *Prnp*-siRNA1and *Prnp*-siRNA4 efficiently downregulated PrP^{C} by more than 80% and 50% (****P<0.0001). **(b)** 2000 cells/well CAD5 cells were plated in a 384-well plate and transfection with *Prnp-siRNA* for 24 hours, then exposed to RML6 for 72 hours. PrP^{Sc}-HPFRET and cell viability assay were performed to quantify PrP^{Sc} protein in cell lysate (Relative PrP^{Sc} level = relative PrP^{Sc}-HPFRET / Relative cell number). *Prnp*-siRNA1 and *Prnp*-siRNA4 efficiently downregulated PrP^{C} and thus significantly blocked PrP^{Sc} replication (****P<0.0001, ***P<0.001).

6.4 Establishment of an automated siRNA HTS platform

Our lab has established the Labcyte Echo acoustic liquid handling platform and a Perkin-Elmer Janus liquid handling platform for high-throughput applications (**Figure 6.3a**). Based on these robotic platforms, I established automated protocols specifically for the murine siRNA screening project. The Labcyte Echo acoustic liquid handling platform is able to make siRNA stamps in 384-well plates with a completely random map (**Figure 6.3b**): 1) siRNA controls are dispensed using “Plate Reformat” program; 2) siRNA samples are dispensed using “Cherry Pick” program with sample picking lists. In each screening plate, there are 48 wells of nontarget-siRNA control, 47 wells of *Prnp*-siRNA1 control, 16 wells of *Prnp*$^{-/-}$ CAD5

cell control, and 192 wells of siRNA samples. I adapted these newly developed assays described above to a Perkin-Elmer Janus liquid handling system integrated with a Envision multilabel plate reader and a Liconic robitic incubator capable of hosting 44 384-well microplates. Under typical production conditions, this translated into a throughput of 15'360 wells/24 hours, enabling sufficient throughput for large-scale HTS applications.

a

Labcyte Echo acoustic and Perkin-Elmer Janus liquid handling platforms

b

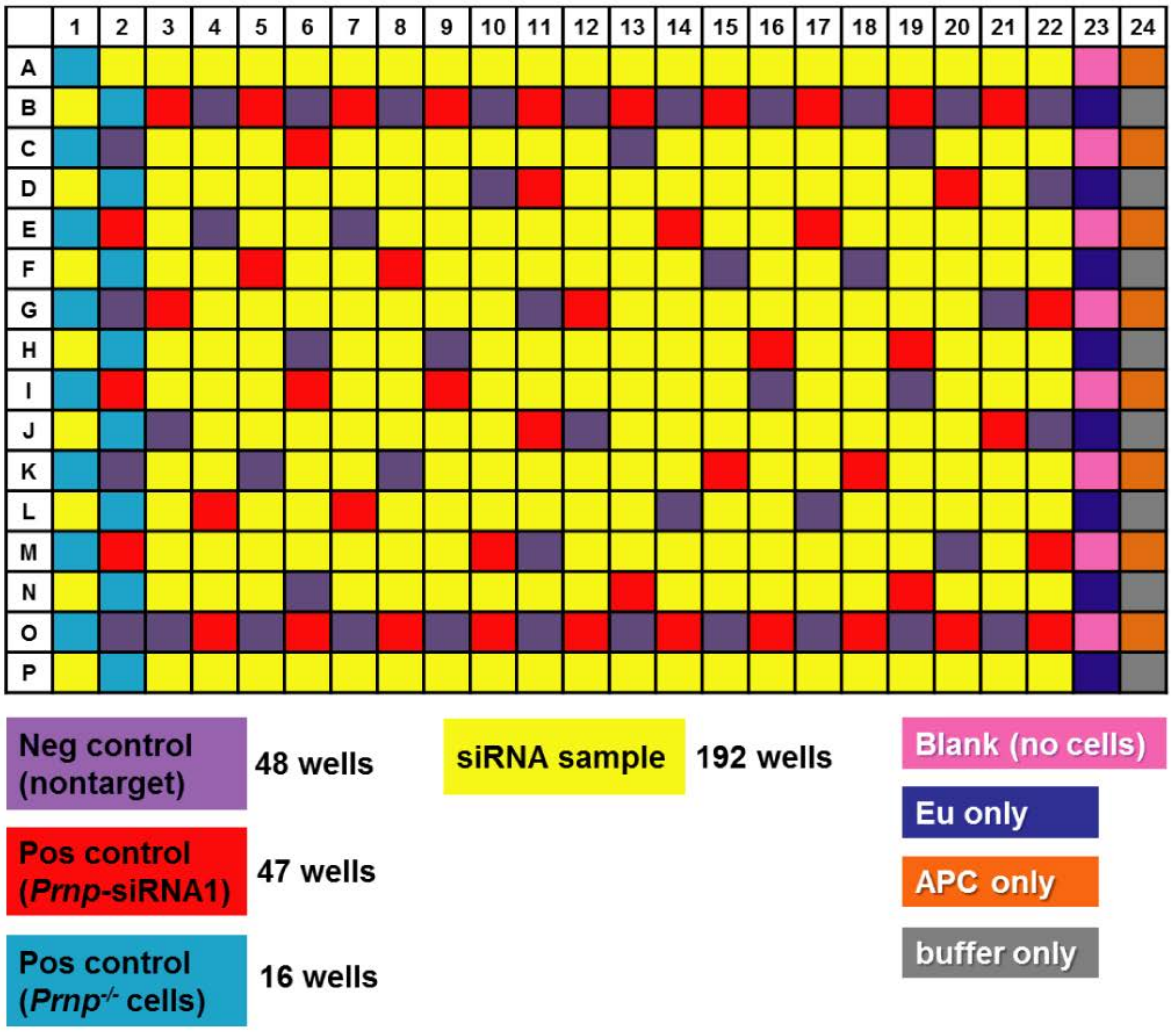

Figure 6.3 An automated RNAi HTS platform. The siRNA stamps in 384-well plates are made on a Labcyte Echo acoustic liquid handling platform; siRNA transfection and HPFRET assays are performed on a Perkin-Elmer Janus liquid handling platform.

6.5 HTS of 3127 murine siRNAs targeting 780 genes involved in endocytosis pathways

6.5.1 Screen of an arrayed murine siRNAs to identify genes regulating endogenous PrP^C expression

First, I did a genome-wide transcriptome analyses in CAD5 cells by RNAseq, which showed that there are 13'752 genes expressed in the CAD5 cells line. Based on RNAseq results, I collected an arrayed murine siRNA library (offered by Novartis Institute for BioMedical Research) including 3'127 siRNAs targeting 780 genes that are expressed in CAD5 cells and involved in endocytic membrane trafficking pathways.

Then, I performed a screen of this library on our automated RNAi HTS platform: 1) All siRNA samples were randomly distributed into 384-well screening plates by the Echo liquid handler according to the completely random map (The screening plates were stored in -40°C freezer and thawed before use); 2) CAD5 cells were plated in screening plates and transfected with siRNAs. After 72 hours incubation, the cell viability assay and PrP^C-HPFRET was performed on automated HTS platforms. The luminescent and FRET signals were read by EnVision multilabel plate reader. All the screening raw data were collected and then analyzed by collaborated bioinformaticians for quality control (QC) reports, normalization, hits selection and pathway analysis.

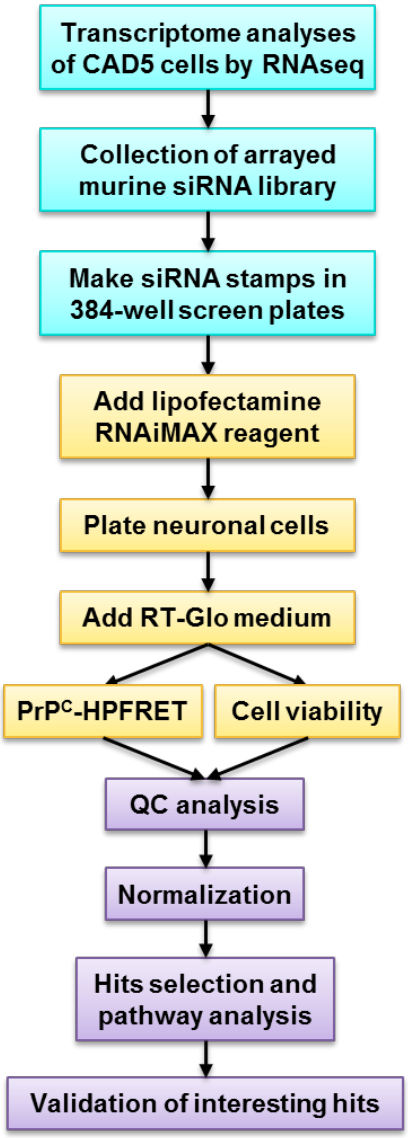

Overview of a murine siRNA library screen.

6.5.2 Screen raw data analysis

Based on screening the raw data, the bioinformaticians did QC analysis to ensure that the resulting data meet minimum quality standards in order to derive valid conclusions. The QC

reports including heat map of PrP^C-HPFRET (**Figure 6.4**) and Realtime-Glo signals (**Figure 6.5**), smoothed histogram of control and sample distributions (**Figure 6.6**), showed that the screening raw data meets acceptable performance criteria for HTS.

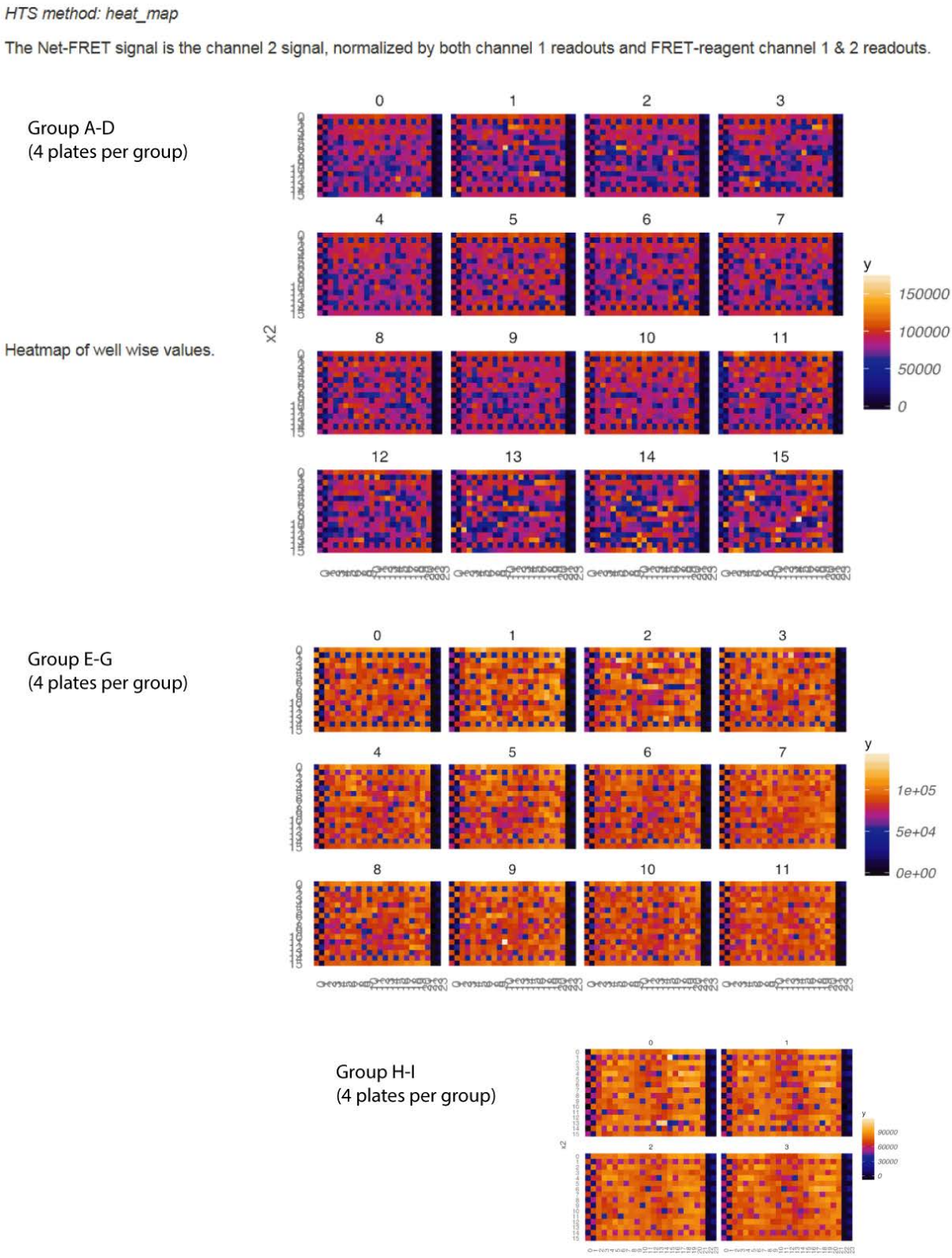

Figure 6.4 QC report: Heat map of PrP^C-HPFRET of screening plates (Group A to I, in total 32 plates)**.**

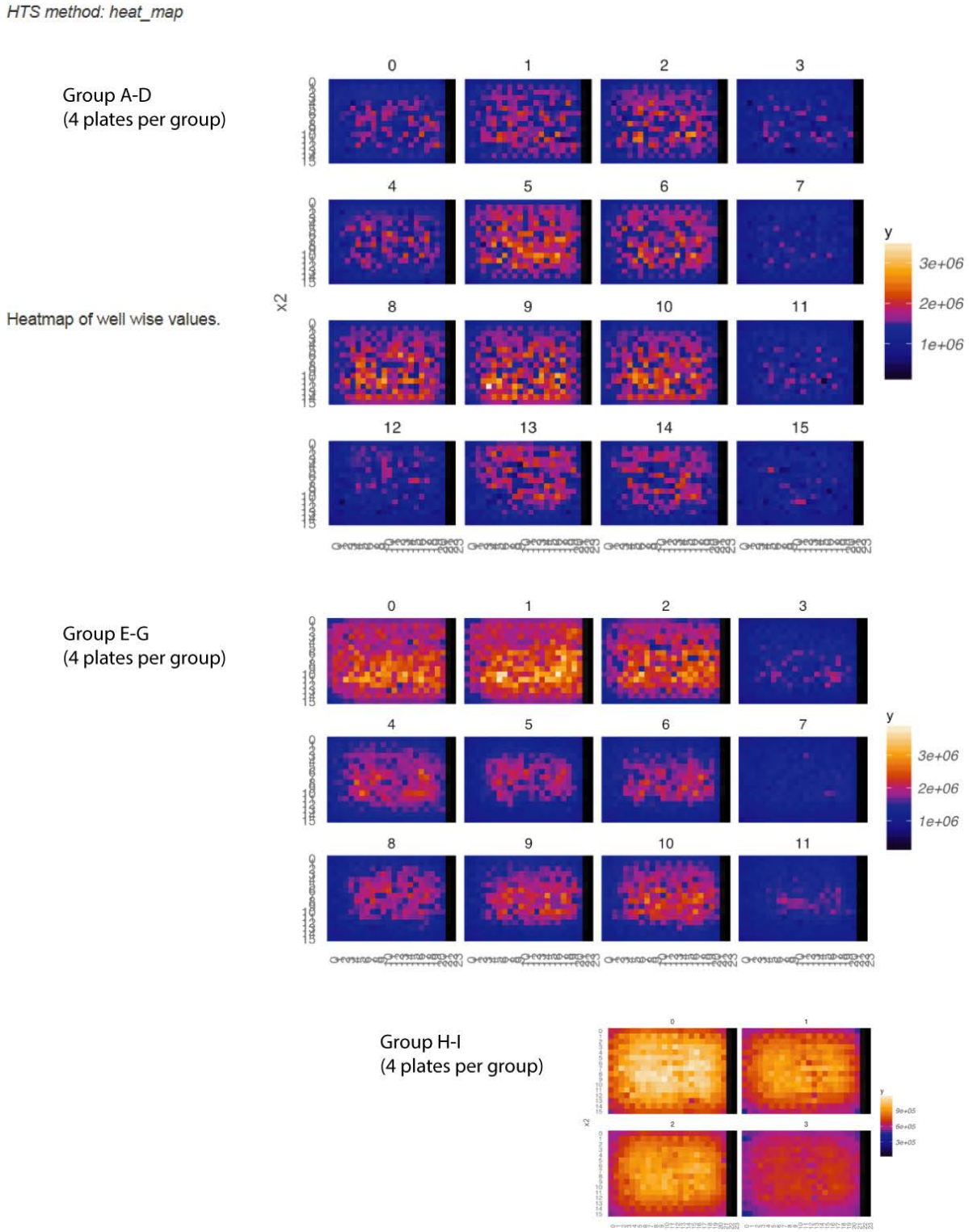

Figure 6.5 QC report: Heat map of Realtime-Glo of screening plates (Group A to I, in total 32 plates)**.**

Figure 6.6 QC report: Smoothed histogram of the control and sample distributions of screening plates (Group A to I, in total 32 plates)**.**

6.5.3 Silencing Tfr1 efficiently downregulated PrP^{C} and blocked PrP^{Sc} replication in neuronal cells

I found an interesting hit transferrin receptor 1 (Tfr1) by noting that three out of four *Tfr1*-siRNA samples showed significantly reduced PrP^{C} levels in CAD5 cells. Next, I validated the candidate Tfr1 using siRNA from another commercial library (Thermo Fisher Scientific). By PrP^{C}-HPFRET and the cell viability assay, I confirmed that silencing Tfr1 in CAD5 cells yields more than a 50% PrP^{C} reduction (**Figure 6.7a**).

I predicted that silencing Tfr1 could inhibit prion replication and thus tested the hypothesis by infecting Tfr1-siRNA transfected CAD5 cells with prion inoculum RML6. We checked the PrP^{Sc} level by PrP^{Sc}-HPFRET and the cell viability assay, and were able to show that PrP^{Sc} replication was significantly blocked by Tfr1-siRNA treatment (**Figure 6.7b**).

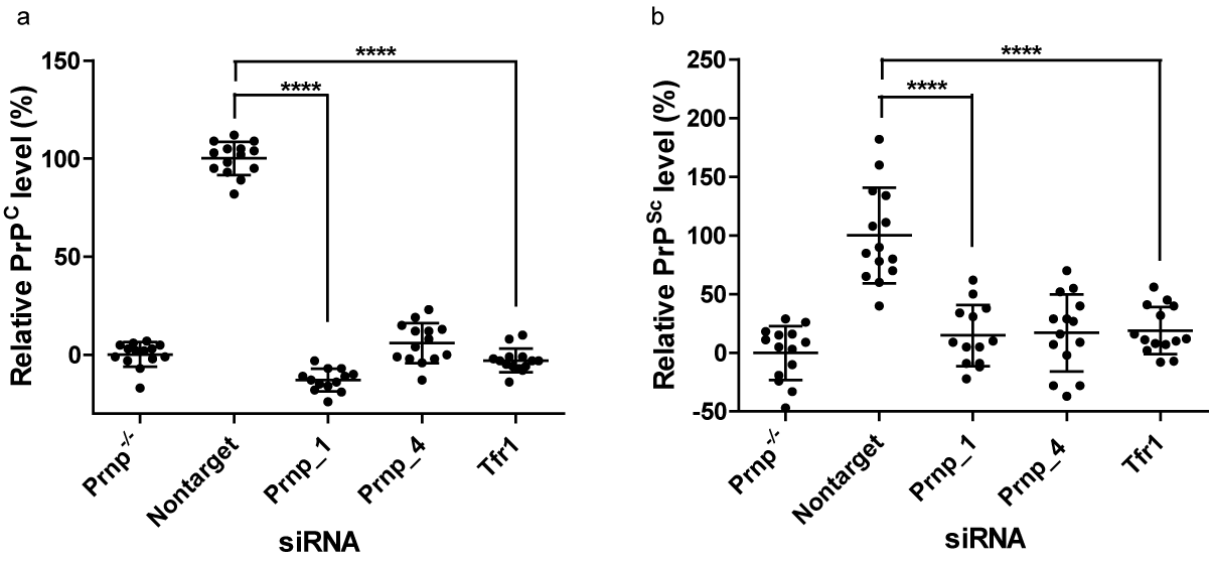

Figure 6.7 Validation of Tfr1-siRNA treatment by PrP^C-HPFRET and PrP^{Sc}-HPFRET. (a) CAD5 cells were plated in a 384-well plate and transfected with Tfr1 and control siRNAs. After 72 hours, the cell viability assay and PrP^C-HPFRET were performed to quantify PrP^C protein in the cell lysate. Tfr1-siRNA treatment significantly reduced PrP^C level in both neuronal cell lines (****P<0.0001). **(b)** CAD5 cells were plated in a 384-well plate and transfected with Tfr1 and control siRNAs for 24 hours, then exposed to RML6 for 72 hours. PrP^{Sc}-HPFRET and cell viability assay was performed to quantify PrP^{Sc} protein in cell lysate. Tfr1-siRNA treatment significantly blocked PrP^{Sc} replication (****P<0.0001).

Furthermore, I checked the specificity of silencing Tfr1 in CAD5 cells by Western blot and confirmed that Tfr1 protein level was efficiently reduced by Tfr1-siRNA treatment (**Figure 6.8**). Meanwhile, PrP^C protein level was significantly decreased, in accordance with the PrP^C-HPFRET results.

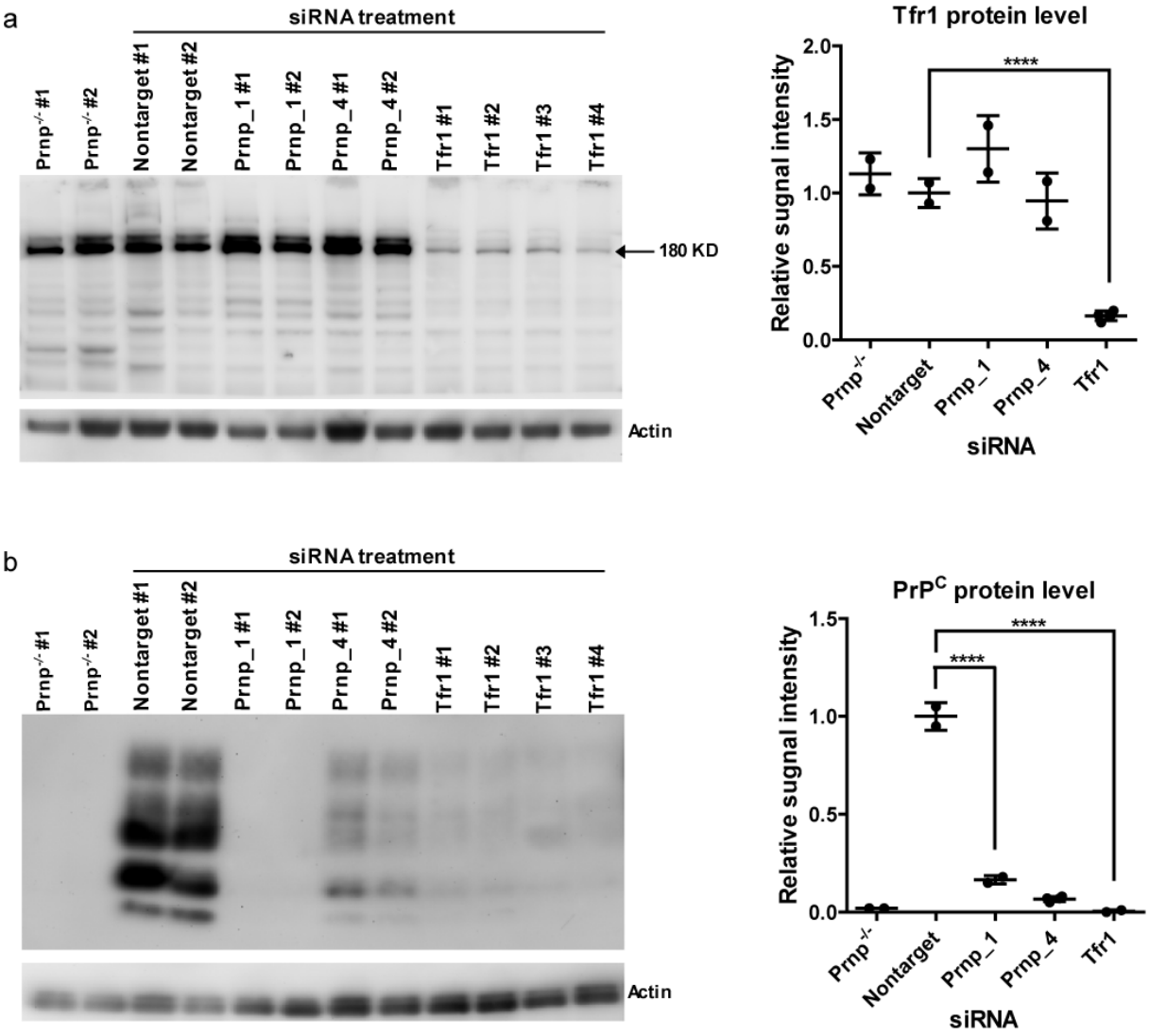

Figure 6.8 Validation of Tfr1-siRNA treatment in CAD5 cells by Western blot. CAD5 cells were plated in a 24-well plate and transfected with Tfr1 and control siRNAs. After 72 hours, cells were harvested and lysed for BCA and Western blot. **(a)** Tfr1 expression was efficiently silenced by Tfr1-siRNA (****P<0.0001). **(b)** PrP^C protein level was significantly reduced by Tfr1-siRNA treatment (****P<0.0001).

6.5.4 Tfr1-siRNA treatment reduced the Prnp mRNA level

To check whether the Tfr1-siRNA mediated regulation of PrP^C expression occurred at the protein-protein interaction or transcriptional/posttranscriptional level, I checked the *Prnp* mRNA in Tfr1-siRNA transfected neuronal cells by qPCR. Interestingly, the *Prnp* mRNA level showed a significant reduction in Tfr1-siRNA treated CAD5 (**Figure 6.9**), suggesting that PrP^C expression could be regulated by Tfr1-siRNA at the transcriptional or posttranscriptional level.

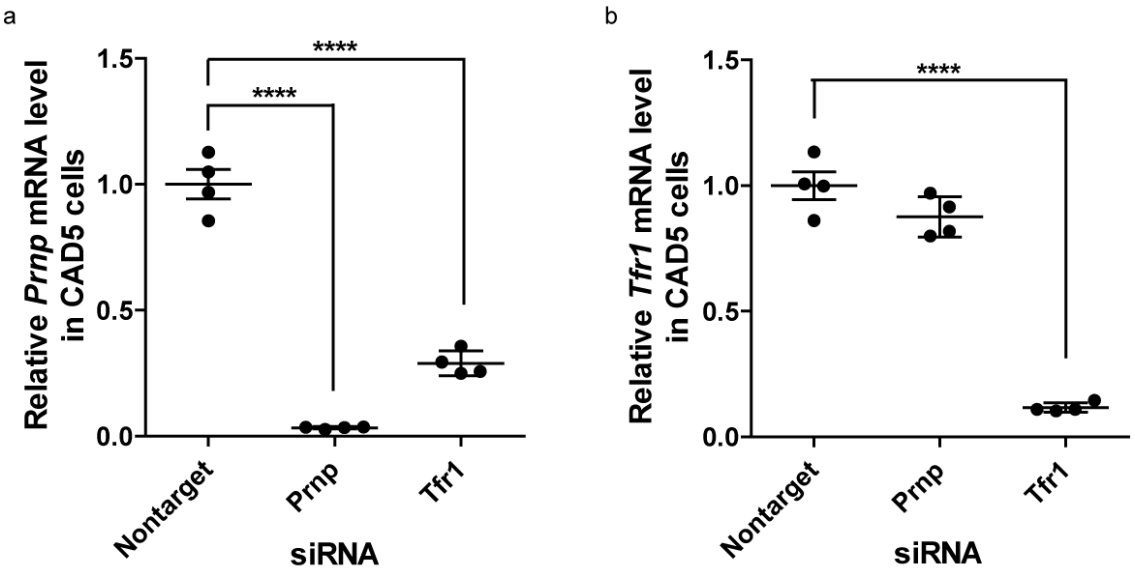

Figure 6.9 qPCR analysis of Prnp mRNA in Tfr1-siRNA transfected neuronal cells. CAD5 cells were plated in a 24-well plate and transfected with Tfr1 and control siRNAs. After 72 hours, cells were harvested. The total RNA was extracted from cells and reversed to cDNA for qPCR. The Prnp mRNA level was significantly reduced by Tfr1-siRNA treatment in CAD5 cells (****P<0.0001, *P<0.05).

I also performed the Tfr1-siRNA treatment in another mouse neuronal cell line N2aPK1 (Klohn, Stoltze et al. 2003), and confirmed the Tfr1-siRNA effect by PrP^C-HPFRET and qPCR (**Figure 6.10**).

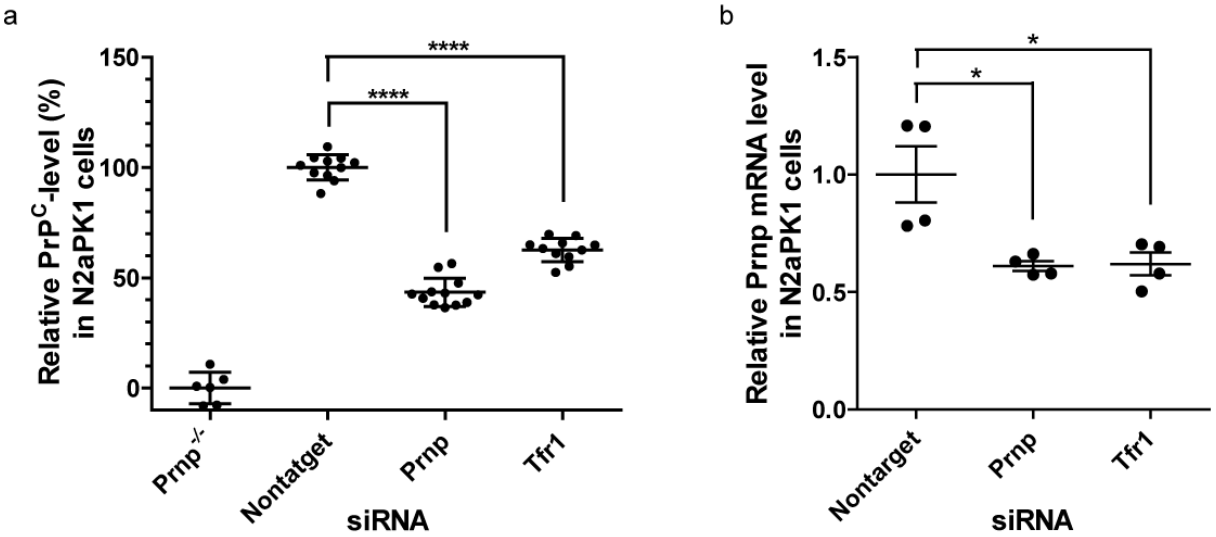

Figure 6.10 Validation of Tfr1-siRNA treatment in N2aPK1 cells. (a) N2aPK1 cells were plated in a 384-well plate and transfected with Tfr1 and control siRNAs. After 72 hours, the cell viability assay and PrP^C-HPFRET were performed to quantify PrP^C protein in the cell lysate. Tfr1-siRNA treatment significantly reduced the PrP^C level (****P<0.0001). **(b)** N2aPK1 cells were plated in a 24-well plate and transfected with Tfr1 and control siRNAs. After 72 hours, cells were harvested. The total RNA was extracted from cells and reversed to cDNA for qPCR. The Prnp mRNA level in CAD5 cells was significantly reduced by Tfr1-siRNA treatment (*P<0.05).

Then, I tested the same siRNA treatment using a new cell line, hyCAD5, which expresses PrP^C under the CMV promoter in *Prnp*$^{-/-}$ CAD5 cells. I transfected the hyCAD5 cells with Tfr1-siRNA, 72 hours later, the PrP^C level was quantified by PrP^C-HPFRET. In contrast wild-type CAD5 cells, PrP^C levels were not reduced in hyCAD5 cells after Tfr1-siRNA transfection (**Figure 6.11**).

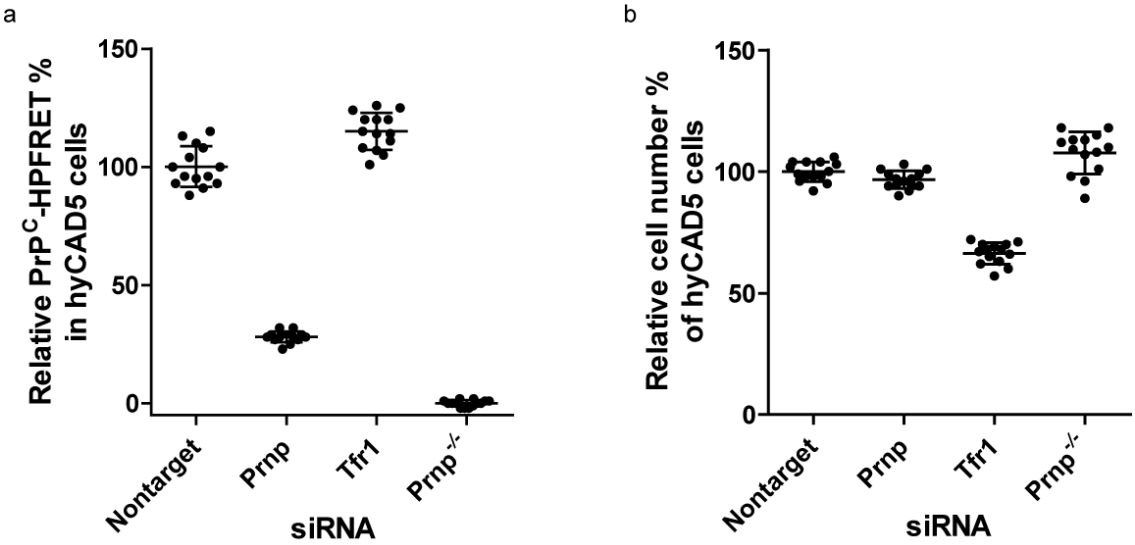

Figure 6.11 Validation of Tfr1-siRNA treatment in hyCAD5 cells. hyCAD5 cells (expressing PrP^C under CMV promoter in Prnp$^{-/-}$ CAD5 cells) were plated in a 384-well plate and transfected with Tfr1 and control siRNAs. After 72 hours, the cell viability assay and PrP^C-HPFRET were performed to quantify PrP^C protein in the cell lysate. The PrP^C protein level was not reduced by Tfr1-siRNA treatment in hyCAD5 cells.

6.5.5 Genome-wide transcriptome analysis of Tfr1-siRNA treated CAD5 by RNAseq

To further check whether other transcriptional changes are induced by silencing Tfr1, I prepared total RNA from Tfr1-siRNA and nontarget-siRNA transfected CAD5 cells. I performed the same treatment twice. In each treatment, there were two groups of samples: nontarget-siRNA and Tfr1-siRNA treatment samples with four biological replicates per group. Then I sent total 16 samples to the Functional Genomics Center Zurich for RNAseq analysis, in order to compare the total RNA between Tfr1-siRNA and nontarget-siRNA treated groups. The RNAseq results showed that there are 1367 significant genes with a threshold p-value < 0.01 and ≥ 2 fold-change (**Figure 6.12-6.13, Table 6.1)**. Furthermore, the expression of 99 genes significantly changed with a >4-fold-change and p-value < 1e-5, in which 48 genes were down-regulated (**Table 6.2**) and 51 genes upregulated (**Table 6.3**). In this result, Tfr1 was the top7 and Prnp the top11 down regulated gene expression. Other interesting genes related to PD and AD diseases, e.g., Park2 (Parkinson disease autosomal recessive, juvenile 2) was significantly upregulated with a 5.2 fold-change, p<1e-5, LRRK2 (leucine-rich repeat kinase 2, encoded by the PARK8 gene in humans) was significantly downregulated with a

2.7 fold-change, p<1e-5, and Mapt (microtubule-associated protein tau) was significantly downregulated with a 2.8 fold-change, p<1e-5.

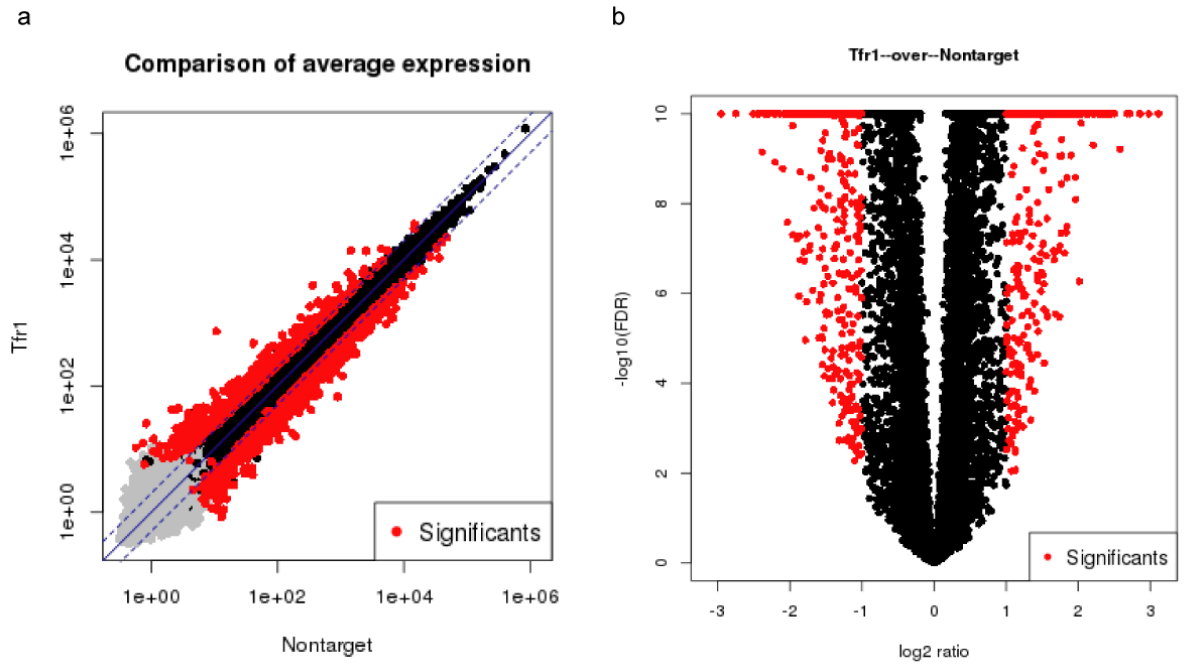

Figure 6.12 Inspection of significant genes. P-value threshold: p <= 0.01. Log ratio threshold: log ratio >= 1. Number of significant genes: 1367. Subsequent plots highlight significant genes in red.

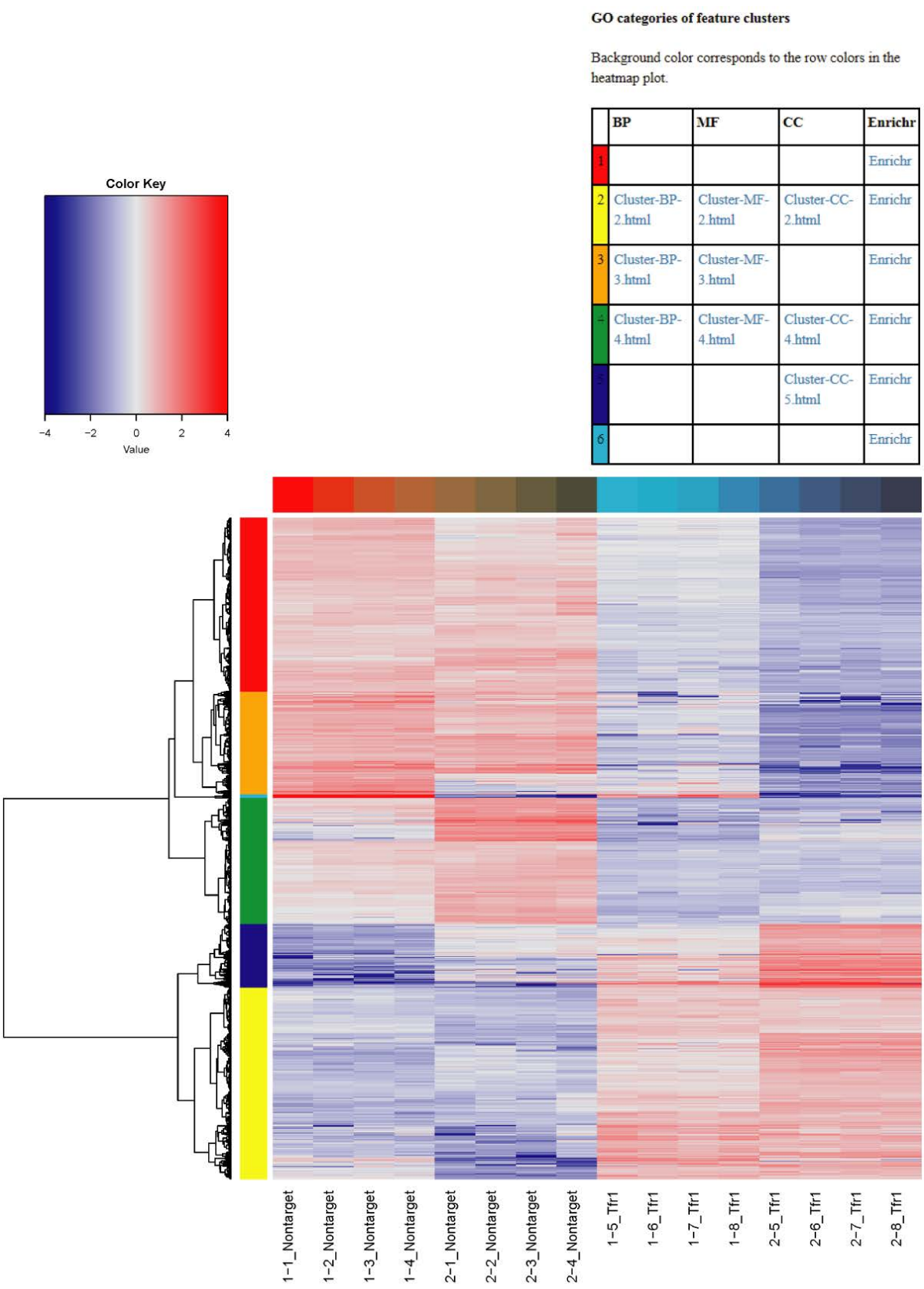

Figure 6.13 Clustering of significant features.

Table 6.1 Number of significant genes according to by p-value and fold-change (fc)

	Number of significants	False Discovery Rate (FDR)	fc >= 1	fc >= 1.5	fc >= 2	fc >= 3	fc >= 4	fc >= 8	fc >= 10
p < 0.1	10101	1.25E-01	10101	3883	1368	317	99	2	0
p < 0.05	9632	6.57E-02	9632	3870	1368	317	99	2	0
p < 0.01	8786	1.44E-02	8786	3803	1367	317	99	2	0
p < 0.001	7784	1.63E-03	7784	3652	1347	317	99	2	0
p < 1e-04	6994	1.81E-04	6994	3489	1301	317	99	2	0
p < 1e-05	6366	1.98E-05	6366	3375	1253	317	99	2	0

Table 6.2 Table of Top 48 genes expression significantly down-regulated with fc >= 4

Top No.	Gene name	Gene description	Is present	Log2 Ratio	P value	FDR
1	Tm7sf2	transmembrane 7 superfamily member 2	TRUE	-2.96	9.7E-25	7.1E-24
2	Slc1a7	solute carrier family 1 (glutamate transporter), member 7	TRUE	-2.75	2.6E-25	2.0E-24
3	Fgf11	fibroblast growth factor 11	TRUE	-2.51	1.9E-20	1.1E-19
4	Sh2d6	SH2 domain containing 6	TRUE	-2.51	1.1E-20	6.3E-20
5	Aoc3	amine oxidase, copper containing 3	TRUE	-2.45	6.5E-22	4.0E-21
6	Gm3448	predicted gene 3448	TRUE	-2.44	1.8E-13	6.7E-13
7	Tfrc	transferrin receptor 1	TRUE	-2.42	6.0E-69	3.6E-67
8	Mettl7b	methyltransferase like 7B	TRUE	-2.39	2.4E-10	7.1E-10
9	Rad23a	RAD23a homolog (S. cerevisiae)	TRUE	-2.36	1.7E-60	7.0E-59
10	2900011O08Rik	RIKEN cDNA 2900011O08 gene	TRUE	-2.36	6.4E-18	3.1E-17
11	Prnp	prion protein	TRUE	-2.35	2.1E-52	5.9E-51
12	Tecr	trans-2,3-enoyl-CoA reductase	TRUE	-2.35	2.0E-51	5.5E-50
13	Pcdhgb1	protocadherin gamma subfamily B, 1	TRUE	-2.35	4.8E-95	7.1E-93
14	Kcnc3	potassium voltage gated channel, Shaw-related subfamily, member 3	TRUE	-2.35	5.3E-41	8.7E-40
15	Plekhg4	pleckstrin homology domain containing, family G (with RhoGef domain) member 4	TRUE	-2.34	7.1E-47	1.6E-45
16	Mst1	macrophage stimulating 1 (hepatocyte growth factor-like)	TRUE	-2.34	4.3E-17	2.0E-16

17	Cdk10	cyclin-dependent kinase 10	TRUE	-2.33	1.4E-37	2.0E-36
18	Ttll11	tubulin tyrosine ligase-like family, member 11	TRUE	-2.30	3.3E-26	2.6E-25
19	Gnb3	guanine nucleotide binding protein (G protein), beta 3	TRUE	-2.29	2.6E-31	2.6E-30
20	Masp2	mannan-binding lectin serine peptidase 2	TRUE	-2.28	1.4E-34	1.7E-33
21	Fam132b	family with sequence similarity 132, member B	TRUE	-2.22	1.2E-32	1.3E-31
22	Olfml2a	olfactomedin-like 2A	TRUE	-2.22	1.5E-56	5.1E-55
23	Pcdha9	protocadherin alpha 9	TRUE	-2.22	1.8E-33	2.1E-32
24	Ndrg4	N-myc downstream regulated gene 4	TRUE	-2.22	1.2E-26	9.8E-26
25	Fam129c	family with sequence similarity 129, member C	TRUE	-2.22	9.0E-17	4.1E-16
26	Fah	fumarylacetoacetate hydrolase	TRUE	-2.21	3.0E-59	1.2E-57
27	Ulbp1	UL16 binding protein 1	TRUE	-2.21	3.6E-16	1.6E-15
28	Liph	lipase, member H	TRUE	-2.20	4.3E-10	1.2E-09
29	Tsacc	TSSK6 activating co-chaperone	TRUE	-2.20	3.7E-17	1.7E-16
30	Dgka	diacylglycerol kinase, alpha	TRUE	-2.19	3.1E-48	7.4E-47
31	Lrsam1	leucine rich repeat and sterile alpha motif containing 1	TRUE	-2.14	1.1E-35	1.5E-34
32	Flot1	flotillin 1	TRUE	-2.13	2.2E-38	3.3E-37
33	Plekhn1	pleckstrin homology domain containing, family N member 1	TRUE	-2.10	5.9E-10	1.7E-09
34	Cdk14	cyclin-dependent kinase 14	TRUE	-2.08	2.5E-80	2.2E-78
35	Tdg	thymine DNA glycosylase	TRUE	-2.06	1.5E-56	5.1E-55
36	Pcdha7	protocadherin alpha 7	TRUE	-2.06	2.1E-33	2.4E-32
37	Prmt2	protein arginine N-methyltransferase 2	TRUE	-2.05	2.1E-23	1.4E-22
38	Pycr1	pyrroline-5-carboxylate reductase 1	TRUE	-2.04	1.0E-31	1.1E-30
39	Inhbe	inhibin beta E	TRUE	-2.04	1.0E-08	2.6E-08
40	Myo7a	myosin VIIA	TRUE	-2.03	3.6E-26	2.9E-25
41	Myrip	myosin VIIA and Rab interacting protein	TRUE	-2.03	5.6E-290	3.6E-286
42	Izumo4	IZUMO family member 4	TRUE	-2.03	6.6E-19	3.4E-18

43	Lgals4	lectin, galactose binding, soluble 4	TRUE	-2.02	7.6E-12	2.5E-11
44	Bche	butyrylcholinesterase	TRUE	-2.01	6.8E-80	5.9E-78
45	Mar-04	membrane-associated ring finger (C3HC4) 4	TRUE	-2.01	1.4E-36	1.9E-35
46	Parp3	poly (ADP-ribose) polymerase family, member 3	TRUE	-2.01	2.5E-41	4.2E-40
47	Lcat	lecithin cholesterol acyltransferase	TRUE	-2.01	7.2E-17	3.3E-16
48	Map4k1	mitogen-activated protein kinase 1	TRUE	-2.00	7.9E-53	2.3E-51

Table 6.3 Table of Top 51 genes expression significantly up-regulated with fc >= 4

Top No.	Gene name	Gene description	Is present	Log2 Ratio	P value	FDR
1	2610524H06Rik	RIKEN cDNA 2610524H06 gene	TRUE	3.12	1.3E-33	1.6E-32
2	Klhdc7a	kelch domain containing 7A	TRUE	3.11	1.1E-37	1.6E-36
3	Ccdc170	coiled-coil domain containing 170	TRUE	2.98	6.0E-25	4.4E-24
4	Rab19	RAB19, member RAS oncogene family	TRUE	2.86	3.7E-14	1.4E-13
5	Cd209c	CD209c antigen	TRUE	2.85	2.0E-26	1.6E-25
6	Gm28041	predicted gene, 28041	TRUE	2.71	2.4E-13	8.5E-13
7	Gpr4	G protein-coupled receptor 4	TRUE	2.68	8.9E-26	6.9E-25
8	Gm10031	predicted pseudogene 10031	TRUE	2.58	2.1E-10	6.1E-10
9	Gm20695	predicted gene 20695	TRUE	2.51	4.6E-13	1.6E-12
10	Rgs2	regulator of G-protein signaling 2	TRUE	2.50	1.5E-21	8.9E-21
11	Mansc1	MANSC domain containing 1	TRUE	2.46	3.3E-56	1.1E-54
12	Cxcr2	chemokine (C-X-C motif) receptor 2	TRUE	2.44	5.3E-89	6.3E-87
13	Foxr1	forkhead box R1	TRUE	2.43	2.2E-22	1.4E-21
14	Trim12c	tripartite motif-containing 12C	TRUE	2.42	1.8E-45	3.7E-44
15	Pbld2	phenazine biosynthesis-like protein domain containing 2	TRUE	2.39	7.4E-123	2.2E-120
16	Park2	Parkinson disease (autosomal recessive, juvenile) 2	TRUE	2.38	7.7E-82	7.5E-80
17	Enkur	enkurin, TRPC channel interacting protein	TRUE	2.37	1.6E-50	4.4E-49
18	Adck3	aarF domain containing kinase 3	TRUE	2.36	9.5E-115	2.4E-112
19	Ccrl2	chemokine (C-C motif) receptor-like	TRUE	2.35	2.3E-16	1.0E-15

		2				
20	Xaf1	XIAP associated factor 1	TRUE	2.34	4.1E-44	7.9E-43
21	Nlrc3	NLR family, CARD domain containing 3	TRUE	2.32	3.0E-109	6.5E-107
22	Pld6	phospholipase D family, member 6	TRUE	2.30	1.1E-12	3.9E-12
23	Grxcr2	glutaredoxin, cysteine rich 2	TRUE	2.30	7.2E-15	2.9E-14
24	C730034F03Rik	RIKEN cDNA C730034F03 gene	TRUE	2.30	5.6E-68	3.2E-66
25	Trim72	tripartite motif-containing 72	TRUE	2.27	9.1E-18	4.4E-17
26	Cyp2e1	cytochrome P450, family 2, subfamily e, polypeptide 1	TRUE	2.24	5.7E-17	2.6E-16
27	Upk1b	uroplakin 1B	TRUE	2.23	2.6E-17	1.2E-16
28	1500015O10Rik	RIKEN cDNA 1500015O10 gene	TRUE	2.23	1.7E-13	6.3E-13
29	Slamf1	signaling lymphocytic activation molecule family member 1	TRUE	2.21	1.3E-131	4.6E-129
30	Ccdc62	coiled-coil domain containing 62	TRUE	2.20	1.6E-105	3.2E-103
31	Edaradd	EDAR (ectodysplasin-A receptor)-associated death domain	TRUE	2.20	1.7E-10	5.0E-10
32	Mmp17	matrix metallopeptidase 17	TRUE	2.20	4.8E-35	6.0E-34
33	Lrriq1	leucine-rich repeats and IQ motif containing 1	TRUE	2.20	1.4E-16	6.2E-16
34	Zfp819	zinc finger protein 819	TRUE	2.19	2.3E-19	1.2E-18
35	1700001P01Rik	RIKEN cDNA 1700001P01 gene	TRUE	2.16	3.4E-34	4.1E-33
36	Thbs4	thrombospondin 4	TRUE	2.15	1.3E-85	1.3E-83
37	Dmbx1	diencephalon/mesencephalon homeobox 1	TRUE	2.14	4.0E-24	2.9E-23
38	Lrrc34	leucine rich repeat containing 34	TRUE	2.13	1.8E-12	6.0E-12
39	Myl9	myosin, light polypeptide 9, regulatory	TRUE	2.13	1.4E-26	1.1E-25
40	Per2	period circadian clock 2	TRUE	2.11	6.7E-235	1.4E-231
41	Zfp791	zinc finger protein 791	TRUE	2.06	3.3E-19	1.8E-18
42	Aqp8	aquaporin 8	TRUE	2.04	5.4E-11	1.6E-10
43	Hacd4	3-hydroxyacyl-CoA dehydratase 4	TRUE	2.03	1.7E-45	3.5E-44
44	Igtp	interferon gamma induced GTPase	TRUE	2.02	3.1E-51	8.5E-50
45	Cx3cl1	chemokine (C-X3-C motif) ligand 1	TRUE	2.02	8.7E-28	7.5E-27

46	Cpne1	copine I	TRUE	2.02	1.1E-17	5.2E-17
47	Fam46b	family with sequence similarity 46, member B	TRUE	2.02	1.9E-14	7.5E-14
48	Tc2n	tandem C2 domains, nuclear	TRUE	2.02	3.7E-13	1.3E-12
49	Nipal1	NIPA-like domain containing 1	TRUE	2.02	2.4E-07	5.4E-07
50	Grb10	growth factor receptor bound protein 10	TRUE	2.00	4.4E-42	7.6E-41
51	Spef1	sperm flagellar 1	TRUE	2.00	1.9E-67	1.0E-65

6.5.6 Regulation of PrP^C expression by iron treatment in cell culture

Because Tfr1 was discovered to be involved in PrP^C expression, I wanted to regulate PrP^C expression by altering the Tfr1 level in cell culture. First, we down regulated Tfr1 in neuronal cells by adding ferric iron supplement. CAD5 cells were treated with ferric ammonium citrate (FAC, formula is $(NH_4)_5Fe(C_6H_4O_7)_2$) for 48 hours in a 384-well plate, then PrP^C protein levels were checked by PrP^C-HPFRET, cell viability assay (**Figure 6.14a**). I further validated the same treatment in a 24-well plate. Cells were harvested and lysed for BCA, then PrP^C and Tfr1 protein levels in cell lysate were checked by western blot (**Figure 6.14b**). The FAC treatment reduced PrP^C protein level in a concentration dependent manner. The 250 µg/mL FAC already yielded 20% Tfr1 reduction and more than 50% PrP^C reduction.

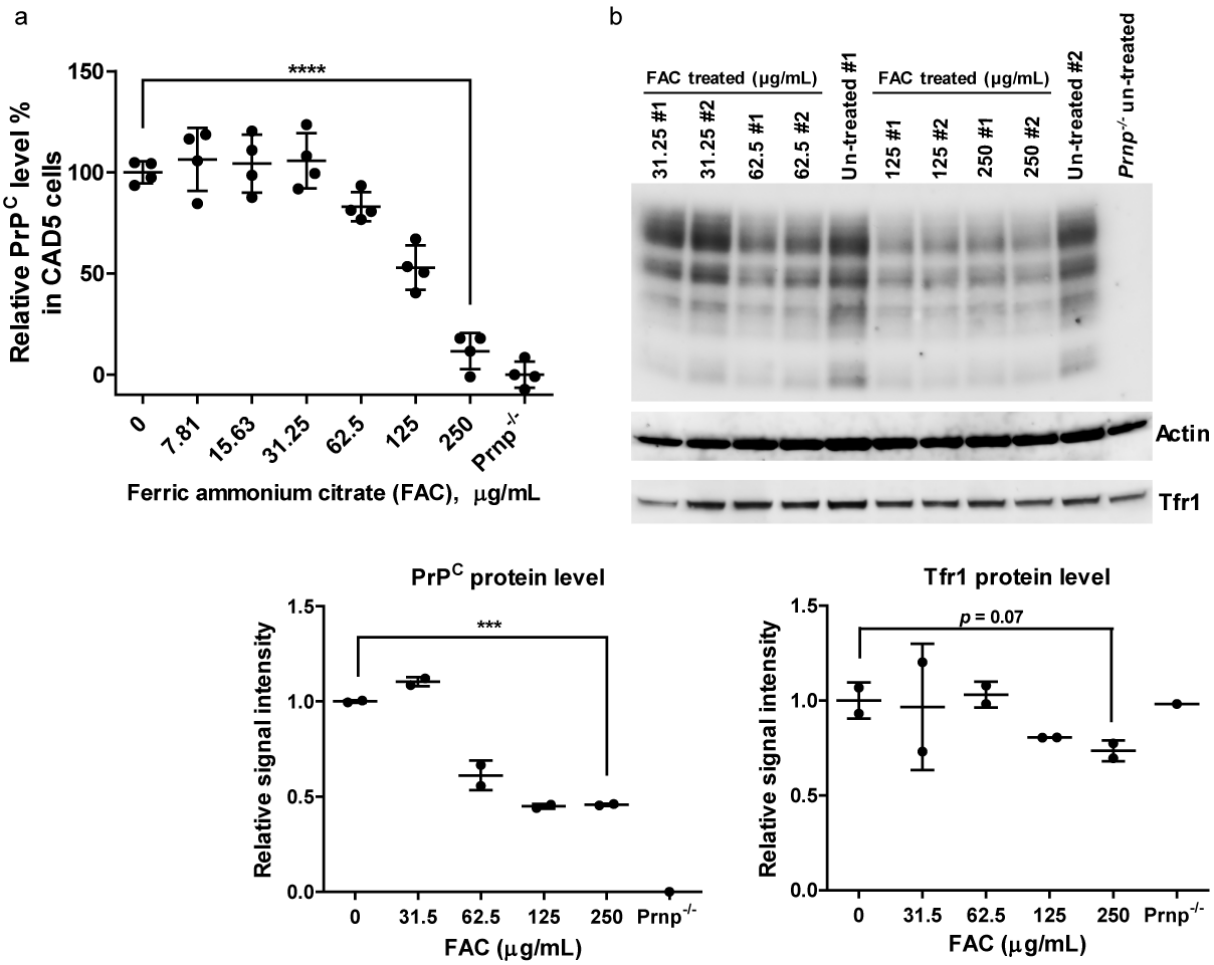

Figure 6.14 Treatment of ferric ammonium citrate in cell culture. (a) CAD5 cells were plated in a 384-well plate and treated with ferric ammonium citrate (FAC) for 48 hours. Then cell viability assay and PrP^C-HPFRET were performed to quantify PrP^C. The FAC treatment reduced PrP^C in a concentration dependent manner. The 250 µg/mL FAC treatment significantly reduced PrP^C by more than 50% (****P<0.0001). **(b)** CAD5 cells were plated in a 24-well plate and treated with FAC for 48 hours. Then cells were harvested and lysed for BCA and Western blot. The 250 µg/mL FAC yielded a 20% Tfr1 reduction and a more than 50% PrP^C reduction (***P<0.001)**.**

Next, I did ferric iron chelator treatment in CAD5 cells. The CAD5 cells were treated with iron chelator deferoxamine mesylate (DFO) for 48 hours, the PrP^C and Tfr1 protein levels were checked by PrP^C-HPFRET, cell viability assay (**Figure 6.15a**) and western blot (**Figure 6.15b**). DFO treatment increased PrP^C level in a concentration dependent manner and the 15 µg/mL DFO induced significant increase of Tfr1 and PrP^C.

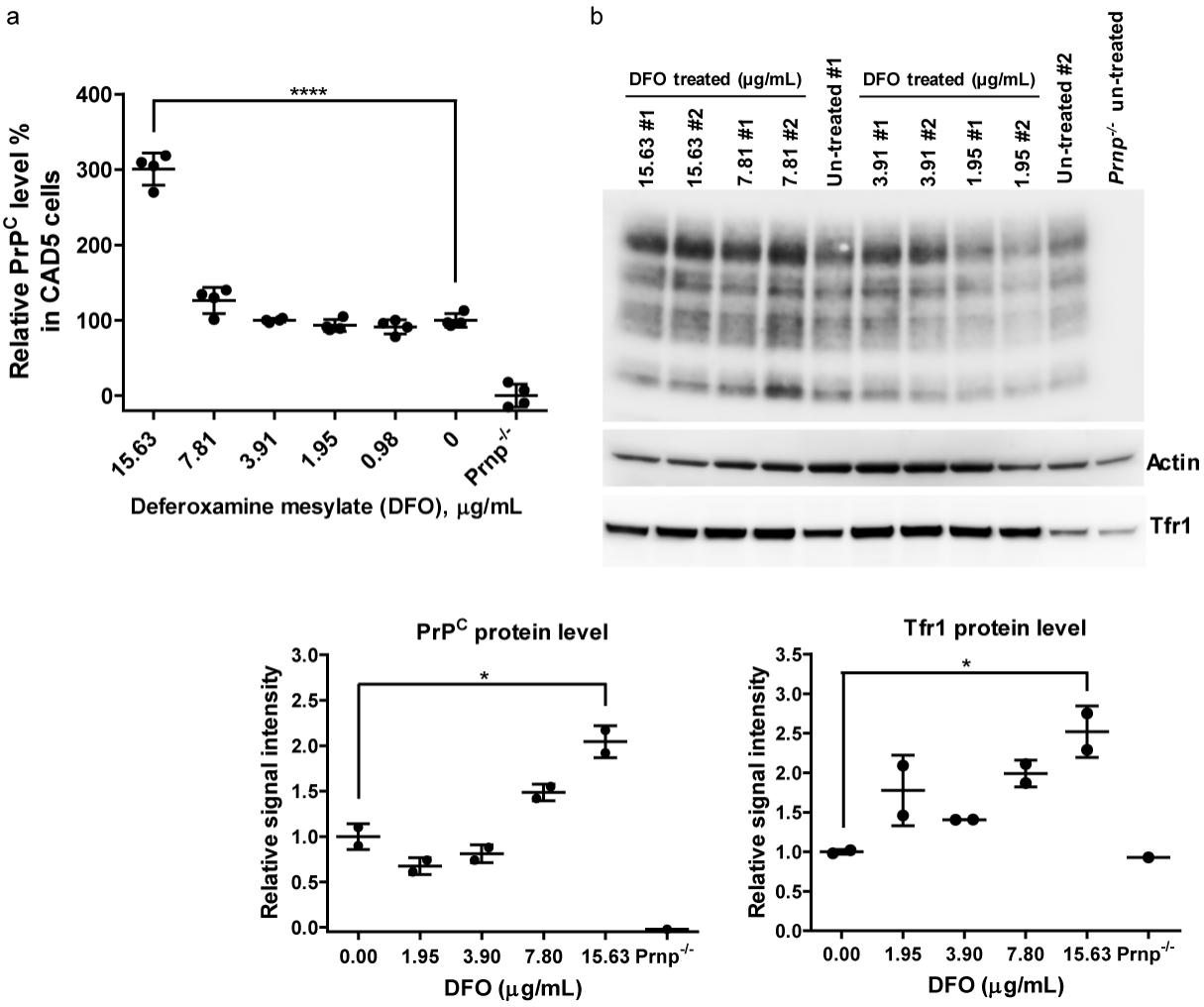

Figure 6.15 Treatment of deferoxamine mesylate in cell culture. (a) The CAD5 cells were plated in a 384-well plate and treated with deferoxamine mesylate (DFO) for 48 hours. Then the cell viability assay and PrP^C-HPFRET were performed to quantify PrP^C. The DFO treatment increased PrP^C in a concentration dependent manner. The 15 µg/mL DFO treatment significantly increased PrP^C (****P<0.0001). **(b)** CAD5 cells were plated in a 24-well plate and treated DFO for 48 hours. Then cells were harvested and lysed for BCA and Western blot. The 15 µg/mL DFO significant increased Tfr1 and PrP^C (*P<0.05).

6.5.7 Inhibition of PrP^{Sc} replication by iron treatment in cell culture

Because 250 µg/mL FAC reduced PrP^C expression by more than 50%, I wanted to inhibit PrP^{Sc} replication by FAC treatment in prion infected CAD5 cells. First, I tested FAC treatment before prion infection. CAD5 cells were treated with 250 µg/mL FAC for 24 hours in a 384-well plate and then infected with 0.1% RML6 BH. 72 hours later, PrP^{Sc} protein levels were checked by PrP^{Sc}-HPFRET, cell viability assay (**Figure 6.15 a-b**). The 250 µg/mL FAC treatment before prion infection efficiently and remarkably blocked PrP^{Sc} replication (**Figure 6.15c**). Next, I tested FAC treatment after prion infection. CAD5 cells were incubated with 0.1% RML6 BH for 24 hours and then treated with 250 µg/mL FAC. 72 hours later, PrP^{Sc} protein

levels were checked by PrP^{Sc}-HPFRET, cell viability assay (**Figure 6.15 d-e**). The 250 µg/mL FAC treatment after prion infection significantly reduced PrP^{Sc} replication (**Figure 6.15f**).

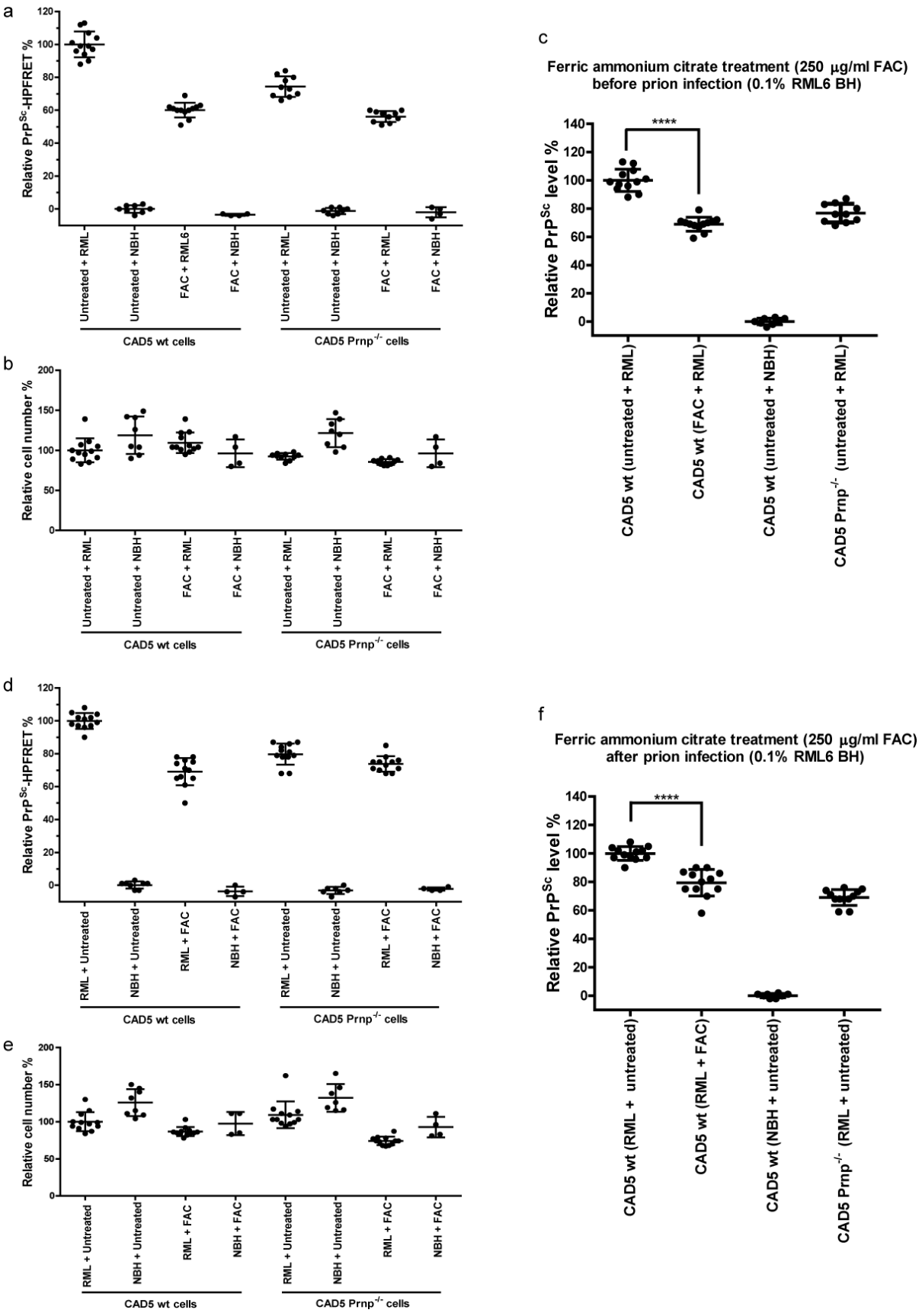

Figure 6.16 Treatment with ferric ammonium citrate before or after prion infection in cell culture. **(a-c)** CAD5 cells were plated in a 384-well plate, treated with 250 µg/mL ferric ammonium citrate (FAC) for 24 hours and then infected with 0.1% RML6 BH. After 72 hours' incubation, cell viability assay and PrP^{Sc}-HPFRET were performed to quantify PrP^{Sc}. The FAC treatment before prion infection efficiently and significantly reduced PrP^{Sc} replication (****P<0.0001). **(e-f)** CAD5 cells were plated in a 384-well plate, infected with 0.1% RML6 BH for 24 hours and then treated with 250 µg/mL ferric ammonium citrate (FAC). After 72 hours' incubation, cell viability assay and PrP^{Sc}-HPFRET were performed to quantify PrP^{Sc}. The FAC treatment after prion infection significantly reduced PrP^{Sc} replication (****P<0.0001).

6.5.8 Regulation of PrP^C expression by iron treatment in mouse model

To explore the potential of iron supplement for prion therapy, I performed the following *in vivo* experiments. 1) The wild-type C57BL/6 mice were fed an iron deficient diet for three weeks. The preliminary result showed that PrP^C levels in brains were significantly increased in the iron deficient diet mice compared to the normal diet mice (**Figure 6.17a**). 2) The intraperitoneal (i.p.) injection of ferri carboxymaltosum (ferinject® from Vifor) into wild-type C57BL/6 mice. The iron injection was performed three times per week for 4 weeks with, and then PrP^C expression level in mouse brain was checked by PrP^C-HPFRET (**Figure 6.17b**) and Western blot (**Figure 6.17c**). PrP^C protein levels in brains were significantly reduced in iron injected mice compared to PBS injected mice.

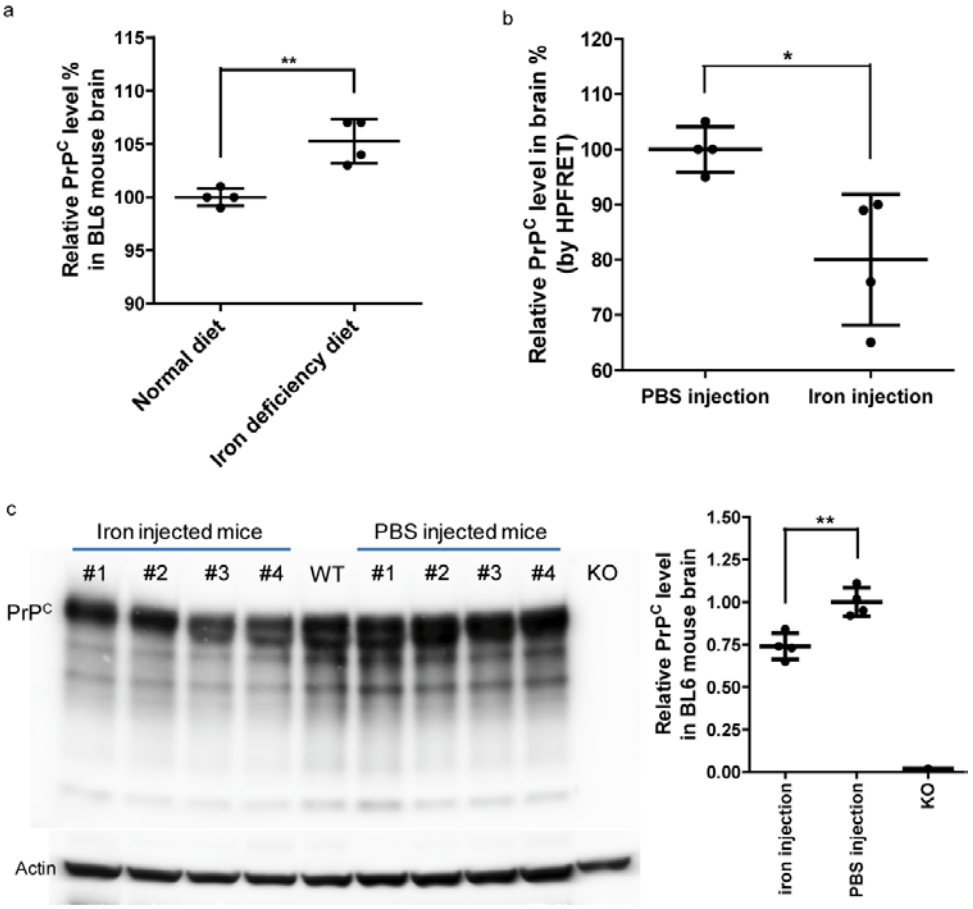

Figure 6.17 Regulation of PrP^C expression in mouse brains by iron treatment. (a) Wild-type C57BL/6 mice were fed an iron deficient diet for three weeks. Control group mice were fed normal diet. The PrP^C proteins in brain homogenate were detected by PrP^C-HPFRET. PrP^C levels in the iron deficient diet mouse brains were significantly increased compared to the normal diet mice (**P<0.01). **(b-c)** Wild-type C57BL/6 mice were intraperitoneal (i.p.) injected with ferri carboxymaltosum (ferinject® from Vifor) for 4 weeks with three times per week. PrP^C expression level in mouse brain was checked by PrP^C-HPFRET and Western blot. PrP^C protein levels in brains were significantly reduced in ferri carboxymaltosum injected mice compared to PBS injected mice (*P<0.05, **P<0.01).

6.6 Discussion

Recent research has revealed novel functions of the endocytic membrane system, implying that endocytosis could be a master organizer of signalling circuits that resolve signals in space and time for cellular communication and interactions with the environment, not only for the internalization of nutrients and membrane associated molecules (Scita and Di Fiore 2010, Liberali, Snijder et al. 2014). However, endocytic RNAi HTS and the relevant systematic analysis have not been achieved in prion research. For the first part of my thesis, I established PrP^C-HPFRET and PrP^{Sc}-HPFRET, which are highly adapted to automated high-throughput screening platforms for basic and applied prion research. Specifically, this technique facilitates high-throughput screening for the identification of chemicals interfering with prion secretion, prion infection, and/or prion replication, and genome-wide RNAi or CRISPR/Cas9 screens aimed at understanding the molecular mechanisms of prion transmissibility and replication. Therefore, for the second part of my thesis, I combined the newly developed PrP-HPFRET assays with RNAi HTS technologies to identify genes regulating endogenous cellular prion protein expression. In addition, I established an automated PrP-HPFRET based high-throughput siRNA screening platform and screened 3153 mouse siRNAs targeting 780 genes that are involved in endocytic membrane trafficking pathways.

From the siRNA HTS of endocytosis genes, I found an interesting candidate gene, Tfr1, that silences Tfr1 efficiently, repressing endogenous PrP^C expression through transcriptional or post-transcriptional regulation, and thus blocks PrP^{Sc} replication in neuronal cells. The well-known function of Tfr1, a homodimeric type II transmembrane glycoprotein, is involved in iron uptake and cell growth regulation (Neckers and Trepel 1986). A Tfr1 protein can internalize up to four ferric ions during one cycle of Tfr1-mediated endocytosis, which has been recently characterized as a useful target for cancer therapy (Daniels, Delgado et al. 2006, Tortorella and Karagiannis 2014). In my experiments, iron treatment in cell culture model confirmed that altering Tfr1 level can affect PrP^C expression in neuronal cells, suggesting that Tfr1 could be a novel therapeutic target to supress cellular prion protein for prion diseases.

6.7 Outlook

To better understand the role of endocytosis-relevant genes on prion protein expression, additional data analysis will continue over the next several months. The raw screening data is still under analysis by our collaborating bioinformaticians for off-targeting analysis, the functional interaction networks and pathways analysis, druggable candidate genes as well as database mining for available compounds. Afterwards, any interesting druggable genes (besides Tfr1) will be validated and relevant compounds will be tested by *in vitro* and *in vivo* models.

To further understand the mechanism of Tfr1 on PrP^C expression, our collaborating bioinformaticians will continue to analyze RNAseq data from the Tfr1-siRNA transfected CAD5 cells. Ninety-nine significant expression changes with >4-fold-change, p<1e-5 were identified. Interestingly, the expression levels of selected important genes related to neurodegenerative diseases were significantly changed by Tfr1-siRNA treatment. For example, the Park2 (Parkinson disease autosomal recessive, juvenile 2) gene expression was significantly up regulated with a 5.2-fold-change, p<1e-5, the Mapt (microtubule-associated protein tau) was significantly downregulated with a 2.8-fold-change, p<1e-5. Therefore, I hope that we will find highly related clusters and pathways based on the RNAseq data, which could provide us with additional insight to guide later studies.

To explore the potential of iron supplement for prion therapy, some *in vivo* experiments have been carried out: 1) Preliminary results showed that PrP^C expression was significantly reduced in the brains of C57BL/6 mice, which were fed an iron-deficient diet for three weeks, compared to the normal diet mice. 2) Another experiment involved was intraperitoneal (i.p.) injection of ferri carboxymaltosum (ferinject® from Vifor) into wild-type C57BL/6 mice for assessment of PrP^C expression in the brains. The results showed that the PrP^C expression was remarkably reduced in the brains of wild-type C57BL/6 mice i.p. injected with ferri carboxymaltosum, Therefore, we propose to treat chronically prion-infected mice with iron, to determine whether the incubation time of prion disease is prolonged.

6.8 Material and Methods

6.8.1 Chemicals and tissue homogenate

Chemicals for buffers were purchased from Sigma-Aldrich. Mouse brain tissue was homogenized in 0.32 M sucrose (or PBS) to 10% (w/v, 100 mg of tissue per 900 µl homogenization buffer) and stored at -80°C. The protein concentration was determined using the bicinchoninic acid assay (Pierce).

6.8.2 Mouse prion susceptible neuronal cell line

Mouse cell line CAD-2A2D5 (CAD5) cells were derived from Cath.a-differentiated cells (Mahal, Baker et al. 2007). Mouse cell line N2aPK1(Klohn, Stoltze et al. 2003) was a subclone of the neuroblastoma cell line (N2a).

6.8.3 Murine siRNA screen

1) Murine siRNA library

An arrayed murine siRNA library in 96-well plates was provided by the Novartis Institute for BioMedical Research. The siRNA samples were reformatted from 96-well source plates into 384-well source plates that were specifically used for making siRNA stamps on the Labcyte Echo acoustic liquid handling platform. Then siRNA controls were dispensed using the “Plate Reformat” program and siRNA samples were dispensed using the “Cherry Pick” program with sample picking lists (**Figure 6.18**). The assay plates were stored in a -40°C freezer.

The sequence of the control Prnp-siRNA (from ambion by life technologies, siRNA ID # s72188) is: 5´-CGUGAAAACAUGUACCGCUtt-3´. The control nontarget-siRNA was purchased from Ambion by Life Technologies as well: Select Negative Control No. 1 siRNA, catalog number is 4390844.

a Printing control siRNA using protocol of Echo Plate Reformat

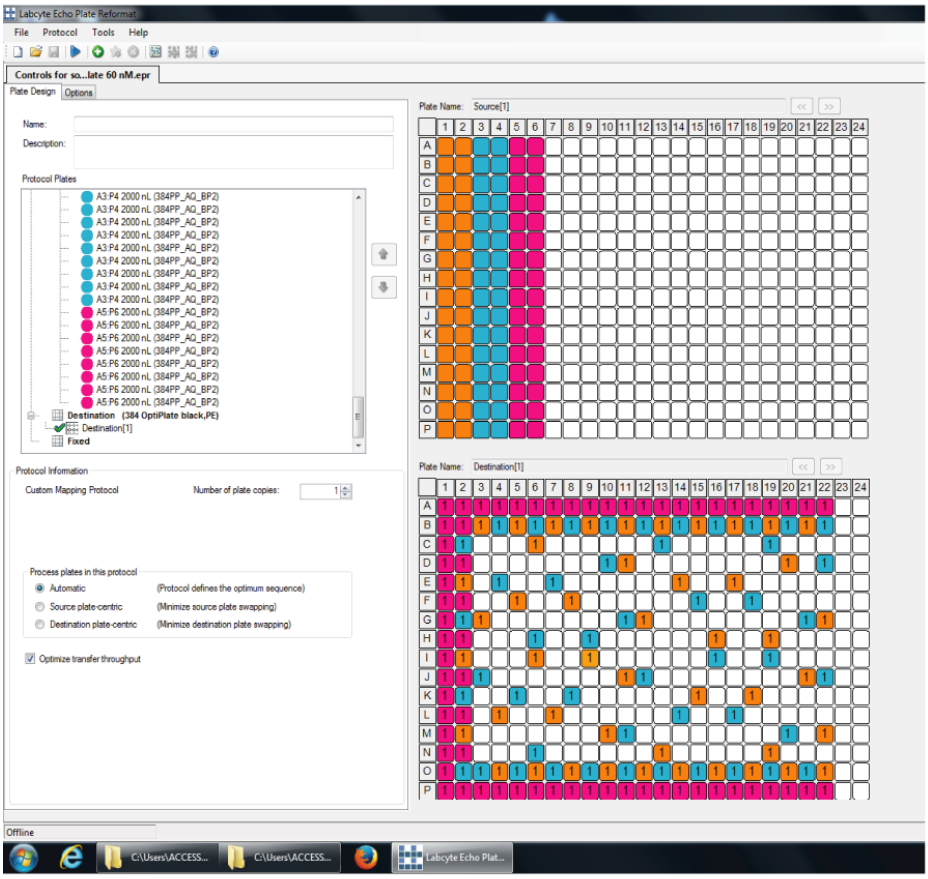

Pos control: Prnp_siRNA1

Neg control: Nontarget-siRNA

Untreated (no siRNA)

b Printing sample siRNA using protocol of Echo Cherry Pick

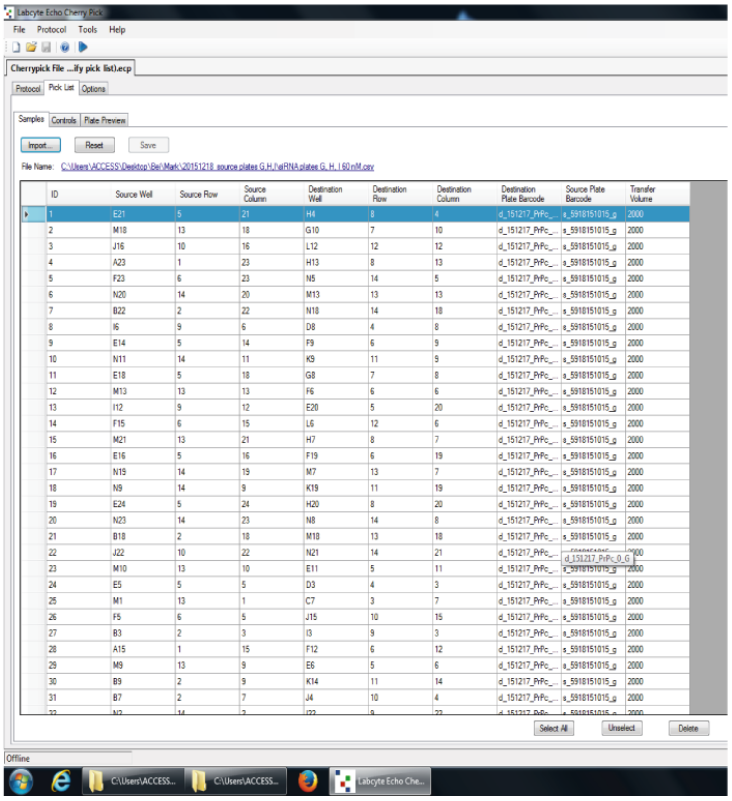

Sample picking list offers unique ID for each siRNA.

Figure 6.18 Making siRNA stamps in 384-well plates by Labcyte Echo acoustic liquid handling platform. (a) siRNA controls were dispensed using the "Plate Reformat" program. **(b)** siRNA samples were dispensed using the "Cherry Pick" program with sample picking lists.

2) siRNA transfection in CAD5 cells

The siRNA stamps were thawed to room temperature. Plates were centrifuged at 2000rpm x 1min. The transfection mix was prepared according to Lipofectamine® RNAiMAX Reagent Protocol. 4ul of transfection mix was dispensed into each well. Plates were centrifuged at 2000rpm x 1min incubated at room temperature for 10 minutes. Cells were harvested when TPP Tissue Culture (T300) flasks were 80% confluent. A cell suspension was made at the desired density in an assay medium that contained the CAD5 cell suspension at 2800 cells/15 µl/well in Opti-MEM® I Reduced-Serum Medium (no phenol red) plus 10% FBS (HyClone). 15 µl of cell suspension was dispensed into each well containing siRNA and the transfection mix. Plates were incubated at 37°C and 5% CO_2 for 24 hrs. Then 20 µl of 0.5x Realtime-Glo (Promega, catalog number is G9713) in OFBS medium was dispensed into each well. Plates were incubated at 37°C and 5% CO_2 for 48 hrs.

3) Cell viability assay and PrP^C-HPFRET assays

72 hours after adding Realtime-Glo, plates were taken out from incubator and the Realtime-Glo luminescence in each well was detected by Envision Multilabel Reader. The RealTime-Glo™ cell viability assay determines the number of viable cells in culture by measuring the reducing potential of cells and thus metabolism. The assay involves adding NanoLuc® luciferase and a cell-permeant prosubstrate, the cell viability substrate, to cells in culture. Viable cells reduce the proprietary prosubstrate to generate a substrate for NanoLuc luciferase. This substrate diffuses from cells into the surrounding culture medium, where it is rapidly used by the NanoLuc enzyme to produce a luminescent signal. The signal correlates with the number of viable cells. Both the cell viability substrate and NanoLuc enzyme are stable in complete cell culture medium at 37°C for at least 72 hours. No cell washing, removal of medium or further reagent addition is required to determine the number of viable cells.

Immediately after reading the Realtime-Glo, PrP^C-HPFRET was performed in 384-well plates with the following steps: 1) cell lysis: 10 µl/well of 5x standard lysis buffer was dispensed in each well without medium removal. The final concentration in each well was 1x standard lysis buffer. The plate was shaken at 37°C for 10 min at 700 rpm. 2) FRET antibody pair incubation: FRET antibody pair Eu^{2+}-POM19 and APC-POM1 stock was diluted with 1x Lance buffer to 30 nM (concentration of POM antibody) and 60 nM (concentration of POM antibody). 5 µl/well of 30 nM Eu^{2+}-POM19 and 5 µl/well of 60nM APC-POM1 were added

separately. The plate was shaken at 37°C for 1 h at 300 rpm. 3) The DPICA plate's clear bottom was sealed with white BackSeal-384 (PerkinElmer) for the top read of time-resolved FRET. The FRET signal of PrP^C in each well was detected by EnVision Multilabel Reader.

Table 6.4 Overview of protocols for the PrP^C screen

	Reagent	Experiment volume	Working conc.	Tool	
siRNA printing	Control siRNA	2 ul/well	60 nM	Echo	
	Seal plates, store plates in -40°C			-40°C freezer	
Day 1	OptiMEM	4 ul/well		Biotek MultiFlo FX (Peristaltic pump)	1 µL cassette
	Lipofectamine RNAiMAX	1 ul/well			1 µL cassette
	For siRNA-lipid mixture formation: 1 min centrifugation at 2000rpm, incubate 10 min at RT			Plate centrifuge	
	WT CAD5 cells	15 ul/well	2800 cells/well	Biotek MultiFlo FX (Peristaltic pump)	5 µL cassette
	KO CAD5 cells	15 ul/well	2800 cells/well		5 µL cassette
Day 2	RT-Glo medium (P/S)	20 ul/well	0.25 x		5 µL cassette
48h incubation				Cell culture incubator	
Day 4	Read RT-Glo luminecence			Envision	
	5x lysis buffer	10 ul/well	1x	Biotek MultiFlo FX (Peristaltic pump)	5 µL cassette
	Seal plates, 700 rpm shaking 15min at RT			multiple-plates shaker	
	Eu^{2+}-POM19	5 ul/well	2.5 nM	Biotek MultiFlo FX (Peristaltic pump)	1 µL cassette
	APC-POM1	5 ul/well	5 nM		1 µL cassette
	Seal plates, 700 rpm shaking 1h at 37°C			multiple-plates shaker	
	Read FRET			Envision Multilabel Reader	

6.8.4 Screen data analysis

The screening raw data was analyzed by collaborating bioinformaticians (Prof. Ioannis Xenarios' lab, University of Lausanne) for the quality control reports, off-targeting analysis, hits selection and network pathway analysis.

6.8.5 RNA sequencing

Total RNA was isolated from cultured CAD5 cells using the RNeasy mini kit (QIAGEN). RNA quality was analyzed by Bioanalyzer 2100 (Agilent Technologies). RNAs with RIN>9 were

used to prepare library for the polyA-selected approach. The TruSeq RNA Sample Prep kit v2 (Illumina) was used in the following steps. In brief, total RNA samples (1 µg) were poly A enriched and reverse transcribed into double-stranded cDNA. TruSeq adapters were ligated to double-stranded cDNA. Fragments containing TruSeq adapters on both ends were selectively enriched with PCR. Quality and the quantity of enriched libraries was validated using Qubit (1.0) Fluorometer and Caliper GX LabChip GX (Caliper Life Sciences). The product was a smear with a mean fragment size of ~260 bp. Libraries were normalized to 10 nM in Tris-Cl 10 mM, pH 8.5, with 0.1% (vol/vol) Tween 20.

TruSeq PE Cluster kit v4-cBot-HS (Illumina) was used for cluster generation using 2 pM of pooled normalized libraries on the cBOT. Sequencing was performed on Illumina HiSeq 2500 at 1 × 100 bp using the TruSeq SBS kit v4-HS (Illumina). Reads were quality-checked using FastQC.

6.8.6 qRT-PCR.

Total RNA from each brain was extracted using RNeasy mini Kit (QIAGEN). The quality of RNA was analyzed by Bioanalyzer 2100 (Agilent Technologies), RNAs with RIN>7 were used for cDNA synthesis. cDNA were synthesized from ~1 µg total RNA using QuantiTect Reverse Transcription kit (QIAGEN) according to the manufacturer's instruction. Quantitative real-time PCR (qRT-PCR) was performed using the SYBR Green PCR Master Mix (Roche) on a ViiA7 Real-Time PCR system (Applied Biosystems). Expression levels were normalized using Gapdh. The sequence of qRT-PCR primers are as follows: Gapdh sense, 5´-CCA CCC CAG CAA GGA GAC T-3´; antisense, 5´-GAA ATT GTG AGG GAG ATG CT-3´. Prnp sense, 5´-GCC AGT GGA TCA GTA CAG CA-3´; antisense, 5´-ATC CCA CGA TCA GGA AGA TG-3´. Tfr1 sense, 5´-CAT GAG GGA AAT CAA TGA TCG TA-3´; antisense, 5´-GCC CCA GAA GAT ATG TCG GAA-3´.

6.8.7 Western blot analysis

To detect PrP^{C}, cells were washed once with PBS and lysed with RIPPA buffer. The cell lysate was centrifuged at 14000g for 20min at 4°C. The supernatant was removed. The total protein concentration was determined using the bicinchoninic acid assay (Pierce). Approximately 15 µg of proteins were loaded and separated on a 12% Bis-Tris polyacrylamide gel (NuPAGE; Invitrogen, Waltham, MA, USA) and then blotted onto a nitrocellulose membrane. Membranes were blocked with 5% wt/vol Topblock (Sigma-Aldrich, Fluka, 37766, manufactured by Juro AG, Lucerne, Switzerland) in PBS supplemented with 0.05% Tween 20 (vol/vol) and incubated with primary antibodies POM1 in 1% Topblock (200 ng mL−1) overnight. After washing, the membranes were incubated with a secondary antibody horseradish peroxidase (HRP)-conjugated rabbit anti–mouse IgG1 (1:10,000,

Zymed). Blots were developed using Luminata Crescendo Western HRP substrate (Millipore, Billerica, MA, USA) was visualized using the Stella system (model 3000, Bio-Rad). To avoid variation in loading, the same blots were striped and incubated with an anti-actin antibody (1:10,000, Millipore). The PrP^C signals were normalized to actin as a loading control.

To detect Tfr1 in cell lysate, approximately 15 µg of proteins were loaded and separated on a 12% Bis-Tris polyacrylamide gel (NuPAGE; Invitrogen, Waltham, MA, USA) and then blotted onto a nitrocellulose membrane. Membranes were blocked with 5% wt/vol Topblock (Sigma-Aldrich, Fluka, 37766, manufactured by Juro AG, Lucerne, Switzerland) in PBS supplemented with 0.05% Tween 20 (vol/vol) and incubated with primary antibodies Tfr1 (1:1,000, Invitrogen) in 1% Topblock overnight. After washing, the membranes were then incubated with secondary antibody horseradish peroxidase (HRP)-conjugated goat anti–mouse IgG1 (1:5,000, Jackson ImmunoResearch). Blots were developed using Luminata Crescendo Western HRP substrate (Millipore, Billerica, MA, USA) and visualized using the Stella system (model 3000, Bio-Rad). To avoid the variation in loading, the same blots were striped and incubated with an anti-actin antibody (1:10,000, Millipore). The Tfr1 signals were normalized to actin as a loading control.

6.8.8 Iron treatment in neuronal cells

CAD5 cells were harvested when TPP Tissue Culture (T150) flasks were 80% confluent. A cell suspension was made at the desired density in OFBS medium. Ammonium iron (III) citrate (sigma, F5879-100G) or deferoxamine mesylate salt (Sigma, D9533-1G) was diluted to the desired concentration with OFBS medium and added to the plates. Plates were incubated at 37°C and 5% CO_2 for 48 hrs. For the 384-well plates, the cell viability assay and PrP^C-HPFRET were performed to quantify PrP^C. For 24-well plates, the cells were harvested from the plates and lysed for BCA and Western blot analysis of the total proteins in the cell lysate.

6.8.9 Iron treatment before or after prion infection in neuronal cells

CAD5 cells were harvested when TPP Tissue Culture (T150) flasks were 80% confluent. A cell suspension was made at the desired density in OFBS medium, 1000 cells/well cells or were added into 384-well plates. CAD5 $Prnp^{-/-}$ cells were used as negative controls.

For iron treatment before prion infection: 1) Ammonium iron (III) citrate (sigma, F5879-100G) was diluted to the desired concentration (end conc. was 250 µg/mL) with OFBS medium and added to the plates, and plates were incubated at 37°C and 5% CO_2 for 24 hrs; 2) RML6 BH was diluted to the desired concentration (end conc. was 0.1%) with OFBS medium and added to the plates, and plates were incubated at 37°C and 5% CO_2 for 24 hrs; 3) Realtime-Glo was diluted to the desired concentration (end conc. was 0.25x) with OFBS medium and

added to the plates, and plates were incubated at 37°C and 5% CO_2 for 48 hrs; 4) The cell viability assay and PrP^{Sc}-HPFRET were performed to quantify PrP^{Sc}.

For iron treatment after prion infection: 1) RML6 BH was diluted to the desired concentration (end conc. was 0.1%) with OFBS medium and added to the plates, and plates were incubated at 37°C and 5% CO_2 for 24 hrs; 2) Ammonium iron (III) citrate (sigma, F5879-100G) was diluted to the desired concentration (end conc. was 250 µg/mL) with OFBS medium and added to the plates, and plates were incubated at 37°C and 5% CO_2 for 24 hrs; 3) Realtime-Glo was diluted to the desired concentration (end conc. was 0.25x) with OFBS medium and added to the plates, and plates were incubated at 37°C and 5% CO_2 for 48 hrs; 4) the cell viability assay and PrP^{Sc}-HPFRET were performed to quantify PrP^{Sc}.

6.8.10 Iron treatment in mice

Wild-type C57BL/6 mice were fed an iron deficient diet for three weeks. Control group mice were fed normal diet. Then brains were collected from mice and homogenized in 0.32M sucrose. The total protein in BH was measured by BCA and then PrP^{C} proteins in BH were detected by PrP^{C}-HPFRET.

Wild-type C57BL/6 mice were intraperitoneal (i.p.) injected with ferri carboxymaltosum (ferinject® from Vifor). The injection dose was 500µg/g body weight. Control group mice were injected by PBS. The injection was performed totally 4 weeks with three times per week. Then brains were collected from mice and homogenized in 0.32M sucrose. The total protein in BH was measured by BCA and then PrP^{C} proteins in BH were detected by PrP^{C}-HPFRET and Western blot.

6.8.11 Statistical analysis.

Results are presented as the mean of replicas ± standard error of the mean (SEM). Statistical significance between experimental groups was assessed using an unpaired Student's t-Test or two-way analysis of variance (ANOVA). *p*-values <0.05 were considered statistically significant.

7 References

Aguzzi, A. (2009). "Cell biology: Beyond the prion principle." Nature **459**(7249): 924-925.

Aguzzi, A., F. Baumann and J. Bremer (2008). "The prion's elusive reason for being." Annual Review of Neuroscience **31**: 439-477.

Aguzzi, A. and A. M. Calella (2009). "Prions: Protein Aggregation and Infectious Diseases." Physiological Reviews **89**(4): 1105-1152.

Aguzzi, A., M. Heikenwalder and M. Polymenidou (2007). "Mechanisms of disease - Insights into prion strains and neurotoxicity." Nature Reviews Molecular Cell Biology **8**(7): 552-561.

Aguzzi, A. and A. K. Lakkaraju (2016). "Cell Biology of Prions and Prionoids: A Status Report." Trends Cell Biol **26**(1): 40-51.

Aguzzi, A., M. Nuvolone and C. Zhu (2013). "The immunobiology of prion diseases." Nat Rev Immunol **13**(12): 888-902.

Aguzzi, A. and M. Polymenidou (2004). "Mammalian prion biology: One century of evolving concepts." Cell **116**(2): 313-327.

Aguzzi, A. and C. Zhu (2012). "Five questions on prion diseases." PLoS Pathog **8**(5): e1002651.

Basler, K., B. Oesch, M. Scott, D. Westaway, M. Walchli, D. F. Groth, M. P. McKinley, S. B. Prusiner and C. Weissmann (1986). "Scrapie and cellular PrP isoforms are encoded by the same chromosomal gene." Cell **46**(3): 417-428.

Bauman, P. A., L. A. Lawrence, L. Biesert, H. Dichtelmuller, F. Fabbrizzi, R. Gajardo, A. Groner, J. I. Jorquera, C. Kempf, T. R. Kreil, I. von Hoegen, D. Y. Pifat, S. R. Petteway, Jr. and K. Cai (2006). "Critical factors influencing prion inactivation by sodium hydroxide." Vox Sang **91**(1): 34-40.

Bellon, A., E. Comoy, S. Simoneau, S. Mornac, C. Dehen, A. Perrin, A. Arzel, S. Arrabal, H. Baron, H. Laude, B. You, J. P. Deslys and B. Flan (2014). "Decontamination of prions in a plasma product manufacturing environment." Transfusion **54**(4): 1028-1036.

Bolton, D. C., M. P. Mckinley and S. B. Prusiner (1982). "Identification of a Protein That Purifies with the Scrapie Prion." Science **218**(4579): 1309-1311.

Borchelt, D. R., M. Scott, A. Taraboulos, N. Stahl and S. B. Prusiner (1990). "Scrapie and Cellular Prion Proteins Differ in Their Kinetics of Synthesis and Topology in Cultured-Cells." Journal of Cell Biology **110**(3): 743-752.

Brandner, S., S. Isenmann, A. Raeber, M. Fischer, A. Sailer, Y. Kobayashi, S. Marino, C. Weissmann and A. Aguzzi (1996). "Normal host prion protein necessary for scrapie-induced neurotoxicity." Nature **379**(6563): 339-343.

Brandner, S., A. Raeber, A. Sailer, T. Blattler, M. Fischer, C. Weissmann and A. Aguzzi (1996). "Normal host prion protein (PrPc) is required for scrapie spread within the central nervous system." Proceedings of the National Academy of Sciences of the United States of America **93**(23): 13148-13151.

Bremer, J., F. Baumann, C. Tiberi, C. Wessig, H. Fischer, P. Schwarz, A. D. Steele, K. V. Toyka, K. A. Nave, J. Weis and A. Aguzzi (2010). "Axonal prion protein is required for peripheral myelin maintenance." Nature Neuroscience **13**(3): 310-U319.

Brown, P., A. Wolff and D. C. Gajdusek (1990). "A simple and effective method for inactivating virus infectivity in formalin-fixed tissue samples from patients with Creutzfeldt-Jakob disease." Neurology **40**(6): 887-890.

Bueler, H., A. Aguzzi, A. Sailer, R. A. Greiner, P. Autenried, M. Aguet and C. Weissmann (1993). "Mice devoid of PrP are resistant to scrapie." Cell **73**(7): 1339-1347.

Bueler, H., M. Fischer, Y. Lang, H. Bluethmann, H. P. Lipp, S. J. Dearmond, S. B. Prusiner, M. Aguet and C. Weissmann (1992). "Normal Development and Behavior of Mice Lacking the Neuronal Cell-Surface Prp Protein." Nature **356**(6370): 577-582.

Caughey, B. and P. T. Lansbury (2003). "Protofibrils, pores, fibrils, and neurodegeneration: Separating the responsible protein aggregates from the innocent bystanders." Annual Review of Neuroscience **26**: 267-298.

Caughey, B., G. J. Raymond, D. A. Kocisko and P. T. Lansbury (1997). "Scrapie infectivity correlates with converting activity, protease resistance, and aggregation of scrapie-associated prion protein in guanidine denaturation studies." Journal of Virology **71**(5): 4107-4110.

Chakrabarti, O., A. Ashok and R. S. Hegde (2009). "Prion protein biosynthesis and its emerging role in neurodegeneration." Trends in Biochemical Sciences **34**(6): 287-295.

Chandler, R. L. (1961). "Encephalopathy in Mice Produced by Inoculation with Scrapie Brain Material." Lancet **1**(719): 1378-&.

Chesebro, B., M. Trifilo, R. Race, K. Meade-White, C. Teng, R. LaCasse, L. Raymond, C. Favara, G. Baron, S. Priola, B. Caughey, E. Masliah and M. Oldstone (2005). "Anchorless prion protein results in infectious amyloid disease without clinical scrapie." Science **308**(5727): 1435-1439.

Cohen, S. I., M. Vendruscolo, C. M. Dobson and T. P. Knowles (2011). "Nucleated polymerization with secondary pathways. III. Equilibrium behavior and oligomer populations." J Chem Phys **135**(6): 065107.

Collins, S., C. A. McLean and C. L. Masters (2001). "Gerstmann-Straussler-Scheinker syndrome,fatal familial insomnia, and kuru: a review of these less common human transmissible spongiform encephalopathies." J Clin Neurosci **8**(5): 387-397.

Cuille J and Chelle PL (1939). "Experimental transmission of trembling to the goat." C R Seances Acad Sci **208**: 1058-1160.

Daniels, T. R., T. Delgado, J. A. Rodriguez, G. Helguera and M. L. Penichet (2006). "The transferrin receptor part I: Biology and targeting with cytotoxic antibodies for the treatment of cancer." Clinical Immunology **121**(2): 144-158.

Daude, N., M. Marella and J. Chabry (2003). "Specific inhibition of pathological prion protein accumulation by small interfering RNAs." Journal of Cell Science **116**(13): 2775-2779.

Dodelet, V. C. and N. R. Cashman (1998). "Prion protein expression in human leukocyte differentiation." Blood **91**(5): 1556-1561.

Dougherty, R. (1964). "Animal virus titration techniques." Tech Exp Virol.: 183-186.

Falsig, J., T. Sonati, U. S. Herrmann, D. Saban, B. Li, K. Arroyo, B. Ballmer, P. P. Liberski and A. Aguzzi (2012). "Prion Pathogenesis Is Faithfully Reproduced in Cerebellar Organotypic Slice Cultures." Plos Pathogens **8**(11).

Fischer, M., T. Rulicke, A. Raeber, A. Sailer, M. Moser, B. Oesch, S. Brandner, A. Aguzzi and C. Weissmann (1996). "Prion protein (PrP) with amino-proximal deletions restoring susceptibility of PrP knockout mice to scrapie." Embo Journal **15**(6): 1255-1264.

Ford, M. J., L. J. Burton, R. J. Morris and S. M. Hall (2002). "Selective expression of prion protein in peripheral tissues of the adult mouse." Neuroscience **113**(1): 177-192.

Forman, M. S., J. Q. Trojanowski and V. M. Lee (2004). "Neurodegenerative diseases: a decade of discoveries paves the way for therapeutic breakthroughs." Nat Med **10**(10): 1055-1063.

Friberg, K. N., G. Hung, E. Wancewicz, K. Giles, C. Black, S. Freier, F. Bennett, S. J. DeArmond, Y. Freyman, P. Lessard, S. Ghaemmaghami and S. B. Prusiner (2012). "Intracerebral Infusion of Antisense Oligonucleotides Into Prion-infected Mice." Molecular Therapy-Nucleic Acids **1**.

Frontzek, K., M. I. Lutz, A. Aguzzi, G. G. Kovacs and H. Budka (2016). "Amyloid-beta pathology and cerebral amyloid angiopathy are frequent in iatrogenic Creutzfeldt-Jakob disease after dural grafting." Swiss Med Wkly **146**: w14287.

Gajdusek, D. C. (1977). "Unconventional viruses and the origin and disappearance of kuru." Science **197**(4307): 943-960.

Gajdusek, D. C. (1988). "Transmissible and Non-Transmissible Amyloidoses - Autocatalytic Post-Translational Conversion of Host Precursor Proteins to Beta-Pleated Sheet Configurations." Journal of Neuroimmunology **20**(2-3): 95-110.

Gajdusek, D. C., C. J. Gibbs and M. Alpers (1966). "Experimental Transmission of a Kuru-Like Syndrome to Chimpanzees." Nature **209**(5025): 794-&.

Gambetti, P., P. Parchi, R. B. Petersen, S. G. Chen and E. Lugaresi (1995). "Fatal Familial Insomnia and Familial Creutzfeldt-Jakob-Disease - Clinical, Pathological and Molecular-Features." Brain Pathology **5**(1): 43-51.

Gibbs, C. J., Jr., D. C. Gajdusek, D. M. Asher, M. P. Alpers, E. Beck, P. M. Daniel and W. B. Matthews (1968). "Creutzfeldt-Jakob disease (spongiform encephalopathy): transmission to the chimpanzee." Science **161**(3839): 388-389.

Golding, M. C., C. R. Long, M. A. Carmell, G. J. Hannon and M. E. Westhusin (2006). "Suppression of prion protein in livestock by RNA interference." Proceedings of the National Academy of Sciences of the United States of America **103**(14): 5285-5290.

Golker, C. F., M. D. Whiteman, K. H. Gugel, R. Gilles, P. Stadler, R. M. Kovatch, D. Lister, M. H. Wisher, C. Calcagni and G. E. Hubner (1996). "Reduction of the infectivity of scrapie agent as a model for BSE in the manufacturing process of Trasylol(R)." Biologicals **24**(2): 103-111.

Gordon, W. S. (1946). "Advances in veterinary research." Vet Rec **58**(47): 516-525.

Greenwood, A. D., M. Horsch, A. Stengel, I. Vorberg, G. Lutzny, E. Maas, S. Schadler, V. Erfle, J. Beckers, H. Schatzl and C. Leib-Mosch (2005). "Cell line dependent RNA expression profiles of prion-infected mouse neuronal cells." Journal of Molecular Biology **349**(3): 487-500.

Harris, D. A. (2003). "Trafficking, turnover and membrane topology of PrP." Br Med Bull **66**: 71-85.

Haybaeck, J., M. Heikenwalder, B. Klevenz, P. Schwarz, I. Margalith, C. Bridel, K. Mertz, E. Zirdum, B. Petsch, T. J. Fuchs, L. Stitz and A. Aguzzi (2011). "Aerosols transmit prions to immunocompetent and immunodeficient mice." PLoS Pathog **7**(1): e1001257.

Heikenwalder, M., N. Zeller, H. Seeger, M. Prinz, P. C. Klohn, P. Schwarz, N. H. Ruddle, C. Weissmann and A. Aguzzi (2005). "Chronic lymphocytic inflammation specifies the organ tropism of prions." Science **307**(5712): 1107-1110.

Hope, J. (2013). "Bovine spongiform encephalopathy: a tipping point in One Health and Food Safety." Curr Top Microbiol Immunol **366**: 37-47.

Hope J, Ritchie L, Farquhar C, Somerville R and Hunter N (1989). "Bovine spongiform encephalopathy: a scrapie-like disease of British cattle." Prog Clin Biol Res **317**: 659-667.

Hruska-Plochan, M., B. Li, D. Kyburz, J. Krutzfeld, U. Landmesser, A. Aguzzi and M. Polymenidou (2015). "New and emerging roles of small RNAs in neurodegeneration, muscle, cardiovascular and inflammatory diseases." Swiss Med Wkly **145**: w14192.

Jarrett, J. T. and P. T. Lansbury (1993). "Seeding One-Dimensional Crystallization of Amyloid - a Pathogenic Mechanism in Alzheimers-Disease and Scrapie." Cell **73**(6): 1055-1058.

Jaunmuktane, Z., S. Mead, M. Ellis, J. D. Wadsworth, A. J. Nicoll, J. Kenny, F. Launchbury, J. Linehan, A. Richard-Loendt, A. S. Walker, P. Rudge, J. Collinge and S. Brandner (2015). "Evidence for human transmission of amyloid-beta pathology and cerebral amyloid angiopathy." Nature **525**(7568): 247-250.

Johnson, R. T. and C. J. Gibbs, Jr. (1998). "Creutzfeldt-Jakob disease and related transmissible spongiform encephalopathies." N Engl J Med **339**(27): 1994-2004.

Julius, C., G. Hutter, U. Wagner, H. Seeger, V. Kana, J. Kranich, P. Klohn, C. Weissmann, G. Miele and A. Aguzzi (2008). "Transcriptional stability of cultured cells upon prion infection." Journal of Molecular Biology **375**(5): 1222-1233.

Kang, S. G., Y. M. Roh, A. Lau, D. Westaway, D. McKenzie, J. Aiken, Y. S. Kim and H. S. Yoo (2011). "Establishment and characterization of Prnp knockdown neuroblastoma cells using dual microRNA-mediated RNA interference." Prion **5**(2): 93-102.

Karapetyan, Y. E., G. F. Sferrazza, M. H. Zhou, G. Ottenberg, T. Spicer, P. Chase, M. Fallahi, P. Hodder, C. Weissmann and C. I. Lasmezas (2013). "Unique drug screening approach for prion diseases identifies tacrolimus and astemizole as antiprion agents." Proceedings of the National Academy of Sciences of the United States of America **110**(17): 7044-7049.

Klohn, P. C., L. Stoltze, E. Flechsig, M. Enari and C. Weissmann (2003). "A quantitative, highly sensitive cell-based infectivity assay for mouse scrapie prions." Proc Natl Acad Sci U S A **100**(20): 11666-11671.

Knowles, T. P. J., C. A. Waudby, G. L. Devlin, S. I. A. Cohen, A. Aguzzi, M. Vendruscolo, E. M. Terentjev, M. E. Welland and C. M. Dobson (2009). "An Analytical Solution to the Kinetics of Breakable Filament Assembly." Science **326**(5959): 1533-1537.

Kovacs, G. G., M. I. Lutz, G. Ricken, T. Strobel, R. Hoftberger, M. Preusser, G. Regelsberger, S. Honigschnabl, A. Reiner, P. Fischer, H. Budka and J. A. Hainfellner (2016). "Dura mater is a potential source of A beta seeds." Acta Neuropathologica **131**(6): 911-923.

Liberali, P., B. Snijder and L. Pelkmans (2014). "A Hierarchical Map of Regulatory Genetic Interactions in Membrane Trafficking." Cell **157**(6): 1473-1487.

Liberski, P. P. (2012). "Historical overview of prion diseases: a view from afar." Folia Neuropathol **50**(1): 1-12.

Ligios, C., C. J. Sigurdson, C. Santucciu, G. Carcassola, G. Manco, M. Basagni, C. Maestrale, M. G. Cancedda, L. Madau and A. Aguzzi (2005). "PrPSc in mammary glands of sheep affected by scrapie and mastitis." Nat Med **11**(11): 1137-1138.

Luk, K. C., V. Kehm, J. Carroll, B. Zhang, P. O'Brien, J. Q. Trojanowski and V. M. Y. Lee (2012). "Pathological alpha-Synuclein Transmission Initiates Parkinson-like Neurodegeneration in Nontransgenic Mice." Science **338**(6109): 949-953.

Mahal, S. P., C. A. Baker, C. A. Demczyk, E. W. Smith, C. Julius and C. Weissmann (2007). "Prion strain discrimination in cell culture: The cell panel assay." Proceedings of the National Academy of Sciences of the United States of America **104**(52): 20908-20913.

Mallucci, G., A. Dickinson, J. Linehan, P. C. Klohn, S. Brandner and J. Collinge (2003). "Depleting neuronal PrP in prion infection prevents disease and reverses spongiosis." Science **302**(5646): 871-874.

Mallucci, G. R., M. D. White, M. Farmer, A. Dickinson, H. Khatun, A. D. Powell, S. Brandner, J. G. Jefferys and J. Collinge (2007). "Targeting cellular prion protein reverses early cognitive deficits and neurophysiological dysfunction in prion-infected mice." Neuron **53**(3): 325-335.

Manson, J. C., A. R. Clarke, P. A. Mcbride, I. Mcconnell and J. Hope (1994). "Prp Gene Dosage Determines the Timing but Not the Final Intensity or Distribution of Lesions in Scrapie Pathology." Neurodegeneration **3**(4): 331-340.

Marbiah, M. M., A. Harvey, B. T. West, A. Louzolo, P. Banerjee, J. Alden, A. Grigoriadis, H. Hummerich, H. M. Kan, Y. Cai, G. S. Bloom, P. Jat, J. Collinge and P. C. Klohn (2014). "Identification of a gene regulatory network associated with prion replication." Embo Journal **33**(14): 1527-1547.

Mathiason, C. K., J. G. Powers, S. J. Dahmes, D. A. Osborn, K. V. Miller, R. J. Warren, G. L. Mason, S. A. Hays, J. Hayes-Klug, D. M. Seelig, M. A. Wild, L. L. Wolfe, T. R. Spraker, M. W. Miller, C. J. Sigurdson, G. C. Telling and E. A. Hoover (2006). "Infectious prions in the saliva and blood of deer with chronic wasting disease." Science **314**(5796): 133-136.

Mead, S., M. P. H. Stumpf, J. Whitfield, J. A. Beck, M. Poulter, T. Campbell, J. B. Uphill, D. Goldstein, M. Alpers, E. M. C. Fisher and J. Collinge (2003). "Balancing selection at the prion protein gene consistent with prehistoric kurulike epidemics." Science **300**(5619): 640-643.

Medori, R., H. J. Tritschler, A. Leblanc, F. Villare, V. Manetto, H. Y. Chen, R. Xue, S. Leal, P. Montagna, P. Cortelli, P. Tinuper, P. Avoni, M. Mochi, A. Baruzzi, J. J. Hauw, J. Ott, E. Lugaresi, L. Autiliogambetti and P. Gambetti (1992). "Fatal Familial Insomnia, a Prion Disease with a Mutation at Codon-178 of the Prion Protein Gene." New England Journal of Medicine **326**(7): 444-449.

Meyer, R. K., M. P. Mckinley, K. A. Bowman, M. B. Braunfeld, R. A. Barry and S. B. Prusiner (1986). "Separation and Properties of Cellular and Scrapie Prion Proteins." Proceedings of the National Academy of Sciences of the United States of America **83**(8): 2310-2314.

Nazor Friberg, K., G. Hung, E. Wancewicz, K. Giles, C. Black, S. Freier, F. Bennett, S. J. Dearmond, Y. Freyman, P. Lessard, S. Ghaemmaghami and S. B. Prusiner (2012). "Intracerebral Infusion of Antisense Oligonucleotides Into Prion-infected Mice." Mol Ther Nucleic Acids **1**: e9.

Neckers, L. M. and J. B. Trepel (1986). "Transferrin Receptor Expression and the Control of Cell-Growth." Cancer Investigation **4**(5): 461-470.

Nuvolone, M., V. Kana, G. Hutter, D. Sakata, S. M. Mortin-Toth, G. Russo, J. S. Danska and A. Aguzzi (2013). "SIRP alpha polymorphisms, but not the prion protein, control phagocytosis of apoptotic cells." Journal of Experimental Medicine **210**(12): 2539-2552.

Oesch, B., D. Westaway, M. Walchli, M. P. Mckinley, S. B. H. Kent, R. Aebersold, R. A. Barry, P. Tempst, D. B. Teplow, L. E. Hood, S. B. Prusiner and C. Weissmann (1985). "A Cellular Gene Encodes Scrapie Prp 27-30 Protein." Cell **40**(4): 735-746.

Peretz, D., M. R. Scott, D. Groth, R. A. Williamson, D. R. Burton, F. E. Cohen and S. B. Prusiner (2001). "Strain-specified relative conformational stability of the scrapie prion protein." Protein Sci **10**(4): 854-863.

Pfeifer, A., S. Eigenbrod, S. Al-Khadra, A. Hofmann, G. Mitteregger, M. Moser, U. Bertsch and H. Kretzschmar (2006). "Lentivector-mediated RNAi efficiently suppresses prion protein and prolongs survival of scrapie-infected mice." Journal of Clinical Investigation **116**(12): 3204-3210.

Polymenidou, M., R. Moos, M. Scott, C. Sigurdson, Y. Z. Shi, B. Yajima, I. Hafner-Bratkovic, R. Jerala, S. Hornemann, K. Wuthrich, A. Bellon, M. Vey, G. Garen, M. N. G. James, N. Kav and A. Aguzzi (2008). "The POM Monoclonals: A Comprehensive Set of Antibodies to Non-Overlapping Prion Protein Epitopes." Plos One **3**(12).

Polymenidou, M., S. Prokop, H. H. Jung, E. Hewer, D. Peretz, R. Moos, M. Tolnay and A. Aguzzi (2011). "Atypical Prion Protein Conformation in Familial Prion Disease with PRNP P105T Mutation." Brain Pathology **21**(2): 209-214.

Priola, S. A., B. Chesebro and B. Caughey (2003). "A view from the top - Prion diseases from 10,000 feet." Science **300**(5621): 917-+.

Proske, D., S. Gilch, F. Wopfner, H. M. Schatzl, E. L. Winnacker and M. Famulok (2002). "Prion-protein-specific aptamer reduces PrPSc formation." Chembiochem **3**(8): 717-725.

Prusiner, S. B. (1982). "Novel proteinaceous infectious particles cause scrapie." Science **216**(4542): 136-144.

Prusiner, S. B. (1991). "Molecular-Biology of Prion Diseases." Science **252**(5012): 1515-1522.

Prusiner, S. B., D. Groth, A. Serban, N. Stahl and R. Gabizon (1993). "Attempts to Restore Scrapie Prion Infectivity after Exposure to Protein Denaturants." Proceedings of the National Academy of Sciences of the United States of America **90**(7): 2793-2797.

Prusiner, S. B., D. F. Groth, M. P. McKinley, S. P. Cochran, K. A. Bowman and K. C. Kasper (1981). "Thiocyanate and hydroxyl ions inactivate the scrapie agent." Proc Natl Acad Sci U S A **78**(7): 4606-4610.

Pulford, B., N. Reim, A. Bell, J. Veatch, G. Forster, H. Bender, C. Meyerett, S. Hafeman, B. Michel, T. Johnson, A. C. Wyckoff, G. Miele, C. Julius, J. Kranich, A. Schenkel, S. Dow and M. D. Zabel (2010). "Liposome-siRNA-Peptide Complexes Cross the Blood-Brain Barrier and Significantly Decrease PrPC on Neuronal Cells and PrPRES in Infected Cell Cultures." Plos One **5**(6).

Reed J, M. H. (1938). "A simple method for estimating fifty per cent end points." Am. J. Epidemiol. **27**(3): 493-497.

Riek, R., S. Hornemann, G. Wider, M. Billeter, R. Glockshuber and K. Wuthrich (1996). "NMR structure of the mouse prion protein domain PrP(121-231)." Nature **382**(6587): 180-182.

Rissin, D. M., C. W. Kan, T. G. Campbell, S. C. Howes, D. R. Fournier, L. Song, T. Piech, P. P. Patel, L. Chang, A. J. Rivnak, E. P. Ferrell, J. D. Randall, G. K. Provuncher, D. R. Walt and D. C. Duffy (2010). "Single-molecule enzyme-linked immunosorbent assay detects serum proteins at subfemtomolar concentrations." Nature Biotechnology **28**(6): 595-U525.

Rissin, D. M. and D. R. Walt (2006). "Digital concentration readout of single enzyme molecules using femtoliter arrays and Poisson statistics." Nano Letters **6**(3): 520-523.

Saba, R., C. D. Goodman, R. L. C. H. Huzarewich, C. Robertson and S. A. Booth (2008). "A miRNA Signature of Prion Induced Neurodegeneration." Plos One **3**(11).

Sandberg, M. K., H. Al-Doujaily, B. Sharps, A. R. Clarke and J. Collinge (2011). "Prion propagation and toxicity in vivo occur in two distinct mechanistic phases." Nature **470**(7335): 540-542.

Sandberg, M. K., H. Al-Doujaily, B. Sharps, M. W. De Oliveira, C. Schmidt, A. Richard-Londt, S. Lyall, J. M. Linehan, S. Brandner, J. D. F. Wadsworth, A. R. Clarke and J. Collinge (2014). "Prion neuropathology follows the accumulation of alternate prion protein isoforms after infective titre has peaked." Nature Communications **5**.

Scita, G. and P. P. Di Fiore (2010). "The endocytic matrix." Nature **463**(7280): 464-473.

Seeger, H., M. Heikenwalder, N. Zeller, J. Kranich, P. Schwarz, A. Gaspert, B. Seifert, G. Miele and A. Aguzzi (2005). "Coincident scrapie infection and nephritis lead to urinary prion excretion." Science **310**(5746): 324-326.

Sigurdson, C. J. and A. Aguzzi (2007). "Chronic wasting disease." Biochim Biophys Acta **1772**(6): 610-618.

Silveira, J. R., G. J. Raymond, A. G. Hughson, R. E. Race, V. L. Sim, S. F. Hayes and B. Caughey (2005). "The most infectious prion protein particles." Nature **437**(7056): 257-261.

Sonati, T., R. R. Reimann, J. Falsig, P. K. Baral, T. O'Connor, S. Hornemann, S. Yaganoglu, B. Li, U. S. Herrmann, B. Wieland, M. Swayampakula, M. H. Rahman, D. Das, N. Kav, R. Riek, P. P. Liberski, M. N. G. James and A. Aguzzi (2013). "The toxicity of antiprion antibodies is mediated by the flexible tail of the prion protein." Nature **501**(7465): 102-+.

Stahl, N., D. R. Borchelt, K. Hsiao and S. B. Prusiner (1987). "Scrapie Prion Protein Contains a Phosphatidylinositol Glycolipid." Cell **51**(2): 229-240.

Steele, A. D., S. Lindquist and A. Aguzzi (2007). "The Prion Protein Knockout Mouse A Phenotype Under Challenge." Prion **1**(2): 83-93.

Stohr, J., C. Condello, J. C. Watts, L. Bloch, A. Oehler, M. Nick, S. J. DeArmond, K. Giles, W. F. DeGrado and S. B. Prusiner (2014). "Distinct synthetic Abeta prion strains producing different amyloid deposits in bigenic mice." Proc Natl Acad Sci U S A **111**(28): 10329-10334.

Tateishi, J., T. Kitamoto, S. Mohri, S. Satoh, T. Sato, A. Shepherd and M. R. Macnaughton (2001). "Scrapie removal using Planova((R)) virus removal filters." Biologicals **29**(1): 17-25.

Taylor, D. M., J. M. Brown, K. Fernie and I. McConnell (1997). "The effect of formic acid on BSE and scrapie infectivity in fixed and unfixed brain-tissue." Vet Microbiol **58**(2-4): 167-174.

Telling, G. C., M. Scott, J. Mastrianni, R. Gabizon, M. Torchia, F. E. Cohen, S. J. Dearmond and S. B. Prusiner (1995). "Prion Propagation in Mice Expressing Human and Chimeric Prp Transgenes Implicates the Interaction of Cellular Prp with Another Protein." Cell **83**(1): 79-90.

Tilly, G., J. Chapuis, D. Vilette, H. Laude and J. L. Vilotte (2003). "Efficient and specific down-regulation of prion protein expression by RNAi." Biochemical and Biophysical Research Communications **305**(3): 548-551.

Tortorella, S. and T. C. Karagiannis (2014). "Transferrin Receptor-Mediated Endocytosis: A Useful Target for Cancer Therapy." Journal of Membrane Biology **247**(4): 291-307.

Trevitt, C. R. and J. Collinge (2006). "A systematic review of prion therapeutics in experimental models." Brain **129**: 2241-2265.

Tuite, M. F. and B. S. Cox (2003). "Propagation of yeast prions." Nat Rev Mol Cell Biol **4**(11): 878-890.

Unal, A., J. Thyer, E. Uren, D. Middleton, M. Braun and D. Maher (2007). "Investigation by bioassay of the efficacy of sodium hydroxide treatment on the inactivation of mouse-adapted scrapie." Biologicals **35**(3): 161-164.

Watts, J. C., C. Condello, J. Stohr, A. Oehler, J. Lee, S. J. DeArmond, L. Lannfelt, M. Ingelsson, K. Giles and S. B. Prusiner (2014). "Serial propagation of distinct strains of Abeta prions from Alzheimer's disease patients." Proc Natl Acad Sci U S A **111**(28): 10323-10328.

Weiss, S., D. Proske, M. Neumann, M. H. Groschup, H. A. Kretzschmar, M. Famulok and E. L. Winnacker (1997). "RNA aptamers specifically interact with the prion protein PrP." Journal of Virology **71**(11): 8790-8797.

Weissmann, C. (1991). "A Unified Theory of Prion Propagation." Nature **352**(6337): 679-683.

Weissmann, C. (1999). "Molecular genetics of transmissible spongiform encephalopathies." Journal of Biological Chemistry **274**(1): 3-6.

Weissmann, C. (2005). "Birth of a prion: spontaneous generation revisited." Cell **122**(2): 165-168.

Weissmann, C. and A. Aguzzi (1997). "Bovine spongiform encephalopathy and early onset variant Creutzfeldt-Jakob disease." Curr Opin Neurobiol **7**(5): 695-700.

Weissmann, C., J. Li, S. P. Mahal and S. Browning (2011). "Prions on the move." EMBO Rep **12**(11): 1109-1117.

Wells, G. A., A. C. Scott, C. T. Johnson, R. F. Gunning, R. D. Hancock, M. Jeffrey, M. Dawson and R. Bradley (1987). "A novel progressive spongiform encephalopathy in cattle." Vet Rec **121**(18): 419-420.

White, M. D., M. Farmer, I. Mirabile, S. Brandner, J. Collinge and G. R. Mallucci (2008). "Single treatment with RNAi against prion protein rescues early neuronal dysfunction and

prolongs survival in mice with prion disease." Proceedings of the National Academy of Sciences of the United States of America **105**(29): 10238-10243.

Williams, E. S. and S. Young (1980). "Chronic Wasting Disease of Captive Mule Deer - Spongiform Encephalopathy." Journal of Wildlife Diseases **16**(1): 89-98.

Wongsrikeao, P., S. Sutou, M. Kunishi, Y. J. Dong, X. J. Bai and T. Otoi (2011). "Combination of the somatic cell nuclear transfer method and RNAi technology for the production of a prion gene-knockdown calf using plasmid vectors harboring the U6 or tRNA promoter." Prion **5**(1): 39-46.

Xanthopoulos, K., M. Polymenidou, S. J. Bellworthy, S. L. Benestad and T. Sklaviadis (2009). "Species and Strain Glycosylation Patterns of PrPSc." Plos One **4**(5).

8 ACKNOWLEDGMENTS

I would like to express my gratitude to all the people who supported me during the time of my thesis and contributed to making it such a memorable journey:

I would like to express my deepest thanks to my supervisor, Prof. Adriano Aguzzi, for offering me the precious opportunity of pursuing a Ph.D. thesis in his lab. In addition I would like to express my gratitude for his constant support, brilliant ideas, inspiring discussions and guidance throughout my Ph.D. thesis.

I would like to express my deepest thanks to Prof. Charles Weissmann, Prof. Ben Schuler and Prof. Tuomas P.J. Knowles for supporting me over these years with their time for discussions and participation in my PhD committee.

Furthermore, I would like to express my warm gratitude to a number of people who have helped me throughout my training:

Prof. Elisabeth Rushing for her kind help with correcting my thesis and insightful comments on the thesis.

Dr. Caihong Zhu for fascinating discussions, teaching me *in vitro* and *in vivo* biological methods, as well as collaborations on several interesting projects.

Prof. Ioannis Xenarios from the Swiss Institute of Bioinformatics at the University of Lausanne, and his team members including Elke Schaper, Jerome Dauvillier for their contribution to the systematic data analysis to siRNA screening project.

Dr. Frank V. Girardi from Novartis Institute BioMedical Research, for offering us the murine siRNA library. Prof. Lucas Pelkmans from the Institute of Molecular Life Science at the University of Zurich, for his discussions and collaborations on the siRNA screening project. Dr. Philip Gribbon from the Fraunhofer Institute for Molecular Biology and Applied Ecology IME, for his suggestions and discussions on siRNA screening performance.

Dr. Simone Hornemann for her guidance and teaching of bio-safety performance, biochemistry methods.

Clemence Tournaire for her technical support, including the organization and maintenance of automated platforms HTS users.

Dr. Mario Nuvolone and Dr. Sorce Silvia for their contribution to the mouse bio-bank brain samples.

Valeria Eckhardt, Mark Zurbrügg, Dr. Karl Frontzek and Daniel Pease for their contribution to the generation and validation of new cell lines for the small RNAi screening projects.

Chapter 8 ACKNOWLEDGMENTS

The lab technician team Rita Moos, Petra Schwarz, Irina Abakumova, Karina Arroyo, Rajlakshmi Marpakwar, Lisa Caflisch and Mirzet Delic for help with everything in the lab.

The secretary team Jacqueline Wiedler, Isabella Gianella and Meike Nau-Lüber for help in organizational and administrative work.

Norbert Wey, André Wethmar and Monika Bieri for the IT support.

The current and former members of the lab for their help in the lab, discussions and the fun moments: Dr. Asvin Lakkaraju, Dr. Senatore Assunta, Dr. Henning Leske, Dr. Regina Reimann, Dr. Daniel Kirschenbaum, Dr. Vijay Chandrasekar, Dr. Rehwald Claudia, Dr. Cinzia Tiberi, Dr. Yingjun Liu, Melanie Einsiedler, Despina Goniotaki, Prof. Magda Polymenidou, Dr. Tiziana Sonati, Dr. Sergey Yakushev, Ahmet Varol, Cédric Doucerain, Dr. Alexander Küffer, Dr. Veronika Kana, Dr. Christian Kempf.

I would like to express my extreme gratitude to my parents and my husband for their constant support and unconditional love.

9 CURRICULUM VITAE

Name: BEI LI

First name: Bei

Date of birth: December 20th, 1983

Nationality: China

Education:

04/2011 – 09/2016 PhD student

University of Zurich, Molecular Life Science Ph.D. program.

Institute of Neuropathology, University Hospital of Zurich

Supervisor: Professor. Adriano Aguzzi

PhD thesis title: Establishment of an automated digital prion infectivity cell assay and PrP-HPFRET based high-throughput siRNA screening platform.

09/2005 – 03/2008 Master of Science in Biochemistry and Molecular Biology

School of Life Sciences and Technology, Tongji University, Shanghai, China

Supervisor: Prof. Guoxiang Cheng

Master thesis title: Knockout of the gene encoding IgH in goat fetal fibroblasts.

09/2001 – 06/2005 Bachelor of Science in Biology Science and Technology

College of Bioscience and Biotechnology, Yangzhou University, China

Supervisor: Prof. Guoxiang Cheng

Bachelor thesis title: Production and purification of fully humanized anti-VEGF monoclonal antibody.

Publications:

Marian Hruska-Plochana*, **Bei Li***, Diego Kyburz, Jan Krützfeldt, Ulf Landmesser, Adriano Aguzzi, Magdalini Polymenidou. New and emerging roles of small RNAs in neurodegeneration, muscle, cardiovascular and inflammatory diseases. **Swiss Med Wkly.** 2015 Sep 16;145:w14192. doi: 10.4414/smw.2015.14192. eCollection 2015 (co-first author).

Uli S. Herrmann, Anne K. Schütz, Hamid Shirani, Danzhi Huang, Dino Saban, Mario Nuvolone, **Bei Li**, Boris Ballmer, Andreas K. O. Åslund, Jeffrey J. Mason, Elisabeth Rushing, Herbert Budka, Sofie Nyström, Per Hammarström, Anja Böckmann, Amedeo Caflisch, Beat H. Meier, K. Peter R. Nilsson, Simone Hornemann, Adriano Aguzzi. Structure-based drug

design identifies polythiophenes as antiprion compounds. **Sci Transl Med.** 2015 Aug 5;7(299):299ra123. doi: 10.1126/scitranslmed.aab1923.

Caihong Zhu, Uli S. Herrmann, **Bei Li**, Irina Abakumova, Rita Moos, Petra Schwarz, Elisabeth J. Rushing, Marco Colonna, Adriano Aguzzi. Triggering receptor expressed on myeloid cells-2 is involved in prion-induced microglial activation but does not contribute to prion pathogenesis in mouse brains. **Neurobiol Aging.** 2015 May;36(5):1994-2003. doi: 10.1016/j.neurobiolaging.2015.02.019. Epub 2015 Feb 27.

Uli S. Herrmann, Tiziana Sonati, Jeppe Falsig, Regina R. Reimann, Paolo Dametto, Tracy O'Connor, **Bei Li**, Agnes Lau, Simone Hornemann, Silvia Sorce, Uli Wagner, Despina Sanoudou, Adriano Aguzzi. Prion infections and anti-PrP antibodies trigger converging neurotoxic pathways. **PLoS Pathog.** 2015 Feb 24;11(2):e1004662. doi: 10.1371/journal.ppat.1004662. eCollection 2015.

Tiziana Sonati, Regina R. Reimann, Jeppe Falsig, Pravas Kumar Baral, Tracy O'Connor, Simone Hornemann, Sine Yaganoglu, **Bei Li**, Uli S. Herrmann, Barbara Wieland, Mridula Swayampakula, Muhammad Hafizur Rahman, Dipankar Das, Nat Kav, Roland Riek, Pawel P. Liberski, Michael N. G. James, Adriano Aguzzi. The toxicity of antiprion antibodies is mediated by the flexible tail of the prion protein. **Nature.** 2013 Sep 5;501(7465):102-6. doi: 10.1038/nature12402. Epub 2013 Jul 31.

Jeppe Falsig, Tiziana Sonati, Uli S. Herrmann, Dino Saban, **Bei Li**, Karina Arroyo, Boris Ballmer, Pawel P. Liberski, Adriano Aguzzi. Prion pathogenesis is faithfully reproduced in cerebellar organotypic slice cultures. **PLoS Pathog.** 2012;8(11):e1002985. doi: 10.1371/journal.ppat.1002985. Epub 2012 Nov 1.

Bei Li, Elke Schaper, Caihong Zhu, Clemence Tournaire, Valeria Eckhardt, Mark Zurbrügg, Karl Frontzek, Simone Hornemann, Ioannis Xenarios, Adriano Aguzzi. An automated PrP-HPFRET based siRNA HTS uncovering Tfr1 modulating cellular prion protein expression (Manuscript in preparation).

Bei Li, Georg Meisl, Sergey Yakushev, Elke Schaper, Caihong Zhu, Simone Hornemann, Mario Nuvolone, Silvia Sorce, Clemence Tournaire, Tuomas P.J.Knowles, Adriano Aguzzi. High-throughput prion infectivity detection with an automated digital prion infectivity cell assay (DPICA) (Manuscript in preparation).